Midterm Report

AETHERIA

Group 11: Hydrogen-powered long-range eVTOL designed for crashworthiness

B.A. van Battum	5100771	D.M. Keijzer	5303206
B. Sarıgöl	5252016	S. de Rijke	5109345
C. Karaca	5211123	E. Hadzhiyski	5229022
L. Middendorp	5067049	C. Simon Soria	5220491
W. Albers	5040019	J. Arends	5243637

Delft University of Technology

Midterm Report

AETHERIA

by

Group 11: Hydrogen-powered long-range eVTOL designed for crashworthiness

B.A. van Battum	5100771	D.M. Keijzer	5303206
B. Sarıgöl	5252016	S. de Rijke	5109345
C. Karaca	5211123	E. Hadzhiyski	5229022
L. Middendorp	5067049	C. Simon Soria	5220491
W. Albers	5040019	J. Arends	5243637

Tutor: Saullo Giovanni Pereira Castro and Fulvio Scarano
Coaches: Justus Benad and Marina Barahona Lopez
Teaching Assistant: Koen Smit

Institution: Delft University of Technology
Faculty: Faculty of Aerospace Engineering

Submission date: Friday 2nd June 2023

TU Delft

Summary

There has been a significant increase in research and development for alternative modes of transportation in the quest for faster, more effective, and more sustainable travel options in recent years. Additionally, the need for solutions has become more urgent due to air pollution and traffic congestion. Electric Vertical Take-Off and Landing (eVTOL) aircraft may hold the key to this issue's resolution. The addition of hydrogen-based propulsion to the eVTOL design is a development that will increase the aircraft's potential range. Therefore, the goal of this DSE project is to use hydrogen to improve the performance of battery-powered long-range eVTOLs. The Mission Need Statement (MNS) of the project is as follows:

Design a safe and sustainable long-range hydrogen eVTOL that can transport four passengers

This report will serve as the basis for creating the final, detailed design of an eVTOL called Aetheria. Trade-offs will be performed based on three predetermined configurations. Preliminary estimates are made for parameters in each technical department for each configuration, and given a score relative to one another. Finally, the scores will be used to pick one design to pursue in the final report.

Team Organisation and Project Plan

The team has organized itself into both managerial and technical roles, with each team member connected to a specific department.
The workflow diagram (WFD) and the work breakdown structure (WBDS) were updated and presented in more depth in order to demonstrate the tasks as they become clearer and more specific. Furthermore, an N2 chart is presented to illustrate the flow of information between the different subsystems of Aetheria. Additionally, a project design and development logic diagram demonstrates the progression of the project beyond the preliminary design phase, including detailed design, prototype construction, testing, certification, mass production, commercialization, regular inspections, and eventual recycling and disposal.

Design Options and Trade-Off Criteria

The three designs that will be evaluated are presented. This involves a design called J1, which has been inspired by Joby Aviation, and has two tilting rotors on each wing, and another tilting rotor on the horizontal stabiliser. The second one is the L1, inspired by Lilium, which features a tandem wing and has tilting ducted fans on each wing. The last one is the W1, inspired by the Wigeon group, and has tilting tandem wings with fixed rotors.
To assess each design, trade-off criteria have been made, each with its own score. These are the mission energy, stability & controllability, crashworthiness, noise, production costs, and operational costs excluding fuel criteria. Each has been given relative weights of 30%, 20%, 20%, 10%, 10% and 10%, respectively.

Technical Risk Assessment

The risk assessment was a build-up on the risk analysis performed in the baseline report as new risks were identified during the detailed design stages. The power and propulsion, control and stability, structures and operations departments posed the highest risks, amongst a few more risks from other departments. These high risks corresponding to the orange and red sections of the risk matrix were mitigated to more acceptable levels by applying prevention and contingency measures. Finally, an updated risk map representing all the risks until this design phase was shown on the post mitigation risk matrix.

Preliminary sizing

In order to start with department-specific design, a starting point for the mass, power, and wing surface area is required. This is done in preliminary sizing. Wing and power loading diagrams were created for each of the designs to obtain the required power and wing surface area. The initial mass was estimated with a Class I weight estimation. A dataset of existing eVTOLs was used to determine the maximum take-off mass from the payload mass via linear regression. The size of the dataset was initially 24 but was reduced to 10 to only include eVTOLs with functioning prototypes. This improved the accuracy of the linear regression. The Class I estimation resulted in an MTOM of 2510 [kg] and OEM of 2000 [kg].

Aerodynamics & Flight Performance

In order to estimate an accurate mission energy (required for the trade-off), the aerodynamic and flight performance parameters of the design were evaluated. The first step was to calculate the wing planform param-

eters. After the wing planforms were complete the airfoil was chosen. In order to simplify the trade-off, the same airfoil was chosen for each of the three designs. Whether this airfoil is the best for each design will be investigated after the trade-off in the optimization phase. The airfoil chosen was the NACA44017, the same airfoil used by the Wigeon final design [1].
A class I drag estimation was performed, using the wetted area to calculate the C_{D_0} and using XFLR5 to find C_L. This gave the W1 the highest L/D at cruise conditions. After completing the class II drag estimation, for which the component drag method is used, the L1 had the highest L/D, while the J1 had the lowest. Using the L/D values, the mission energy during cruise can be calculated. This accounts for more than 50% of the total energy used. After running the convergence loop, the J1 has by far the lowest mission energy (199.0 [kWh]), followed by the W1 (313.9 [kWh]), and lastly the L1 (527.3 [kWh]). This makes the J1 the most preferred design for mission energy.

Structural Design

To start the structural analysis, the ultimate load factors and critical load cases need to be established. The ultimate load factor is obtained from the manoeuvring and gust diagram. For the structural analysis, the critical defect types were identified to be overload, delamination, and fatigue. For the first two types, a stress analysis was performed on the wing root. The normal stress, shear and critical buckling stress were found for two load cases: vertical flight and cruise. J1 experienced the least stress, followed by W1 and L1. Regarding buckling, W1 performed the best, meaning that it would require the least amount of stiffeners. The fatigue analysis showed that the cycle life was dependent on the stress range, meaning that J1 has the best fatigue performance. Subsequently, an initial planform of the fuselage was designed. The length and width of the fuselage were determined to be 9295 [mm] and 1700 [mm] respectively.
The class II weight estimation was performed using the Cessna and Torenbeek methods [2]. All main structural components were taken into account and, additionally, miscellaneous sub-components such as electrical systems were added. Each design was converged through an iterative process until a design that meets performance requirements is reached. The final weights were determined to be 2014 [kg], 4584 [kg] and 3351 [kg] for J1, L1 and W1 respectively.
The "safe" component of the MNS refers to the crashworthiness study which demonstrates that there are two important factors to consider: engine & wing placement, propeller penetration into the cabin, and the effective cross-section area used to store hydrogen. It was concluded that the effect of both factors was similar for the three configurations. Secondly, a safe energy absorption system shall be designed to absorb all kinetic energy. With a certain honeycomb structure, it was found that L1 requires a cuboid structure with a length of 3.63 [m], which is more than the cabin length. J1 and W1 both do not require a redesign to fit the crash structure and are therefore the best option in a structural context.

Power System

The power system options considered and analysed were hydrogen cruise and hybrid cruise. To compare these two options, trade-offs were performed on the type of battery, fuel cell and hydrogen storage options, in order to chose the best option for this design and use the corresponding configuration values to size the overall power system.
In the battery trade-off, although obtaining the lowest total score, lithium-ion batteries were chosen since they successfully passed the imposed hard pass/fail criteria. The other options, excluding super-capacitors, didn't. However, super-capacitors were discarded, since they have extremely low energy densities which would result in a very heavy infeasible design. Solid-state batteries were also analysed, for use in future applications due to their very high potential. In the fuel cell trade-off, PEM fuel cells outscored any other options. Finally, in the storage tank trade-off, compressed and liquid storage methods had the same score. However, due to high complexity of liquid storage methods, a compressed hydrogen storage method was chosen.
Following the trade-offs, it was found that a hybrid cruise option turned out to be better than using only hydrogen for cruise. In this hybrid cruise, the optimum mass values obtained were by using hydrogen for 82% of cruise and batteries for the remaining 18% of cruise and for hovering. For this option, the power system mass would be 400[kg] for lithium-ion and 300 [kg] for solid state batteries. Finally, it was found that the volume was not the limiting case, therefore a 350 bar compression storage system is chosen. With this storage system, a total volume of 500 liters was obtained.

Propulsion & Power

To estimate the propulsive parameters, the actuator disk theory has been used. Using the MTOW for each design, a total propeller area was found. Once these were found, the exhaust velocity in hover and cruise was found. Together with the freestream velocity, the propulsive efficiency of each design was calculated. This showed that the J1 was best, followed by W1, then L1. This calculation proved that the J1 should be pursued in the final report with respect to propulsion.
The hover power requirements were also estimated based on an equation found in Lilium's technology paper. Here, the thrust was estimated as the MTOW, which produced a hover power requirement. By multiplying the MTOW by the maximum thrust-to-weight ratio found in the preliminary sizing, a maximum power requirement was found. Finally, using the MTOW, C_L/C_D, freestream velocity, and propulsive efficiency, the required power during cruise was also found. This showed that the J1 used the least amount of power, followed by the W1, then the L1. The J1's low disk loading was able to both increase the propulsive efficiency and decrease the power required.
Noise estimations were based on an empirical method to find the noise per propeller. This equation relied on a number of parameters, some of which were estimated, and some of which were found from literature. The L1's many distributed fans made L1 the winner in terms of noise, followed by the J1, then the W1.

Stability & Control

Based on stability and control criteria, a program has been created, that produces a cg envelope for each conceptual design. The cg envelope shows the required cg excursion, derived from the "potato" loading diagram; the shift of foremost and aftmost cg due to different wing positions; and the shift of foremost and aftmost cg due to an increased allowed maximum power per engine (above nominal conditions). Based on the cg envelopes, a trade-off value has been given to each conceptual design based on how restrictive stability and control is for them. A high value corresponds to a low compromise, flexible design concept. If a design cannot meet the cg excursion requirements it is automatically discarded. The design J2 was introduced, an improvement on the J1, due to J1's unacceptable vertical flight controllability characteristics.

Operations & Logistics, Sustainability Development Plan and Production Plan

For operations, the following have been considered: standby, cargo & passenger loading, and refueling & charging. This showed that for standby, the J1 and W1 are more suitable, for cargo & passenger loading, the L1 and W1 are more suitable, and for refueling & charging, all perform similarly. When the eVTOL is out of service, performing maintenance, repairs, and end-of-life concerns are discussed. Each design performs similarly in all of these phases. A RAMS (reliability, availability, maintainability, and safety) analysis was performed on each design, which generally showed that the J1 was the most optimal.
The sustainability development plan is split up into three sectors: Environmental sustainability, economical sustainability and social sustainability. From this analysis the conclusion was drawn that the environmental and economical sustainability of the three designs is not that different, while the social is due to noise of which L1 has the best noise performance.
The manufacturing, assembly, and integration determine how the eVTOL will go from being raw material to the finished product. For this, a line assembly will be used. Following this, the individual components will be assembled. This will lead to the subassembly of each aircraft section, which will then be all assembled and finished. Testing will also take place in parallel when possible.

Financial Analysis

In order to put a price on the production costs and operational costs of the eVTOLs, a financial analysis was conducted. The equations that were used to assess the costs were found in a textbook that conducted this research on GA aircraft [3], which were deemed close enough to eVTOLs to provide a preliminary cost analysis. The analysis showed that fixed costs were the same for each eVTOL, but the J1 was much cheaper when it came to the unit variable cost, and the operational cost. Next was the W1, and then the L1. The break-even unit number for the J1 was also much lower than the other designs, which is a very important parameter.

Trade-Off

Based on the trade-off criteria, the design J2 was chosen as it received a score of 2.4/3, a big lead compared to the other W1 which received a score of 1.8/3 and L1 which received a score of 1.5/3. Design J1 was discarded, as it did not meet control & stability requirements.

Contents

1
Introduction

Today, sustainable urban air mobility is in great demand and more and more conceptual designs on short and long range eVTOLs are being produced. Some have even gone as far as building a working prototype already such as the Lilium or Joby aircraft. However, working prototypes for eVTOLs incorporating hydrogen in their design do not exist yet. The main advantage of using hydrogen originates from its high energy density with respect to current state-of-the-art batteries. This will allow for an increased range, while still providing a sustainable way of transport. Aetheria is the name of the aircraft that will be designed to fill this gap in the current eVTOL market.

The aim of this report is to present the analysis of three possible Aetheria designs, of which the final chosen configuration shall be a sustainable long-range eVTOL designed for crashworthiness and capable of carrying four passengers. This will be done by comparing each design through six technical aspects, each focusing on a particular performance parameters: mission energy, control & stability, crashworthiness, noise, CAPEX and OPEX (excl. fuel costs). First, preliminary sizing is conducted consisting of Class I weight estimations and wing and power loading diagrams. This will be used by the aerodynamics department to design three wing planforms and assess their performance using XFLR5 software. Following this, the power and structures departments will compute power requirements, noise performance and crashworthiness. Finally, an iteration procedure is performed to ensure all designs have converged such that performance requirements are met. The aircraft parameters are then used in the final trade-off where the designs are graded on each performance criteria.

2
Team Organisation & Project Plan

This chapter provides the team organisation and project plan to ensure a smooth operation and clear organisation. The team organisation regards the role divisions and its responsibilities, and it presented in a organogram in Section 2.1. The main objectives of the project plan are to divide the tasks into departments and show the logical order of activities. A graphical representation of these objectives are displayed in the Work Break-down Structure and the Work Flow Diagram. The interaction between the subsystems (departments) in shown in a N^2 chart in Section 2.3. Furthermore, a Gantt chart in presented in Section 2.2 lists all the tasks to be performed. Lastly, Section 2.4 presents the order of activities that shall be performed to get Aetheria produced and flying.

2.1. Organogram

For the purpose of the organization, the group has split itself into different roles, both technical and managerial. The departments have been given in green to indicate where the technical roles come from. As of the first session, the group has assigned itself the roles as illustrated in Figure 2.1.

The responsibilities of each managerial role can also be summarized as:

1. The project manager will lead the meetings and manage deliverables, conflicts, and ensure that the project efficiency is as high as possible. Furthermore, the project manager will be responsible for the distribution of tasks and shares responsibility with the secretary and project administrator for the planning.

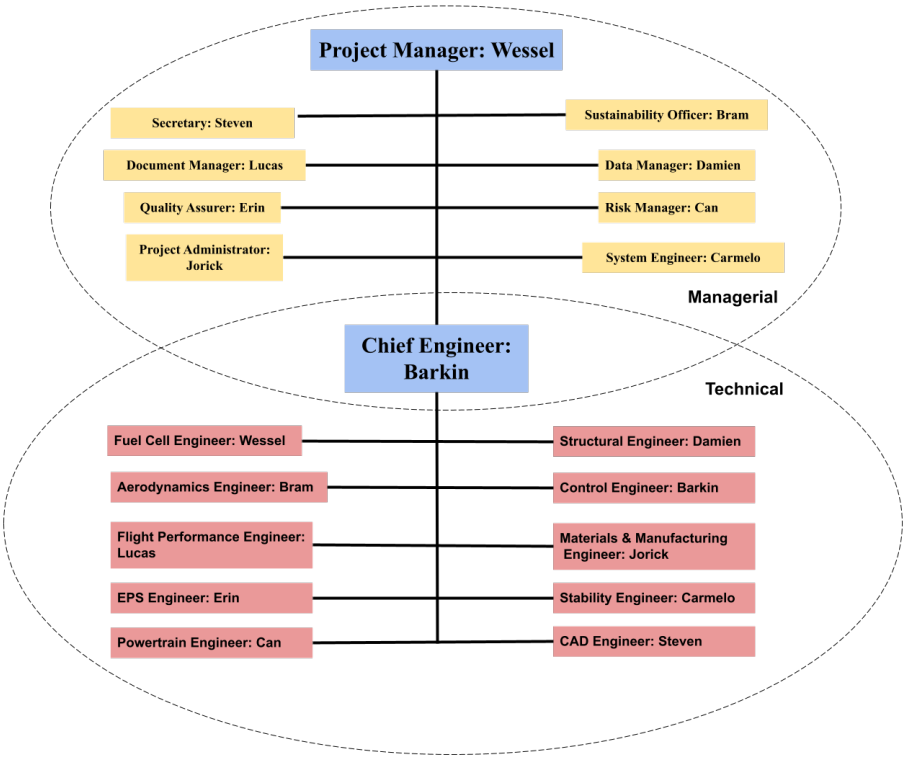

Figure 2.1: *The organogram containing the roles of the team members*

2. The secretary will document meetings, and take notes. The secretary, project administrator, and project manager share the responsibility of the planning

3. The project administrator will manage the logbook, 3Dexperience, and check if the team is on track with the Gantt chart

4. The document manager will handle, organize, and arrange all documents accrued during project hours. This includes the organization of the Overleaf files.

5. The data manager will handle all of the code that is being produced, and also set up the GitHub.

6. The system engineer ensures that all the subsystems can integrate well, and will communicate with each department so that all engineering teams are working on compatible products.

7. The sustainability officer confirms that each step taken toward the final product will be conducted in a sustainable manner, taking into account environmental, economic, and social aspects.

8. The quality assurer implements activities within the system to provide confidence that the product will meet the user requirements.

9. The risk manager manages technical risk, implements contingencies, and makes sure operations are conducted in an attainable and safe manner.

10. The chief engineer designs trade off's, creates design options trees, defines the engineering system, and does checks on each subsystem.

2.2. Planning diagrams

These are the workflow diagram, the work breakdown structure and the gantt chart. These list the required tasks of the project in an increasing amount of detail. It also shows dependencies and a time frame in which the task will be completed. These diagrams can be found below at the end of this chapter in the following order: work flow diagram, work breakdown structure and the gantt chart.

2.3. N^2 chart

This section provides the N^2 chart, which displays the interaction between the different subsystems. The yellow blocks are the subsystems, except for **Inputs**. The outputs of each subsystem are in the rows and the columns shows the outputs of each subsystem.

Table 2.1: *N^2 chart of the Aetheria vehicle illustrating the flow of information between the various subsystem. The arrows have been omitted for clarity reasons.*

Inputs	V_{cr} V_s V_{max} ROC_{climb} ROC_{hover}	n_{max} n_{min} n_{pax} gust speeds, payload			A_{disk}		A, A_h, n_{ult}, $P_{density}$	initial geometry
	Preliminary Sizing	OEM, W/S, C_{root}	W/S, S, b	W/P			S, b	
		Structure	l_{fus} l_{cab} l_{cp} l_{tail} d_{fus}				Φ_f, l_{fus}	l_{fus}
	$C_{L_{max}}$ C_L – C_D AR e	$C_{L_{max}}$ C_{L_α} C_m	**Aero**	C_L/C_D	C_L/C_D	C_D	t_{r_h}	C_m C_{m_α} $C_{m_{ac}}$ C_L C_{L_α} c
				Flight Performance			E_{req} P_{cr}	
	T/A				**Propulsion**	P_{max}	W_{prop}	T/A
		V_{H2}				**Power Sizing**	P_{max} W_{bat} V_{bat} W_{FCS} V_{FCS} W_{H_2} V_{H_2}	
	MTOM	MTOM		MTOM	MTOM	MTOM	**Weight Estimation**	MTOM
							S_h	**Stability & Control**

2.4. Project Design & Development Logic

The course this project will follow post DSE can be seen in the form of a project development diagram [4]. Figure 2.2 represents this process. Once the DSE ends, the preliminary design that has been made in the final report will be iterated over, to see whether it is feasible. This includes wind tunnel tests and general finalization of the design to rid it of small errors that could have been overlooked. Areas of the design that would have taken too long, or were too expensive to further investigate could be pursued in this step. Once the design is deemed feasible by each technical team, and complies with the regulations, the detailed design can begin.

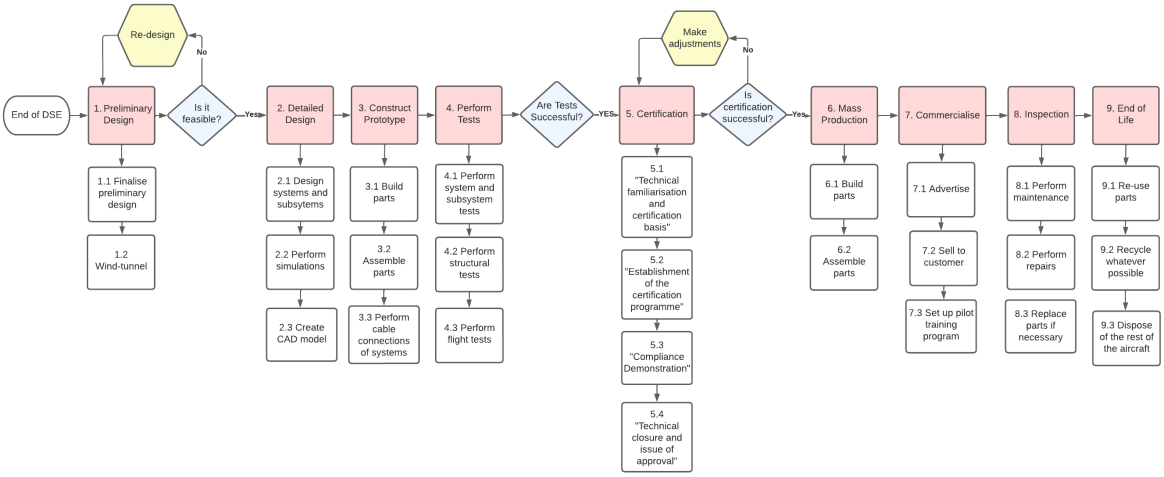

Figure 2.2: *Project Development Diagram*

The detailed design consists of designing each subsystem in full accuracy. For example, not only will the turboshaft design of the propeller be made, it should be clear whether an off-the-shelf item will be used, or one will be designed and constructed by the team. Detailed CAD models will be made of each part that will contribute to the eVTOL. Assemblies will also be made, such that the product in its entirety is designed, and the blueprints can be passed onto a manufacturing team. Simulations will be made of the CAD models as well to ensure that the design performs in the way that is expected. Using the CAD designs and the blueprints, a few prototypes will be constructed. This involves building each part and assembling them. In order to have a fully functioning prototype, the cable management of the eVTOL should also be made clear, and be present on the prototype. These will allow for marketing, but also testing.

Each subsystem of the prototype can be subjected to its respective tests. These tests can include both ground tests, to fit regulations, and necessary flight tests in hover and cruise, to prove the theoretical values. Structural tests can be performed to match the expected speculative behavior of the structure, with the test results. This would ensure safety. Once the testing of the prototypes has been successful, the eVTOL has to be certified in order to be able to be commercialised. This certification process consists of 4 phases [1]. These phases can be seen in Figure 2.2. Following these steps, if the certification is successful, mass production of the eVTOL can commence. However, if the certification process is unsuccessful, adjustments should be made in order for successful certification and tried again.

In the mass production, phase 5, a production line will be necessary to build and assemble parts simultaneously for rapid production of many eVTOLs. Once enough production of eVTOLs has taken place, the brand Aetheria can start to be commercialised. Aetheria can be commercialised by placing advertisements in order to encourage large companies to buy eVTOLs from us. Since this design is the first in the eVTOL market to use hydrogen as a power source, it should drag a lot of interest from potential customers to which we would sell. Furthermore, pilot training programs will be set up so that companies that we would sell Aetheria eVTOLs can use them to train their pilots.

After, Aetheria eVTOLs have been sold to customers, regular inspections in terms of maintenance will be applied in order to ensure the quality of the highest standards. In case necessary, repairs and possible part replacements will also be provided. After 15 years, which is the designated operational lifetime for Aetheria eVTOLs, the product will be brought in from the customer. Recyclable parts will be recycled and parts that can be re-used will be taken out and applied wherever possible. As the very final stage of the product, the eVTOL will be disposed of.

[1] Accessed May 17th 2023, https://www.easa.europa.eu/en/domains/aircraft-products/aircraft-certification

Work flow diagram

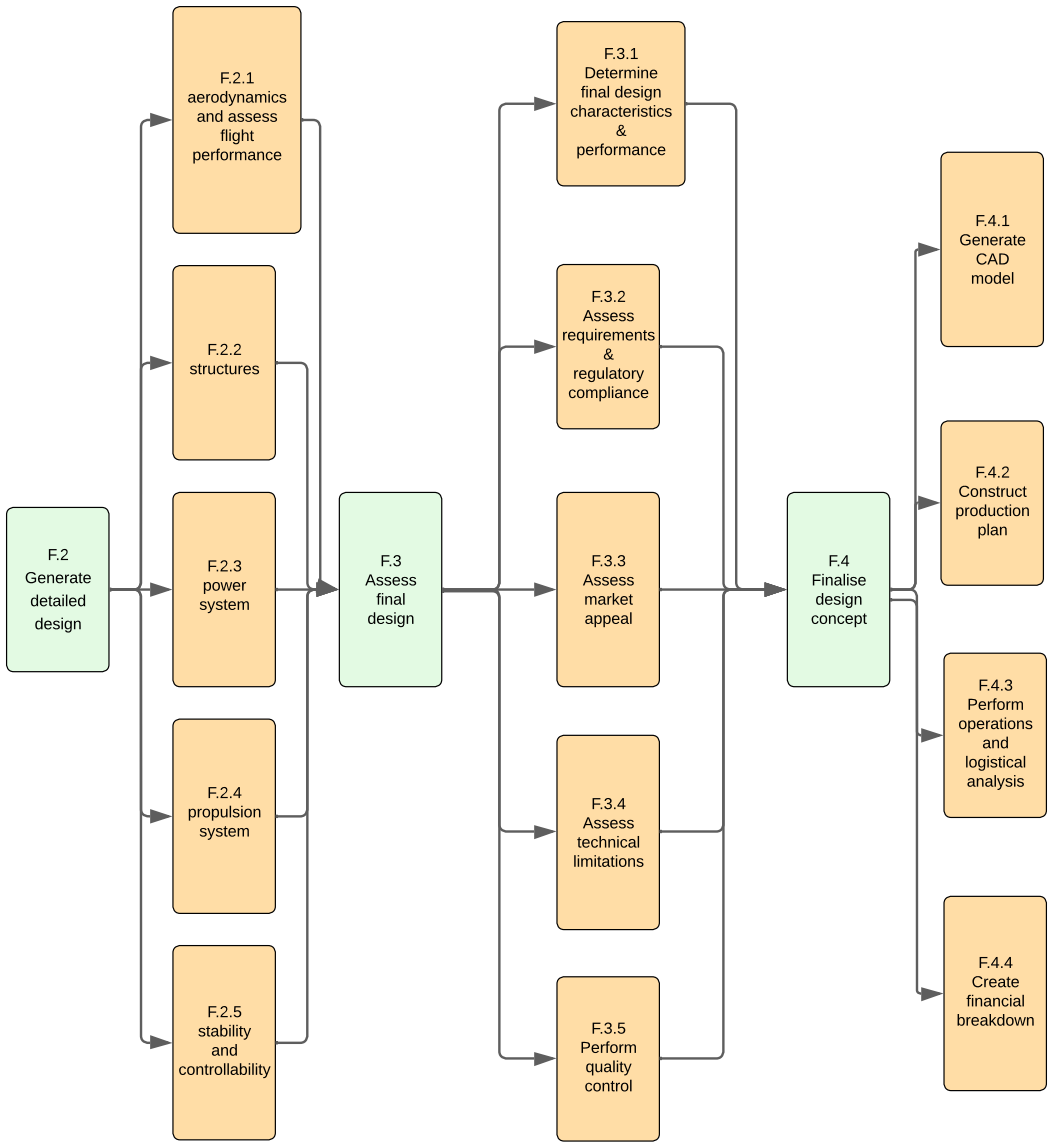

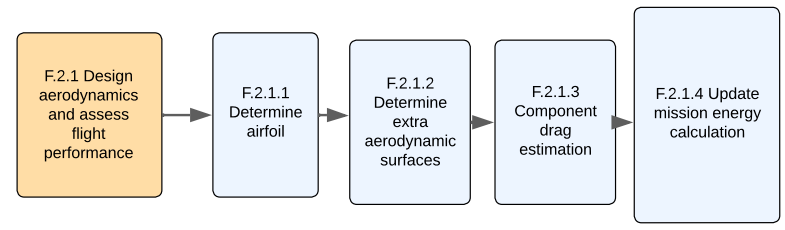

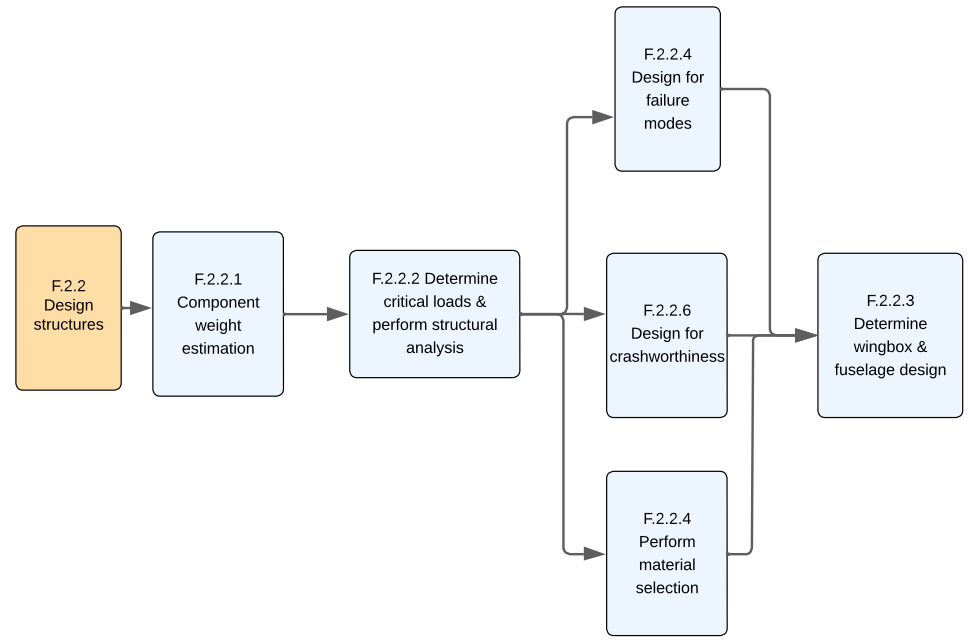

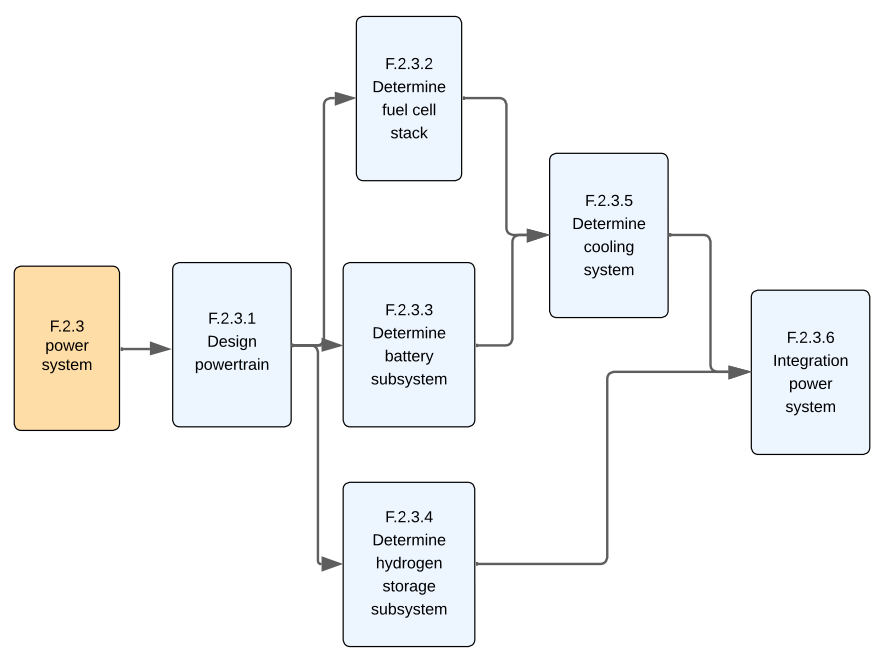

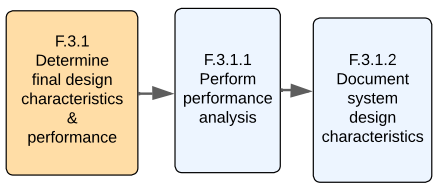

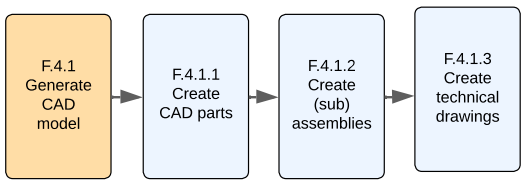

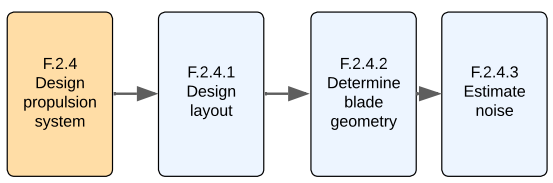

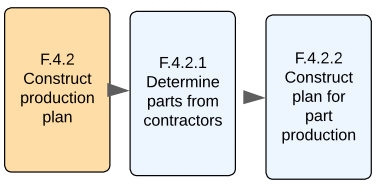

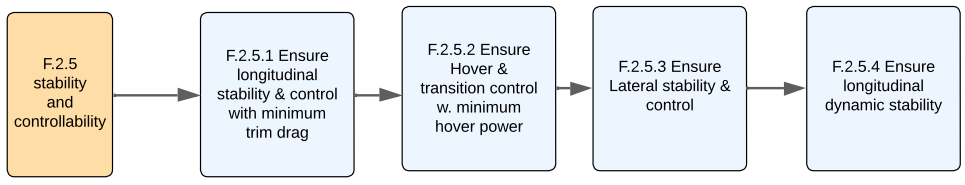

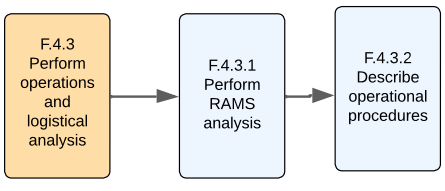

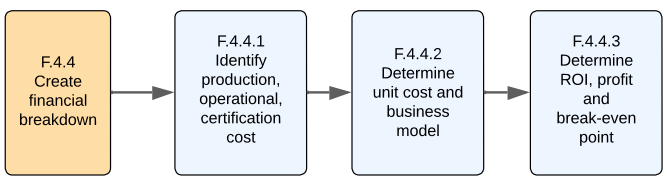

Work Breakdown Structure

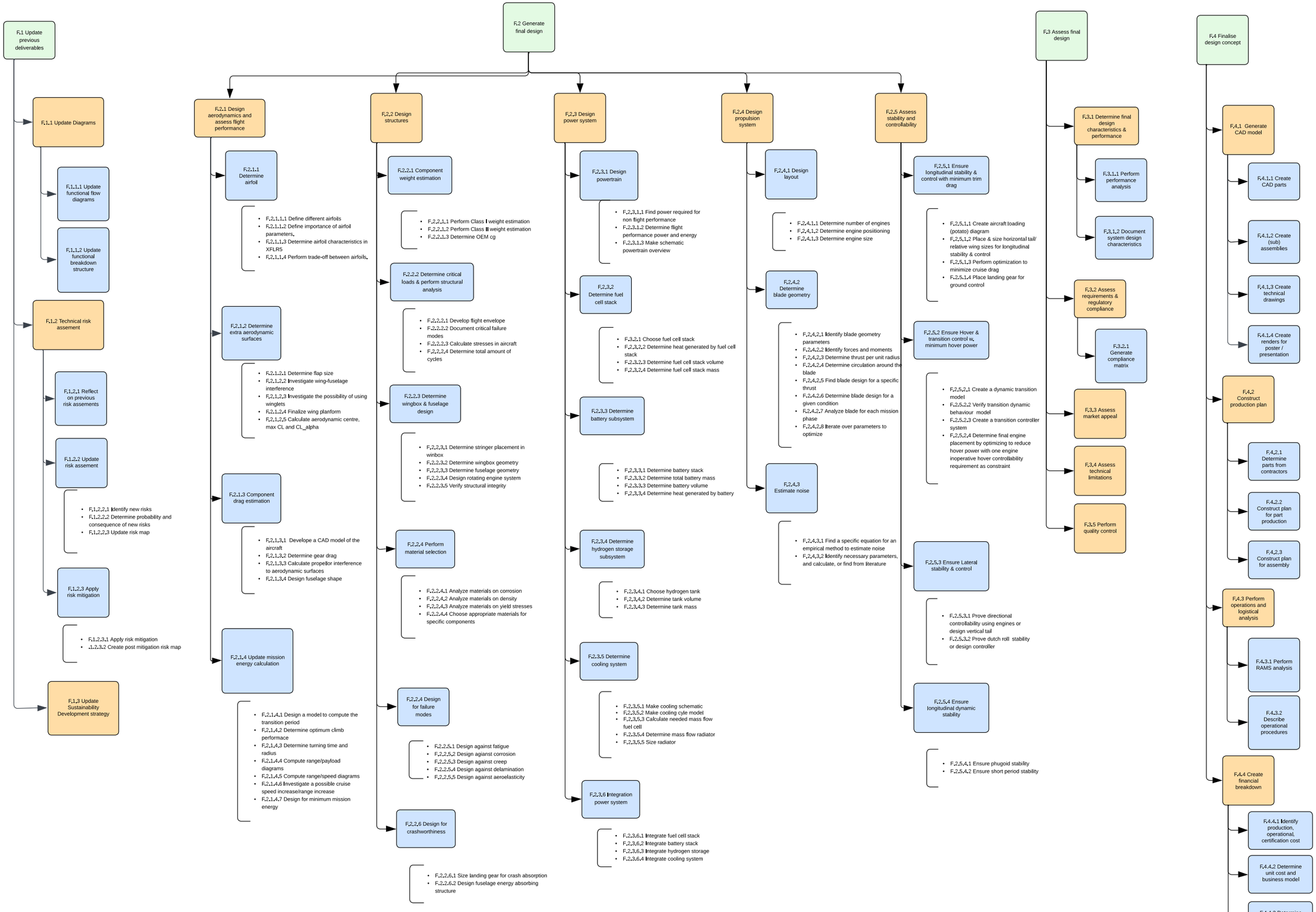

Gantt Chart

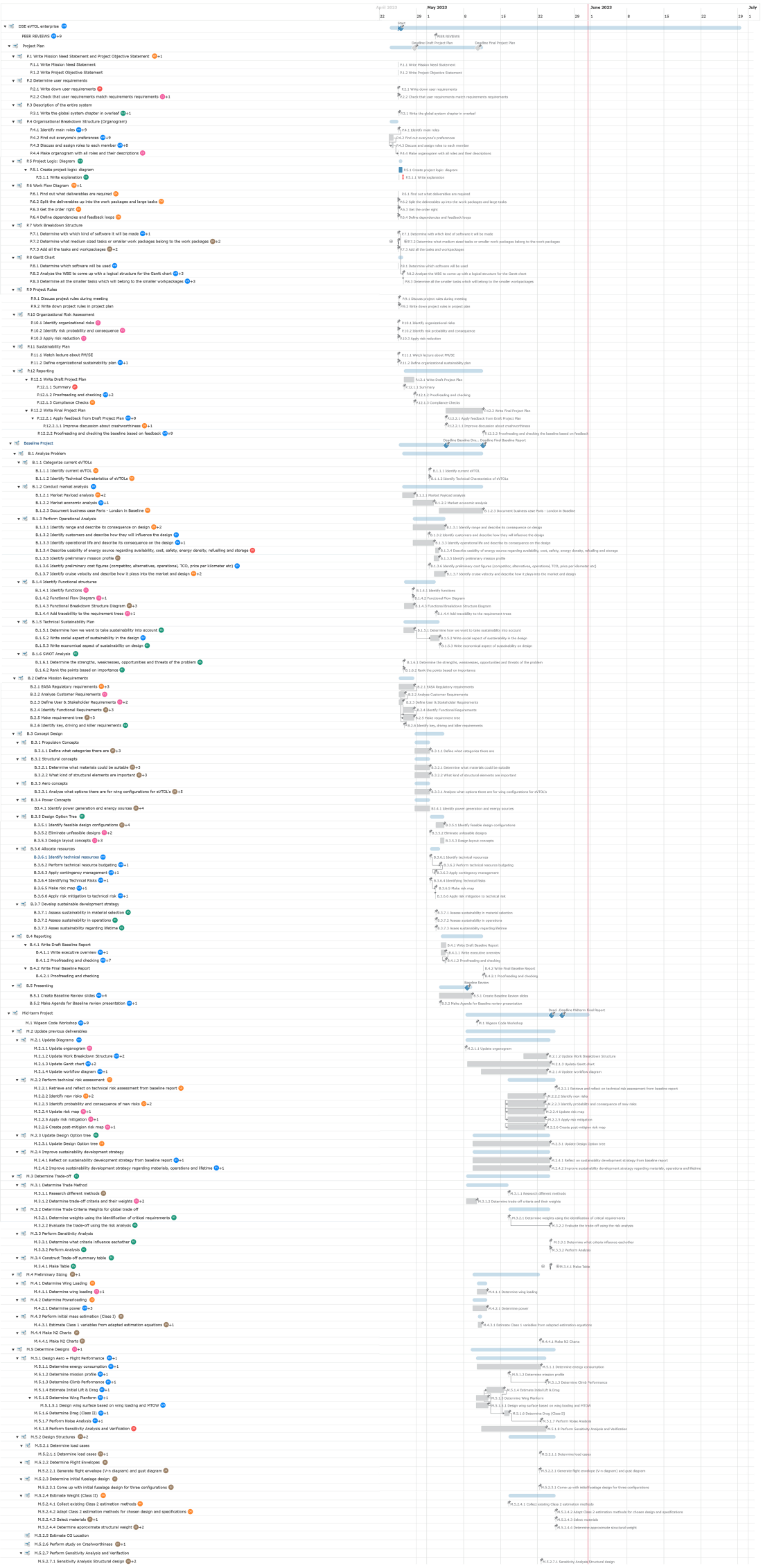
April 2023
May 2023
June 2023
July
DSE eVTOL enterprise
PEER REVIEWS +9
Project Plan
P.1 Write Mission Need Statement and Project Objective Statement +1
P.1.1 Write Mission Need Statement
P.1.2 Write Project Objective Statement
P.2 Determine user requirements
P.2.1 Write down user requirements
P.2.2 Check that user requirements match requirements requirements +1
P.3 Description of the entire system
P.3.1 Write the global system chapter in overleaf +1
P.4 Organisational Breakdown Structure (Organogram)
P.4.1 Identify main roles +9
P.4.2 Find out everyone's preferences +9
P.4.3 Discuss and assign roles to each member +8
P.4.4 Make organogram with all roles and their descriptions
P.5 Project Logic Diagram
P.5.1 Create project logic: diagram
P.5.1.1 Write explanation
P.6 Work Flow Diagram +1
P.6.1 Find out what deliverables are required
P.6.2 Split the deliverables up into the work packages and large tasks
P.6.3 Get the order right
P.6.4 Define dependencies and feedback loops
P.7 Work Breakdown Structure
P.7.1 Determine with which kind of software it will be made +1
P.7.2 Determine what medium sized tasks or smaller work packages belong to the work packages +2
P.7.3 Add all the tasks and workpackages +2
P.8 Gantt Chart
P.8.1 Determine which software will be used
P.8.2 Analyze the WBS to come up with a logical structure for the Gantt chart +3
P.8.3 Determine all the smaller tasks which will belong to the smaller workpackages +3
P.9 Project Rules
P.9.1 Discuss project rules during meeting
P.9.2 Write down project rules in project plan
P.10 Organizational Risk Assessment
P.10.1 Identify organizational risks
P.10.2 Identify risk probability and consequence
P.10.3 Apply risk reduction
P.11 Sustainability Plan
P.11.1 Watch lecture about PM/SE
P.11.2 Define organizational sustainability plan +1
P.12 Reporting
P.12.1 Write Draft Project Plan
P.12.1.1 Summary
P.12.1.2 Proofreading and checking +2
P.12.1.3 Compliance Checks
P.12.2 Write Final Project Plan
P.12.2.1 Apply feedback from Draft Project Plan +9
P.12.2.1.1 Improve discussion about crashworthiness +1
P.12.2.2 Proofreading and checking the baseline based on feedback +9
Baseline Project
B.1 Analyze Problem
B.1.1 Categorize current eVTOLs
B.1.1.1 Identify current eVTOL
B.1.1.2 Identify Technical Characteristics of eVTOLs
B.1.2 Conduct market analysis +2
B.1.2.1 Market Payload analysis +2
B.1.2.2 Market economic analysis +1
B.1.2.3 Document business case Paris - London in Baseline
B.1.3 Perform Operational Analysis
B.1.3.1 Identify range and describe its consequence on design +2
B.1.3.2 Identify customers and describe how they will influence the design
B.1.3.3 Identify operational life and describe its consequence on the design +1
B.1.3.4 Describe usability of energy source regarding availability, cost, safety, energy density, refuelling and storage
B.1.3.5 Identify preliminary mission profile
B.1.3.6 Identify preliminary cost figures (competitor, alternatives, operational, TCO, price per kilometer etc)
B.1.3.7 Identify cruise velocity and describe how it plays into the market and design +2
B.1.4 Identify Functional structures
B.1.4.1 Identify functions
B.1.4.2 Functional Flow Diagram +1
B.1.4.3 Functional Breakdown Structure Diagram +3
B.1.4.4 Add traceability to the requirement trees +1
B.1.5 Technical Sustainability Plan
B.1.5.1 Determine how we want to take sustainability into account
B.1.5.2 Write social aspect of sustainability in the design
B.1.5.3 Write economical aspect of sustainability on design
B.1.6 SWOT Analysis
B.1.6.1 Determine the strengths, weaknesses, opportunities and threats of the problem
B.1.6.2 Rank the points based on importance
B.2 Define Mission Requirements
B.2.1 EASA Regulatory requirements +3
B.2.2 Analyse Customer Requirements
B.2.3 Define User & Stakeholder Requirements +2
B.2.4 Identify Functional Requirements +3
B.2.5 Make requirement tree +3
B.2.6 Identify key, driving and killer requirements
B.3 Concept Design
B.3.1 Propulsion Concepts
B.3.1.1 Define what categories there are +3
B.3.2 Structural concepts
B.3.2.1 Determine what materials could be suitable +3
B.3.2.2 What kind of structural elements are important +3
B.3.3 Aero concepts
B.3.3.1 Analyze what options there are for wing configurations for eVTOL's +5
B.3.4 Power Concepts
B3.4.1 Identify power generation and energy sources +4
B.3.5 Design Option Tree
B.3.5.1 Identify feasible design configurations +4
B.3.5.2 Eliminate unfeasible designs +2
B.3.5.3 Design layout concepts +3
B.3.6 Allocate resources
B.3.6.1 Identify technical resources
B.3.6.2 Perform technical resource budgeting +1
B.3.6.3 Apply contingency management +1
B.3.6.4 Identifying Technical Risks +1
B.3.6.5 Make risk map +1
B.3.6.6 Apply risk mitigation to technical risk +1
B.3.7 Develop sustainable development strategy
B.3.7.1 Assess sustainability in material selection
B.3.7.2 Assess sustainability in operations
B.3.7.3 Asses sustainability regarding lifetime
B.4 Reporting
B.4.1 Write Draft Baseline Report
B.4.1.1 Write executive overview +1
B.4.1.2 Proofreading and checking +7
B.4.2 Write Final Baseline Report
B.4.2.1 Proofreading and checking
B.5 Presenting
B.5.1 Create Baseline Review slides +4
B.5.2 Make Agenda for Baseline review presentation +1
Mid-term Project
M.1 Wigeon Code Workshop +9
M.2 Update previous deliverables
M.2.1 Update Diagrams
M.2.1.1 Update organogram
M.2.1.2 Update Work Breakdown Structure +2
M.2.1.3 Update Gantt chart +2
M.2.1.4 Update workflow diagram +1
M.2.2 Perform technical risk assessment
M.2.2.1 Retrieve and reflect on technical risk assessment from baseline report
M.2.2.2 Identify new risks +2
M.2.2.3 Identify probability and consequence of new risks +2
M.2.2.4 Update risk map +1
M.2.2.5 Apply risk mitigation +1
M.2.2.6 Create post-mitigion risk map +1
M.2.3 Update Design Option tree
M.2.3.1 Update Design Option tree
M.2.4 Improve sustainability development strategy
M.2.4.1 Reflect on sustainability development strategy from baseline report +1
M.2.4.2 Improve sustainability development strategy regarding materials, operations and lifetime +1
M.3 Determine Trade-off
M.3.1 Determine Trade Method
M.3.1.1 Research different methods
M.3.1.2 Determine trade-off criteria and their weights +2
M.3.2 Determine Trade Criteria Weights for global trade off
M.3.2.1 Determine weights using the identification of critical requirements
M.3.2.2 Evaluate the trade-off using the risk analysis
M.3.3 Perform Sensitivity Analysis
M.3.3.1 Determine what criteria influence eachother
M.3.3.2 Perform Analysis
M.3.4 Construct Trade-off summary table
M.3.4.1 Make Table
M.4 Preliminary Sizing +1
M.4.1 Determine Wing Loading
M.4.1.1 Determine wing loading +1
M.4.2 Determine Powerloading
M.4.2.1 Determine power +3
M.4.3 Perform initial mass estimation (Class I)
M.4.3.1 Estimate Class 1 variables from adapted estimation equations +1
M.4.4 Make N2 Charts
M.4.4.1 Make N2 Charts
M.5 Determine Designs +1
M.5.1 Design Aero + Flight Performance +1
M.5.1.1 Determine energy consumption +1
M.5.1.2 Determine mission profile +1
M.5.1.3 Determine Climb Performance +1
M.5.1.4 Estimate Initial Lift & Drag +1
M.5.1.5 Determine Wing Planform +1
M.5.1.5.1 Design wing surface based on wing loading and MTOW
M.5.1.6 Determine Drag (Class II) +1
M.5.1.7 Perform Noise Analysis +1
M.5.1.8 Perform Sensitivity Analysis and Verification
M.5.2 Design Structures +2
M.5.2.1 Determine load cases
M.5.2.1.1 Determine load cases +1
M.5.2.2 Determine Flight Envelopes
M.5.2.2.1 Generate flight envelope (V-n diagram) and gust diagram
M.5.2.3 Determine initial fuselage design
M.5.2.3.1 Come up with initial fuselage design for three configurations
M.5.2.4 Estimate Weight (Class II)
M.5.2.4.1 Collect existing Class 2 estimation methods
M.5.2.4.2 Adapt Class 2 estimation methods for chosen design and specifications
M.5.2.4.3 Select materials +1
M.5.2.4.4 Determine approximate structural weight +2
M.5.2.5 Estimate CG Location
M.5.2.6 Perform study on Crashworthiness +1
M.5.2.7 Perform Sensitivity Analysis and Verifaction
M.5.2.7.1 Sensitivity Analysis Structural design +2
M.5.3 Design Power & Propulsion +1
M.5.3.1 Determine required energy and maximum power
M.5.3.2 Determine required volume +2
M.5.3.3 Determine resulting mass from power subsystem
M.5.3.4 Do Fuel Cell Trade-off
M.5.3.5 Do battery trade-off
M.5.3.6 Do hydrogen storage trade-off +1
M.5.3.7 Determine Noise
M.5.3.8 Final Trade-off +1
M.5.3.9 Sensitivity Analysis +2
M.5.3.10 Verification and Validation plan +2
M.5.4 Design Stability & Control +1
M.5.4.1 Determine general fuselage shape options
M.5.4.2 Determine Controllability in Hover +1
M.5.4.3 Determine Stability in Hover +1
M.5.4.4 Determine Controllability in Cruise +1
M.5.4.5 Determine Stability in Cruise +1
M.5.4.6 Perform Sensitivity Analysis and Verification
M.6 General Deliverables
M.6.1 Operations and logistics concept description +1
M.6.1.1 Create operations and logistics deliverables +1
M.6.1.2 create RAMS report +1
M.6.2 Project design & development logic
M.6.2.1 Project Design and Development logic +1
M.6.3 Make general verification and validation plan
M.6.3.1 Determine what types of tests we want for code
M.6.3.2 Determine how to verify future concepts using computer programs (like CAD, FEM, CFD, etc.)
M.6.4 Make Financial Analysis
M.6.4.1 Make return on investment analysis +1
M.6.4.2 Market price and volume of the evtol +1
M.6.4.3 Development cost of the eVTOL +1
M.7 Presenting
M.7.1 Create Midterm review slides
M.8 Reporting
M.8.1 Write Draft Midterm Report
M.8.1.1 Write an introduction
M.8.1.2 Write a conclusion
M.8.1.3 Proof reading and checking +9
M.8.2 Write Final Midterm Report
Final report
F.1 Update previous deliverables
F.1.1 Update Diagrams
F.1.1.1 Update Functional Flow Diagram
F.1.1.2 Update Functional Breakdown Structure
F.1.2 Technical Risk Assessment
F.1.2.1 Reflect on Technical Risk Assessment from Midterm Report
F.1.2.2 Update risk assement
F.1.2.2.1 Identify new risks
F.1.2.2.2 Identify probability and consequence of new risks
F.1.2.2.3 Update risk map
F.1.2.3 Apply risk mitigation
F.1.2.3.1 Apply risk mitigation
F.1.2.3.2 Create post mitigation risk map
F.1.3 Update Sustainability Development Strategy
F.1.3.1 Improve and update sustainability development strategy
F.2 Final Design Generation
F.2.1 Design aerodynamics and assess flight performance +1
F.2.1.1 Determine airfoil of the aircraft
F.2.1.1.1 Do research on different kinds of airfoils +1
F.2.1.1.2 Define important airfoil characteristics to consider during trade-off +1
F.2.1.1.3 Determine airfoil characteristics in XFLR5 for 3 selected airfoils +1
F.2.1.1.4 Perform trade-off for the selected airfoils +1
F.2.1.2 Determine extra aerodynamic surfaces
F.2.1.2.1 Determine flap size, type and angle if deemed necessary +1
F.2.1.2.2 Investigate aerodynamic body-wing interactions +1
F.2.1.2.3 Investigate the possibility and advantages of using winglets +1
F.2.1.2.4 Finalize wing planform +1
F.2.1.2.5 Determine final parameter values for Cm_ac, CL_max and CL_alpha using XFLR5 +1
F.2.1.3 Component drag estimation
F.2.1.3.1 Develop or or obtain CAD model from structures department +1
F.2.1.3.2 Determine gear drag +1
F.2.1.3.3 Determine effect of propellor-wing interferences +1
F.2.1.3.4 Determine skin friction drag of fuselage and wing using CAD model +1
F.2.1.3.5 Perform CFD analysis for high-fidelity drag and lift estimations using CAD model +1
F.2.1.4 Update mission energy calculations
F.2.1.4.1 Write code to compute required transition energy +1
F.2.1.4.2 Determine optimum climb performance +1
F.2.1.4.3 Determine turning time and radius +1
F.2.1.4.4 Compute range/payload diagrams +1
F.2.1.4.5 Compute range/speed diagrams +1
F.2.1.4.6 Investigate optimizations for cruise speed and range +1
F.2.1.4.7 Design for minimum mission energy +1
F.2.2 Design structures
F.2.2.1 Perform component weight estimation
F.2.2.1.1 Perform class I weight estimation
F.2.2.1.2 Perform class II weight estimation
F.2.2.1.3 Determine OEM cg
F.2.2.2 Determine critical loads & perform structural analysis
F.2.2.2.1 Develop flight envelope
F.2.2.2.2 Document critical failure modes
F.2.2.2.3 Calculate stresses in aircraft
F.2.2.2.4 Determine total amount of cycles before fatigue
F.2.2.3 Determine wingbox & fuselage design
F.2.2.3.1 Determine stringer placement in wingbox
F.2.2.3.2 Determine wingbox geometry
F.2.2.3.3 Determine fuselage geometry
F.2.2.3.4 Design rotating engine system
F.2.2.3.5 Verify structural integrity
F.2.2.4 Perform material selection
F.2.2.4.1 Analyze materials on corrosion
F.2.2.4.2 Analyze materials on density
F.2.2.4.3 Analyze materials on yield stresses
F.2.2.4.4 Choose appropriate materials for specific components
F.2.2.5 Design for failure modes
F.2.2.5.1 Design against fatigue
F.2.2.5.2 Design against corrosion
F.2.2.5.3 Design against creep
F.2.2.5.4 Design against aeroelasticity
F.2.2.6 Design for crashworthiness
F.2.2.6.1 Size landing gear for crash absorption
F.2.2.6.2 Design fuselage energy absorbing structure
F.2.3 Design power system
F.2.3.1 Design powertrain
F.2.3.1.1 Find power required for non flight performance
F.2.3.1.2 Determine flight performance power and energy
F.2.3.1.3 Make schematic powertrain overview
F.2.3.2 Determine fuel cell stack
F.2.3.2.1 Choose fuel cell stack
F.2.3.2.2 Determine heat generated by fuel cell stack
F.2.3.2.3 Determine fuel cell stack volume
F.2.3.2.4 Determine fuel cell stack mass
F.2.3.3 Determine battery subsystem
F.2.3.3.1 Determine battery stack
F.2.3.3.2 Determine total battery mass
F.2.3.3.3 Determine battery volume
F.2.3.3.4 Determine heat generated by battery
F.2.3.4 Determine hydrogen storage subsystem
F.2.3.4.1 Choose hydrogen tank
F.2.3.4.2 Determine tank volume
F.2.3.4.3 Determine tank mass
F.2.3.5 Determine cooling system
F.2.3.5.1 Make cooling schematic
F.2.3.5.2 Make cooling cycle model +1
F.2.3.5.3 Calculate needed mass flow fuel cell
F.2.3.5.4 Determine mass flow radiator
F.2.3.5.5 Size radiator +1
F.2.3.5.6 Optimize cooling system +1
F.2.3.6 Integration power system
F.2.3.6.1 Integrate fuel cell stack
F.2.3.6.2 Integrate battery stack
F.2.3.6.3 Integrate hydrogen storage
F.2.3.6.4 Integrate cooling system
F.2.4 Design propulsion system
F.2.4.1 Design layout
F.2.4.1.1 Determine number of engines
F.2.4.1.2 Determine engine positioning
F.2.4.1.3 Determine engine size
F.2.4.2 Determine blade geometry
F.2.4.2.1 Identify blade geometry parameters
F.2.4.2.2 Identify forces and moments
F.2.4.2.3 Determine thrust per unit radius
F.2.4.2.4 Determine circulation around the blade
F.2.4.2.5 Find blade design for a specific thrust
F.2.4.2.6 Determine blade design for a given condition
F.2.4.2.7 Analyze blade for each mission phase
F.2.4.2.8 Iterate over parameters to optimize
F.2.4.3 Estimate noise
F.2.4.3.1 Find a specific equation for an empirical method to estimate noise
F.2.4.3.2 Identify necessary parameters, and calculate, or find from literature
F.2.5 Assess stability and controllability
F.2.5.1 Ensure longitudinal stability & control with minimum trim drag
F.2.5.1.1 Create aircraft loading (potato) diagram
F.2.5.1.2 Place & size horizontal tail/ relative wing sizes for longitudinal stability & control
F.2.5.1.3 Perform optimization to minimize cruise drag
F.2.5.1.4 Place landing gear for ground control
F.2.5.2 Ensure Hover & transition control w. minimum hover power
F.2.5.2.1 Create a dynamic transition model
F.2.5.2.2 Verify transition dynamic behaviour model
F.2.5.2.3 Create a transition controller system
F.2.5.2.4 Determine final engine placement by optimizing to reduce hover power with one engine inoperative hover controllability
F.2.5.3 Ensure Lateral stability & control
F.2.5.3.1 Prove directional controllability using engines or design vertical tail
F.2.5.3.2 Prove dutch roll stability or design controller
F.2.5.4 Ensure longitudinal dynamic stability
F.2.5.4.1 Ensure phugoid stability
F.2.5.4.2 Ensure short period stability
F.2.5.5 Make verification and validation plan
F.2.5.6 Perform sensitivity analysis
F.3 Final Design Assessment
F.3.1 Determine final design characteristics and performance
F.3.1.1 Perform performance analysis
F.3.1.2 Document system design characteristics
F.3.2 Assess requirements & regulatory compliance
F.3.2.1 Generate compliance matrix
F.3.2.2 Assess requirements compliance
F.3.2.3 Assess regulatory compliance
F.3.3 Assess market appeal
F.3.3.1 Look how appealing the aircraft would be in current and future market
F.3.4 Assess technical limitations
F.3.4.1 List and describe the technical limitations regarding range, hover endurance, emergencies etc
F.3.5 Perform quality control
F.3.5.1 Check quality of each (sub)system of the aircraft
F.4 Finalise design concept
F.4.5 Project development and logic diagram +1
F.4.1 Generate CAD model
F.4.1.1 Create CAD parts in 3DEXPERIENCE
F.4.1.2 Create subassemblies and final assembly
F.4.1.3 Create technical drawings for production plan
F.4.1.4 Generate renders for poster/presentations
F.4.2 Construct production plan
F.4.2.1 Determine parts from constructors
F.4.2.2 Construct plan for part production
F.4.2.3 Construct plan for assembly
F.4.3 Perform operations and logistical analysis
F.4.3.1 Perform RAMS analysis +1
F.4.3.2 Describe refuelling procedure
F.4.3.3 Describe payloading on/offloading procedure
F.4.3.4 Describe landing and take off procedures
F.4.3.5 Describe emergency procedures
F.4.3.6 Describe maintenance procedures
F.4.4 Create financial breakdown
F.4.4.1 Identify production, operational, certification, R&D and unit cost +1
F.4.4.2 Generate business model (price per flight/km, airlines/independent flight, operational regions, fleet size etc) +1
F.4.4.3 Determine Return On Investment (ROI), profit and break-even point +1
F.5 Reporting
F.5.1 Write Draft Final Report +9
F.5.1.1 Write an introduction
F.5.1.2 Write a conclusion
F.5.1.3 Proofreading and checking +9
F.5.2 Write Final Report
F.5.2.1 Apply feedback from Draft Final Report +9
F.5.2.2 Proofreading and checking +9
F.5.3 Write summary Red Booklet
F.5.4 Write Jury Summary
F.6 Presenting
F.6.1 Create final review slides
F.6.2 Create poster
F.6.3 Create Symposium slides

- 1.Structure
  - 1.1 Materials
    - Metals Alloys
      - Steel
      - Aluminium
      - Titanium
    - Composites
      - Reinforcement
        - Short Fibres
        - Long Fibres
        - Continuous Fibres
      - Resin
        - Thermoplastic
          - Polyetheretherketone (PEEK)
          - Polyetherketoneketone (PEKK)
          - Polyphenylene sulfide (PPS)
        - Thermoset
          - Polyester
          - Vinyl Ester
          - Epoxy
    - Ceramics ✕
      - Glass
      - Porcelain
  - 1.2 Structural concept
    - Engine mounting
      - Blended in fuselage ×
      - Over wing
      - Below wing
      - On fuselage
      - Blended in wing
      - At nose ×
      - At tail
      - Any combination
    - Wing positioning
      - High wing
      - No wing ×
      - Low wing
      - Blended wing
- 2.Aerodynamics
  - 2.1 Wing configurations
    - No wings ×
      - Helicopter
      - Multicopter
      - Balloon/blimp ×
    - 1 wing
      - Flying V
      - Conventional configuration
      - 2 fuselage configuration
    - 2 wings
      - Biplane
      - Closed wing
      - Tandem wing
    - More than two wings ×
      - Quadwing ×
      - Triplane ×
  - 2.2 Winglets
    - Blended
    - Sharklets
    - Raked
    - No Winglets ×
  - 2.3 Longitudinal stability
    - Tail
      - Conventional Tail
      - T-tail
      - H-tail
      - Cruciform
    - No Tail
    - Canard ×
    - Canard AND tail ×
      - T-tail
      - Conventional Tail
      - H-tail
      - Cruciform
  - 2.4 Longitudinal controllability
    - Elevator
    - Elevons
    - Thrust vectoring
      - Gimbaled engines ×
      - Differential thrust
      - Rotated thrusters
    - Rudder + ailerons
    - Thrust vectoring + ailerons/elevons
  - 2.5 Lateral controllability
  - 2.6 Lateral stability
    - Thrust vectoring
    - Vertical tail ×
    - V-tail
- 3.Ground movement
  - 3.1 Ground surface movement
    - Wheels on rails ×
    - Tracks ×
    - Wheels
      - Non-retractable
      - Retractable
  - 3.2 Method of propelling forward
    - Self movement
      - Use propulsion system
      - Battery powered
    - Externally assisted movement
      - Transporter Tractor
      - Human powered movement ×
- 4.Crashworthiness & Emergency Response
  - 4.1 Protect passengers from power storage
    - CO2 injection into cabin to prevent fire ×
    - Fire wall
    - Expulsion of propulsion tanks ×
    - Self sealing tanks ×
  - 4.2 Protect Passengers & Payload
    - Passenger compartment removal and parachute ×
    - Emergency exits
    - Life vests
    - Crash cage
    - Internal airbags
    - Oxygen masks
    - Eject passengers via ejection seats ×
  - 4.3 Protect all of eVTOL
    - Parachute ×
    - Collapseble landing gear
    - External airbags
- 5.Cabin configuration
  - 5.1 Single pilot row
    - Four rows ×
      - 1 + 1 + 1 + 1 + 1 ×
      - 1 + 4 ×
      - 1 + 2 + 2
      - 1 + 3 + 1 ×
      - 1 + 2 + 1 + 1
      - 1 + 1 + 2 + 1
      - 1 + 1 + 1 + 2
  - 5.2 Without single pilot row ×
    - 5x1
    - 2 + 3
    - 2 + 2 + 1
    - 2 + 1 + 2
    - 3 + 1 + 1
    - 3 + 2
  - 5.3 Cockpit
    - Open cockpit ×
    - Closed cockpit
- 6.Power/Energy
  - 6.1 Hybrid ×
    - Chemical - mechanical
    - Chemical - radiation
    - Chemical - nuclear
    - Mechanical - radiation
    - Mechanical - nuclear
    - Radiation - nuclear
  - 6.2 Mechanical
    - Buoyancy ×
      - Helium
    - Wind energy ×
    - Human ×
  - 6.3 Nuclear
    - Fission ×
    - Fusion ×
  - 6.4 Radiation ×
    - Solar
  - 6.5 Chemical
    - Combustion ×
      - CO2 emitting fuel ×
        - Fossil fuel
          - Kerosene
          - Gasolene
          - SAF (biofuel)
      - Hydrogen
        - Hydrogen turbojet with eletric generator
        - Hydrogen ICE with eletric generator
        - Hydrogen powered steam engine with electric generator ×
    - Fuel cell
      - Hydrogen
        - Fuel cell type
          - Solid Oxide ×
          - PEM
          - Alkaline ×
          - Phosphoric Acid ×
        - Storage
          - Liquid Hydrogen ×
          - Pressurised Hydrogen
        - Refuelling
          - Refilling fixed tanks
          - Swapping tanks ×
      - Other ×
    - Batteries
      - Without recharging ×
        - Alkaline
        - Not rechargeable battery swap
      - With recharging
        - Recharging process
          - Recharging with fuel
          - Battery swap and on-ground recharging ×
          - On-ground recharging
        - Type
          - Supercapacitor ×
            - Double layer capacitor
            - Pseudocapacitor
          - Solid state ×
          - Lithium ion
            - LFP
            - LiPo
            - NMC
            - NCA
- 7.Propulsion
  - 7.1 Propulsion type
    - Air displacing thrust
      - Rotor engine
        - Efficiency Improvement Methods
          - None
          - Swirl Recovery Vane
          - Duct
        - Propeller thrust
          - Tractor
          - Pusher
        - Rotor number
          - Single rotor
          - Discrete multirotor
          - Distributed multirotor
        - Rotor type
          - Conventional fixed pitch propeller
          - Conventional variable pitch propeller
          - Torodioal
      - Flapping wings ×
      - Jet engine ×
        - Turbojet ×
        - Turbofan
    - Non air displacing thrust
      - Ion propulsion ×
      - Rocket ×
      - Solar sail ×
      - Santa's reindeers ×
  - 7.2 Propulsion rotation
    - Varying axis of rotation
      - Aligned with wing (Tilt wing)
      - Independent of wing (Tilt rotor)
      - Propellers move together
      - Propellers can move independantly
    - Constant axis
      - Propellers oriented in multiple axes ×
      - Single-axis propeller orientation with full aircraft rotation manoeuvre
      - Single-axis propeller orientation with mainly vertical thrust component
  - 7.3 Transition
    - Wing(s)
      - Rotate wing
        - Rotate full wing
        - Rotate part of wing
      - Fixed wing
    - Rotors
      - Rotate rotors
        - All rotors are aligned and rotate together
      - Fixed rotors
        - Vertical and Lateral set of Rotors

Legend

- ✕ Infeasible
- × Unwanted (low TRL, incompatible with mission profile)
- Top level
- Middle level
- Low level
- Sub level
- Sub sub level

3
Design Options

The design option tree has been updated and features the options that are still present and will be subjected to a trade-off in this report. The tree is shown above. The three configurations are J1, L1 and W1, as shown in Figure 3.1 inspired by existing successful designs. During designing, J1 was found not to be stable enough so a second iteration was determined called J2. J2 is the same configuration as J1 except that each rotor is powered by two engines that equally provide the power under nominal conditions. The added redundancy of J2 eliminates the critical one engine inoperative controllability problem of J1 as explained in Subsection 11.2.2. J1 is inspired by the Joby S4 and features 6 large tilt rotors, a main wing and a v-tail. L1 is inspired by the lilium 7-seater jet, it features distributed propulsion with 36 ducted fans and a tandem wing design. W1 is inspired by the Wigeon design, it has tilting tandem wings with 12 propellers.

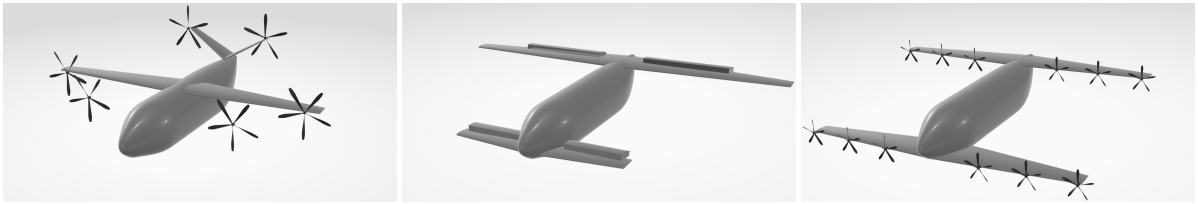

(a) *J1* **(b)** *L1* **(c)** *W1*

Figure 3.1: *Sketches of the different configurations*

4
Trade-Off Criteria

This chapter discusses the trade-off method and criteria used to perform the trade-off. The traditional method of scoring options against weighted criteria is chosen, as the team is the most familiar with this method and it has no disadvantages in this application compared to other trade-off methods, such as the Analytical Hierarchy Process or the graphical comparison method.

In this trade-off, the criteria have been designed such that the configurations are evaluated in terms of whether a chosen design configuration is likely to meet regulations and the design outcomes that are important to users. These outcomes are safety, social and environmental sustainability, and low cost. Each of these outcomes can be further divided into its driving factors or constituents. The cost is driven by production, fuel, and other operational costs (excluding fuel). The perceived cost by the operator and passengers is a reflection of the sum of these costs. Environmental sustainability is heavily dependent on the emissions due to fuel production (based on a life cycle analysis). Weight and the C_L/C_D ratio are not parameters important to the user but are perceived in terms of fuel cost and impact on the environment. Similarly, power is also not important to the user but higher hover power may require more batteries and larger cooling systems which would increase weight and make the aircraft more costly to operate and less environmentally friendly. Since both the fuel cost and impact on the environment depend on how efficient the aircraft is, they can both be measured in terms of the mission energy. The other two costs (production and operational costs excl. fuel) can be their own separate criteria. Although noise is a requirement, it is still desirable to have a lower noise below requirements as it positively affects the stakeholders. Meeting the requirement is a must. Lastly, the final design needs to be safe. This is driven by the likeliness of avoiding a crash, (control and stability) and the consequences, should a crash happen (crashworthiness). Meeting safety requirements is a must but exceeding them is still desirable from the perspective of the user. Finally, this yields the trade-off criteria: mission energy, stability & controllability, crashworthiness, noise, production costs, and operational costs excluding fuel. It is important to note that time to market and development effort is an important criteria as well [5].

However, since the same critical technology (Hydrogen) is used in all designs concepts, this criterion is not useful in distinguishing between different concepts.

Noise, stability & controllability and crashworthiness have requirements. Yet, exceeding the bare minimum is advantageous. Therefore, for these criteria, the following scale as shown in Table 4.1 has been defined.

Table 4.1: *Scoring utilized for noise, stability & controllability and crashworthines.*

0	1	2	3
Fails req.	Meets req. if defici -encies are eliminated	Meets req.	Exceeds req.

Table 4.2: *Scoring utilized for mission energy, production costs and operational costs excluding fuel.*

0	1	2	3
Unacceptable	Acceptable	Good	Excellent

Any design that scores a 0 in any of the criteria is automatically discarded as it cannot meet the requirements and is not considered in the trade-off. However, if a design performs well in all criteria except one and its deficiencies can be easily fixed with small changes to its design, a new design is made and evaluated instead. This makes sure that good ideas are not unnecessarily discarded due to easily fixable shortcomings. A scale out of three rather than a larger number has been defined to avoid arbitrariness in the assigned values.

The criteria of mission energy (driven by fuel cost and environmental sustainability), production costs and operational costs excluding fuel do not have requirements but are still important to the user. And for these, criteria of the same number scale can be defined as shown in Table 4.2.

Weights of Different Criteria

The weights of the criteria sum up to 100% for simplicity. Since the mission energy criterion is representative of two essential design objectives (higher environmental sustainability and fuel cost), the criterion has been given a large weight (30%). In addition, the design must meet safety requirements otherwise it is immediately discarded. However, there is still uncertainty since the designs have not been finalized. A design that barely meets safety requirements now may not meet them at a later design stage or require serious compromises. Since it is beneficial to exceed requirements and lower the risk of not meeting the requirements, safety has been given an importance of 40% and since it is equally important to avoid crashing and surviving a crash, the 40% importance of safety has been split equally between stability & controllability (with importance 20%) and crashworthiness (with importance 20%). Noise has been given an importance of 10% because of the current requirements. Since the UAMs land in the city, the noise requirements are already stringent and exceeding them much more will result in diminishing returns. Lastly, the production and operational costs excluding fuel have been given equals weights (of 10%) because the cost of producing one eVTOL is of the same order of magnitude as the operational costs of operating the eVTOL excluding fuel during its life time as seen in Table 13.3. One may argue that the weights are still somewhat arbitrary despite the above justifications. However, if after a sensitivity study that varies the weights of different criteria, it is observed that the same design is chosen regardless of what the weights of the criteria are, then it can be said that the uncertainty in the weights of the criteria has not affected the trade-off negatively. Indeed, this is the case as seen in Chapter 14. The criteria, their weights, and the trade-off organization (information regarding which criteria are evaluated where in the report) are summarized in Table 4.3.

Table 4.3: *Trade-off summary table*

Criteria	Weight (out of 100)	Trade-off Organization
Mission energy	30	Section 7.4
Stability & Controllability	20	Section 11.3
Crashworthiness	20	Section 8.9
Noise	10	Section 10.5
Production costs	10	Section 13.5
Operational costs excl. fuel	10	Section 13.5

5
Technical Risk Management

As the project has stepped into the next stage, new risks are introduced which have to be managed. These risks are identified by the design team of the different departments by using engineering judgement. This will again be done by identifying them, making a risk map, and performing a mitigation analysis.

Below is a list of all the previous risks, which have already been identified and mitigated in the baseline review so they will not be included in this report. They will be shown in the risk map in Figure 5.1.

- TR-ST-01 - Underestimating the operational empty weight (OEW)
- TR-PP-01 - Underestimating the energy required during the transition phase.
- TR-PP-02 - Propulsive failure
- TR-PP-03 - Hydrogen fuel storage safety
- TR-PP-04 - Loss of hover abilities during flight because of transition failure
- TR-PP-05 - Overheating of the fuel cell
- TR-PP-06 - Loss of power
- TR-PP-07 - Not meeting hydrogen storage requirement
- TR-PP-08 - Running out of hydrogen and energy during flight
- TR-CS-01 - Center of gravity shift during flight
- TR-CS-02 - Aircraft too difficult to control
- TR-OP-01 - Damages during ground operations
- TR-OP-02 - Failing to meet noise requirements
- TR-OP-03 - Bird strike
- TR-OP-04 - Hard landing
- TR-OP-05 - Aircraft is too expensive
- TR-DEV-01 - Numerical/model errors
- TR-DEV-02 - Assumption is not accurate and/or correct
- TR-DEV-03 - Underestimating power requirements during the transition phase

5.1. Additional Risks

Additional new risks identified by the team throughout the current design stage also have to be considered and effectively managed. These risks will be given a score of 1-5 that ranks their likelihood and consequence. From this, the risk is calculated which is likelihood multiplied by consequence. These additional identified risks are divided into their corresponding departments such as PP for power and propulsion, CS for control and stability, ST for structures and AD for aerodynamics. Furthermore, risks associated with operations (OP) of the eVTOL as well as during the development (DV) stage of the eVTOL are also divided and can be seen below:

TR-PP-09: Explosion of Hydrogen due to battery failure. This can happen if a failure in the battery results in a fire which can cause an explosion of hydrogen if they come in contact since hydrogen is a highly explosive element. As a consequence, a potential explosion can be catastrophic as it would cause damage in the structure of the eVTOl causing it to possibly crash and possibly cause fatalities both in the eVTOL and on the ground.
TR-PP-10: Hydrogen boil-off loss underestimated. If cryogenic hydrogen is used, some boil-off is expected. Although a certain amount of hydrogen boil-off is accounted for, if this is underestimated, there would be less fuel onboard, meaning that there would not be not enough fuel for reserve or even to finish the flight.
TR-PP-11: Leakage of ions from fuel cell through coolant liquid. The leakage of ions from the fuel cell through the coolant liquid can result in a slow build-up of electric potential within the aircraft. This build-up can become significant for long operations and cause electrical circuits to short-circuit.
TR-PP-12: Hydrogen fuel loading error. Under-fueling of hydrogen would result in the eVTOL having an

insufficient amount of hydrogen to complete the planned journey. This would result in an emergency landing at a vertiport closer to the take-off location and thus in an unsuccessful mission and unhappy passengers.
TR-PP-13: Corrosion of the fuel cell. If the fuel cell would experience corrosion, then the parts and components of the cell would experience degradation and the overall efficiency would drop. Therefore, the performance of the fuel cell would drop possibly making it insufficient and decreasing its lifespan. Maintenance and replacement costs would also increase. Furthermore, the safety of the fuel cell would be affected.
TR-PP-14: Seal or joint failure of the hydrogen tank. If there is a seal or joint failure in the hydrogen tank, then hydrogen will leak out. If this happens, there might not be enough hydrogen left in the tank to perform the flight between the indicated points. Another possible consequence is a possible explosion of hydrogen if it comes in contact with an ignition source.
TR-PP-15: Failure of the electrolyte in the fuel cell. Possible failure of the electrolyte would result in problems with ion conductivity. This would lead to an inefficiency of the fuel cell. This failure of the fuel cell would result in a failed conversion of hydrogen to electricity. Therefore, the power generated by the fuel cell would be much less.
TR-PP-16: Lithium-ion battery can catch fire. If the battery catches fire, this can lead to the eVTOL catching fire too, which presents a deadly risk. Depending on where the battery is, and how large the fire is, there may not even be a way to land and evacuate everybody safely.
TR-PP-17: Propeller blade breaking. The propeller blade may break at a point either due to accumulated stress, a ground strike, or an external object hitting the blade. The probability of this is quite low but if it happens, it can affect the stability and controllability of the eVTOL, but the broken blade could also hit a part of the eVTOL, causing more damage.
TR-PP-18: Engines using more power than estimated. Empirical methods were used to estimate the power required by the engines. These could prove to be incorrect, and although unlikely, could cause a redesign to take place where the sizing of the eVTOL must be reconsidered. It could even be that during the flight, the power source might not be able to deliver the maximum power required.

Table 5.1: *Scoring for the power and propulsion risks*

Risk (TR)	**PP-01**	**PP-02**	**PP-03**	**PP-04**	**PP-05**	**PP-06**	**PP-07**	**PP-08**	**PP-09**	**PP-10**
Likelihood	1	1	1	1	2	1	2	1	2	2
Consequence	3	4	4	3	3	4	3	3	5	3
Risk (TR)	**PP-11**	**PP-12**	**PP-13**	**PP-14**	**PP-15**	**PP-16**	**PP-17**	**PP-18**		
Likelihood	2	3	1	1	1	2	1	3		
Consequence	3	3	3	4	4	4	4	3		

TR-CS-03: Operational cg range outside longitudinal stability & control and one engine inoperative hover limits
If this were to happen during one of the mission phases, the cg shifting could be catastrophic due to the aircraft not being stable and controllable. The eVTOL could suddenly crash fatally. Even a slight cg shift could induce moments that could be hard for the pilot to control.
TR-CS-04: Aircraft maximum available power does not meet one engine inoperative hover power needs
If one engine becomes inoperative, the other engines need to be able to compensate. This might especially be problematic for designs with fewer number of rotors.

Table 5.2: *Scoring for the control and stability risks*

Risk (TR)	**CS-01**	**CS-02**	**CS-03**	**CS-04**
Likelihood	3	2	3	2
Consequence	2	2	5	5

TR-ST-02: Underestimating the buckling loads
When performing calculations based on structural loads, the buckling load plays a large factor in the dimensions. If these loads are underestimated, the dimensions will be thinner than required, which would lead to a buckling failure mid-flight.
TR-ST-03: Choosing an inadequate material
Since each material has its own strengths, these should be evaluated correctly so that the optimal material is

chosen. If not, this could lead to having to overdesign the dimensions to meet the load requirements, which introduces extra mass.

TR-ST-04: Over-designing the aircraft such that it becomes too heavy

If certain loads are overestimated or, for example, the propeller weight pulling the wing down is not factored in (reducing bending loads), the wing stiffness could be overdesigned which introduces extra mass, which could decrease range.

TR-ST-05: Structural failure of wing-box

The structural failure of the wing box means there could be plastic failure in the wingbox, or even the wings snapping off in extreme cases, which could result in the killing of everybody onboard since no propellers will be attached to the eVTOL anymore to potentially slow the fall.

TR-ST-06: Structural failure of the fuselage

Failure modes like structural fatigue could rip the fuselage, either in a small section or entirely in two. If the rip is small, the eVTOL could perform an emergency landing, but would not be good for PR. If the eVTOL entirely fails, everybody could die.

TR-ST-07: Corrosion damage of important parts

Corrosion of important parts will damage the structural integrity of those parts and decrease their load bearing capabilities. This would result in a weaker part more prone to faster failure and decreased lifespan.

TR-ST-08: Delamination of composite parts

If composites would delaminate, then the mechanical properties of the composites would decrease. This would result in reduced structural integrity of the structure made out of composites. The composites will not be able to carry the initially intended loads and will therefore fail.

TR-ST-09: Landing gear failure

Failing of landing gear would result in a hard landing. With hydrogen on board, landing without gears might be dangerous as the hydrogen tank's structure might be damaged, and could explode.

TR-ST-10: Underestimated structural deformations due to crash events

If the deformations would be underestimated, then the eVTOL will experience higher damage than the calculated, thus this would have a negative effect on safety and weight due to the required reinforcements.

Table 5.3: *Scoring for the structural risks*

Risk (TR)	ST-01	ST-02	ST-03	ST-04	ST-05	ST-06	ST-07	ST-08	ST-09	ST-10
Likelihood	2	2	1	2	1	1	1	1	3	2
Consequence	3	5	3	5	5	4	4	3	2	4

TR-AD-01: Underestimating drag

Underestimating drag would lead to inaccurate calculations of the mission power requirements and characteristics of the eVTOL. The main implication of this would be a decrease in maximum speed as the drag of the eVTOL would be higher than estimated. Furthermore, a decrease in range will also be a consequence.

TR-AD-02: Overestimating Lift

If the lift produced by the wings and rotors is overestimated, this could cause a failing hovering process, which, if not controlled, could be a fatal incident. However, the aircraft should be able to slowly descend if this were the case.

TR-AD-03: Using an inaccurate CFD method

Using an inaccurate CFD method can lead to inaccurate predictions of the airflow around the eVTOL. This in turn would result in inaccurate estimations of the lift and drag of the eVTOL resulting in the consequences mentioned in TR-AD-01 and TR-AD-02. Furthermore, if the flow field around the eVTOL is not estimated correctly, critical phenomena might be missed resulting in underdesigning the eVTOL. This could have implications for the aircraft's stability and control.

Table 5.4: *Scoring for the aerodynamic risks*

Risk (TR)	AD-01	AD-02	AD-03
Likelihood	3	1	2
Consequence	3	4	2

TR-OP-06: Hydrogen not being available at each vertiport

If the eVTOL unknowingly lands at a vertiport location where no hydrogen is available for refueling, it could take a long time, and be expensive, for hydrogen to be brought to the vertiport location. This means the eVTOL could be inoperational for a long time.

TR-OP-07: Operating cost too high

The operating cost being higher than expected means a sudden increase in the asking price would take place. This could affect the number of customers that want to fly on the eVTOL.

TR-OP-08: No available pilot

If pilots were unavailable, then the company would lose customers as the customers' demands would not be met.

Table 5.5: *Scoring for the operational risks*

Risk (TR)	OP-01	OP-02	OP-03	OP-04	OP-05	OP-06	OP-07	OP-08
Likelihood	3	1	1	4	2	3	2	2
Consequence	2	2	3	1	3	5	4	4

TR-DV-04: Inadequate market position establishment

Not being able to receive a certain market share, establishing oneself in the wrong region, and marketing the eVTOL in an incorrect way, can all lead to a decline in customers. This could effectively bankrupt the company.

TR-DV-05: Underestimating the development cost

This also decreases the profits and possibly the time spent on development. If less profit is made, this could risk the future of the company and also means that less equity is put back into the further development of any future eVTOLs the company may produce.

TR-DV-06: Failure of certification

Failure in being certified quickly, and in the first try would result in a longer certification period and therefore higher certification costs. Furthermore, this would result in a delay in entering the market and a decrease in profits. In addition, the reputation of the company may be damaged due to non-compliance with the regulations, resulting in customer loss and a further decrease in profits.

Table 5.6: *Scoring for the developmental risks*

Risk (TR)	DV-01	DV-02	DV-03	DV-04	DV-05	DV-06
Likelihood	2	3	1	2	3	2
Consequence	3	2	3	4	2	3

Following the assignment of likelihood and consequence values for the newly identified additional risks, the risk map from the baseline report can be updated. The new version of the risk map, prior to risk mitigation, can be found in Figure 5.1.

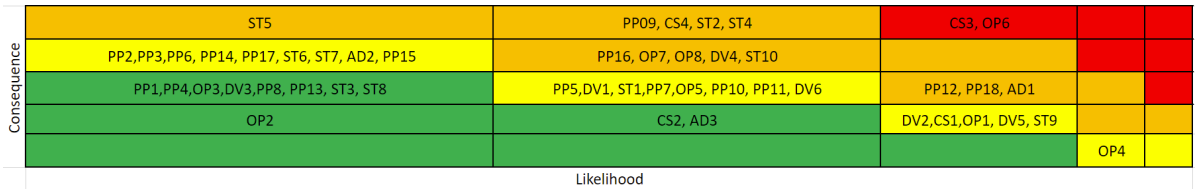

Figure 5.1: *Technical Risk matrix before mitigation*

5.2. Risk Prevention and Mitigation

A risk mitigation strategy can be applied, in order to reduce risk as much as possible. The main risks to mitigate will be those visible in the orange and red sections of the risk map as those correspond to higher danger. The prevention mitigation for these high risks can be seen below.

TR-PP-09: Explosion of Hydrogen

Prevention measure: To prevent this, regular maintenance should be made in order to check for possible

hydrogen leaks from the tank. Furthermore, gas detection systems can be integrated into the eVTOL to detect for possible leaks and then ventilate the hydrogen out of the eVTOL to stop a potential explosion.
Contingency measure: If this happens, it is best to store the hydrogen as far away as possible from batteries in order to prevent a bigger explosion. Furthermore, fire extinguishers should be available so that the explosion and possible fire is contained as fast as possible.

TR-PP-12: Hydrogen fuel loading error
Prevention measure: For prevention, a few extra kilograms of hydrogen more than the necessary amount for the mission can be added.
Contingency measure: If this was to happen, constant communication with ground support should be maintained for possible emergency landing locations. Furthermore, possible emergency fueling locations can also be identified in order to fuel-up and continue to finish the initial flight route.

TR-PP-16: Lithium-ion battery can catch fire
Prevention measure: Keep the area with the battery well-ventilated and cooled. Install a smoke detection system, and possibly a small automatic fire extinguisher that deploys once the smoke detection system is activated.
Contingency measure: The pilot should instantly be notified of this and try to stop the hovering attempt and land the eVTOL. The vertiport workers should instantly use a fire extinguisher to remove all risks of combustion.

TR-PP-18: Engines using more power than estimated
Prevention measure: Perform comprehensive tests beforehand to ensure that the engines will not use more power, even in extreme conditions. Ensure that the power source can still deliver a certain amount of power more than what the engines would need.
Contingency measure: If a maneuver is performed where the engines require more power, immediately stop the maneuver and perform an emergency landing if necessary. Redesign the eVTOL in a way where this maneuver either does not need to take place or where it can perform it and still meet power requirements.

TR-CS-03: Operational cg range outside longitudinal stability & control and one engine inoperative hover limits
Prevention measure: To prevent this, a trade-off that considers whether a certain design can be controllable and stable within the operational cg range can be designed. Furthermore, during the sizing, a 10% margin can be applied for this cg range so that this risk does not take place.
Contingency measure: If this were to take place, the design should be re-iterated and re-designed so that an adequate controllable and stable cg range can be achieved.

TR-CS-04: Aircraft maximum available power does not meet one engine inoperative hover power needs
Prevention measure: An estimation should be made of scenarios where each of the engines fails, and the required power per engine in case of failure. This power requirement should be designed for, by changing the battery parameters.
Contingency measure: Abort the hover attempt and if you are able to descend in a controllable manner, land the eVTOL. Fix the one engine inoperative, and see what the maximum power required would have been. Adapt the batteries so that this power can be given.

TR-ST-02: Underestimating the buckling loads
Prevention measure: Use a safety factor. This will help cover all possible loads encountered during the flight. A detailed analysis of the loads during the flight should also be performed to reduce the possibility of underestimating them.
Contingency measure: If there are signs that a failure may take place due to the buckling loads, instantly land the eVTOL. Retire the aircraft and perform observations to ensure this never happens again.

TR-ST-04: Over-designing the aircraft such that it becomes too heavy
Prevention measure: Make sure all the factors that determine the aircraft dimensions are taken into account. Use literature to see which parameters are the most important. The safety factors used should be enough, but not too large.

Contingency measure: If it turns out the aircraft is over-designed, change the design as soon as possible to decrease mass. Another option is to change the mission as to fit the over-designed eVTOL, such as increasing the amount of passengers and payload.

TR-ST-05: Structural failure of wing-box
Prevention measure: To prevent this, the loads acting on the wing-box should be carefully analysed so that the wing-box is designed accordingly, including a safety factor of 1.5. Structural testing should also be performed during the design stage before actual flights to make sure the wing-box can sustain the loads without failing structurally.
Contingency measure: In case of failure, immediate maintenance and repair should take place to reinforce the structure or replace it. Furthermore, the wing-box should be continuously monitored in order to prevent future failures.

TR-ST-10: Underestimating structural deformations due to crash events
Prevention measure: A higher safety factor can be applied while designing the structure of the eVTOL for crashworthiness.
Contingency measure: In case this would take place, all the eVTOLs could be withdrawn so that they can be redesigned, possibly by reinforcing the structure.

TR-AD-01: Underestimating drag
Prevention measure: Perform adequate wind tunnel tests to have a good idea of how much drag can be expected. Imitate the mission profile conditions in the wind tunnel. A very small safety factor can be used.
Contingency measure: Bring 10% more fuel onboard so that the extra drag can be compensated.

TR-OP-06: Hydrogen not being available at each vertiport
Prevention measure: When designing the routes that the eVTOL will fly, call ahead and ensure that all vertiports always have a hydrogen fueling system and hydrogen fuel.
Contingency measure: If it turns out that a vertiport has run out of fuel, bring a few extra kilograms of fuel to be able to fly to another vertiport that has hydrogen.

TR-OP-07: Operating cost too high
Prevention measure: When determining the operating cost, a range of costs can be found. When the financial analysis is made, the return on investment should be produced taking into account the fact that the operating cost could be the highest in the given range.
Contingency measure: If the operating cost is too high, the fuel cost being lowered would have the most effect. Try to negotiate with the vertiports, potentially attempting to make more trips to that vertiport if the fuel cost can be lowered.

TR-OP-08: No available pilot
Prevention measure: Pilots should be given work contracts, renewed constantly in order to prevent running out of pilots. At least the twice the number of pilots as the number of eVTOLs should be working with a contract at the company so that there are at least two available pilots per eVTOL to operate.
Contingency measure: Backup pilots should always be on standby. Furthermore, pilots performing different routes that do not have a flight at the given time can be transported to the desired location for the desired flight route.

TR-DV-04: Inadequate market position establishment
Prevention measure: A thorough market research should be conducted where the target market and the possible competitors are analysed in detail. Furthermore, a strong branding program can be presented in order to attract customers.
Contingency measure: The product price can be reduced to a price much lower than the competitors with minimum profit in order to attract customers. People usually prefer low prices, therefore this would be desirable. Furthermore, continuous market monitoring should take place so that the design can be adapted to ever-changing markets to create a breakthrough.

Table 5.7: *Scoring per risk after risk mitigation*

Risk (TR)	PP-09	PP-12	PP-16	PP-18	CS-03	CS-04	ST-02	ST-04	ST-05
Likelihood	1	3	2	2	1	2	1	1	1
Consequence	4	1	3	2	4	3	3	3	3
Risk (TR)	**ST-10**	**AD-01**	**OP-06**	**OP-07**	**OP-08**	**DV-04**			
Likelihood	1	2	1	2	1	1			
Consequence	4	2	3	3	4	3			

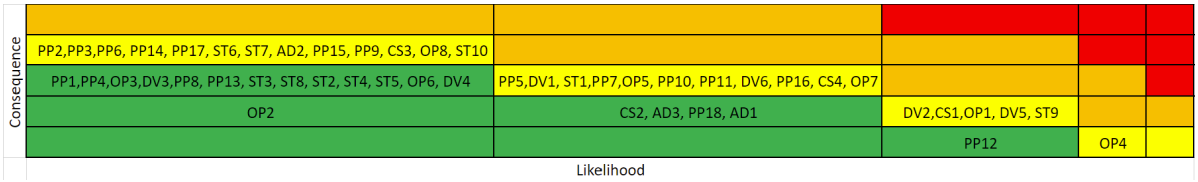

Figure 5.2: *Technical Risk matrix after mitigation*

6
Preliminary Sizing

In this chapter, the first technical characteristics of the aircraft will be determined. This will be done by performing the preliminary sizing. This is done by estimating the wing- and power loading in Section 6.1, after which a class I weight estimation is performed. Most of these values and equations are referenced from the Wigeon midterm report since this group designs a very similar aircraft [4].

6.1. Wing and Power Loading Diagrams

In these diagrams, the wing loading (W/S) is on the x-axis, and the power loading (W/P) is on the y-axis. Multiple constraints are plotted on the graph to envelop an area from which one can determine the optimal wing- and power loading. This can be found at the top right of this envelope since one wants the highest amount of weight per wing surface area and the highest amount of weight per power unit. All the equations below are taken from the third Aerospace Design and System Engineering Elements lecture from Delft University of Technology. [1]

Stall speed

The first constraint on the wing loading is a requirement set by the stall speed. This applies to this aircraft as it is required to be able to make an emergency landing in case the propulsion system fails. A low stall speed is furthermore beneficial for a lower transition time, which improves mission energy. The stall speed has been set to 45 [m/s] and is based on Wigeon [4] while taking into account the higher cruise speed. The equation that governs the stall conditions wing loading is seen in Equation 6.1. It has to be noted that the stall speed and $C_{L_{max}}$ are considered in clean configuration. In the final design high lift devices might be implemented to improve transition characteristics. The density has been used at sea level (ρ_0).

$$\left(\frac{W}{S}\right)_{stall} = C_{Lmax} \cdot \frac{1}{2} \cdot \rho_0 \cdot V_{stall}^2 \tag{6.1}$$

[1] Accessed May 9th 2023, https://brightspace.tudelft.nl/d2l/le/content/213451/viewContent/1472039/View

Climb rate

The equation constraining the climb rate is shown in Equation 6.2. The $\frac{C_D}{C_L^{3/2}}$ term has to be minimized to make sure that minimal power is required. To achieve this, the values for C_L and C_D can be approximated by Equation 6.3 and Equation 6.4. The variables in these equations are taken from Subsection 7.1.3, which will also be the case for the other power constraints. Minimizing power will save weight and increase range so it is crucial to consider. The initial estimate for the rate of climb (ROC) is 5 [m/s], which is roughly double the 500 [ft/min] that Lilium [2] and Uber [3] use. This has been chosen to reach cruise as fast as possible. The density is considered at cruise conditions.

$$\frac{W}{P_{br}} = \left(ROC + \sqrt{\frac{W}{S}\frac{2}{\rho}} \left(\frac{C_D}{C_L^{3/2}} \right)_{opt} \right)^{-1} \eta_{prop} \tag{6.2}$$

$$C_L = \sqrt{3 C_{D_0} \pi A e} \tag{6.3}$$

$$C_D = 4 C_{D_0} \tag{6.4}$$

Climb gradient

The equation constraining the climb gradient is shown in Equation 6.5. The climb gradient (G) is determined by EASA and shall not be less than 4.5% [6]. This equation is optimised with maximum aerodynamic efficiency, where C_L and C_D are specified by Equation 6.6 and Equation 6.7 respectively. Again, the density is considered at cruise.

$$\frac{W}{P_{br}} = \left(\sqrt{\frac{W}{S}\frac{2}{\rho}\frac{1}{C_L}} \left(G + \frac{C_D}{C_L} \right) \right)^{-1} \eta_{prop} \tag{6.5}$$

$$C_L = \sqrt{\pi A e C_{D0}} \tag{6.6}$$

$$C_D = 2 C_{D0} \tag{6.7}$$

Turning load factor

A constraint by the turning load factor can also be specified. It is checked if the aircraft is able to maintain speed during a turn. It is not known at which speed the turning load factor is going to constrain the envelope. The speeds considered are the cruise speed and the maximum speed. Equation 6.8 assesses the above-mentioned ability to supply power during a turn. The load factor (n_{turn}) is set to 2, as this is the load factor during a turn with a bank angle of 60 °. It is assumed that Aetheria will not perform turns with a higher bank angle.

$$\frac{W}{P_{br}} = \left(\frac{C_{D_0} \frac{1}{2} \rho V^3}{W/S} + \left(\frac{W}{S} \right) \frac{n_{turn}^2}{\pi A e \frac{1}{2} \rho V} \right)^{-1} \eta_{prop} \tag{6.8}$$

Vertical Flight

Since the aircraft takes off vertically and has to be able to hover, another constraint is added which is not present for conventional aircraft. There are not any established procedures or formulas for these kinds of eVTOLs since the industry is very young. After some research, formulas were found that constrain the power loading based on the power required during vertical take-off. These two formulas are used for different types of propeller engines. Equation 6.9 is used for ducted fans and Equation 6.10 is used for open propellers. Both are taken from a report from Lilium [7], equation (4) and equation (5) respectively. They have been adapted to describe the power loading.

$$\left(\frac{W}{P_{br}} \right)_{duct} = \left(\frac{1}{2} \frac{T}{W} \sqrt{\frac{T}{A}\frac{1}{\rho}} \right)^{-1} \cdot \eta_{hover} \tag{6.9}$$

$$\left(\frac{W}{P_{br}} \right)_{prop} = \left(\frac{T}{W} \sqrt{\frac{T}{A}\frac{1}{2\rho}} \right)^{-1} \cdot \eta_{hover} \tag{6.10}$$

Where η_{hover} is the propulsive efficiency of the propeller or duct during hover, which is different for each type of engine. These efficiencies describe the relationship between the power used by the electric engines and the kinetic energy flux of the jet. The efficiencies of the electronics, fuel cells, and batteries are not included. T/A is the disk loading (in N/m^2) and is taken from Section 10.2, together with the propulsive efficiencies. T/W is determined using Equation 6.11. This equation is adapted from [8], which describes the thrust required for the vertical take-off phase.

[2] Accessed May 12th 2023, https://lilium.com/newsroom-detail/taking-to-the-skies-flight-testing-the-lilium-jet#:~:text=As%20well%20as%20exceeding%20100,of%20500%20feet%20per%20minute.

[3] Accessed May 12th 2023, https://s3.amazonaws.com/uber-static/elevate/Summary+Mission+and+Requirements.pdf

$$\left(\frac{T}{W}\right)_{\text{climb}}^{\text{VTOL}} = 1.2\left(1 + \frac{1}{W/S}\rho(\text{ROC})^2\frac{S_{\text{tot}}}{S_w}\right) \tag{6.11}$$

This takes 20% extra thrust to accommodate for the gusts and winds and control ability. The last term in the parenthesis describes the drag the eVTOL experiences during vertical flight. *ROC* for vertical flight is set to 2 [m/s] and $\frac{S_{tot}}{S_w}$ describes the ratio between the projected area as seen from above and the wing area, with a value of 1.2 for each configuration. In Table 6.1 it shows the disk-loading and hover efficiency.
Using the results the following graphs for J1 (Figure 6.1a), L1 (Figure 6.1b) and W1 (Figure 6.1c) can be generated.

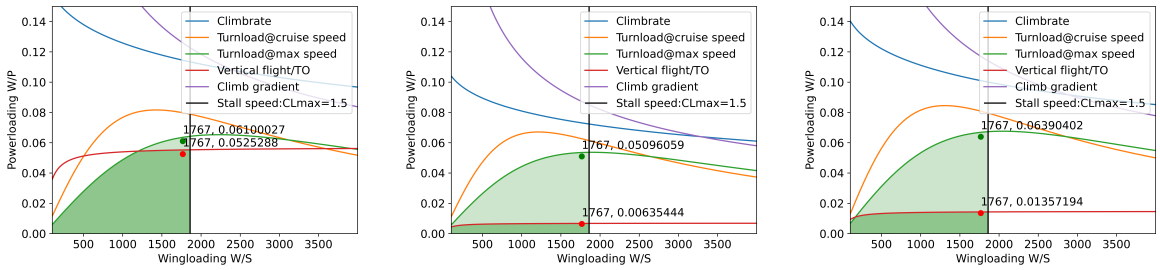

(a) *J1* **(b)** *L1* **(c)** *W1*

Figure 6.1: *Wing- and power loading graphs*

This results in the following wing- and power loadings which can be found in Table 6.1. As can be seen, the darker green area and the red design point include the constraint from the vertical flight constraint. The lighter area does not include this area, so the required power can be determined for both the take-off phase and the normal flight phase. The design point for this area is displayed with a green dot. Both design points have a margin of 5% applied. The bottom row includes these values for the normal flight. The subscript *'novf* is added to specify that it does not take 'vertical flight' into account.

Table 6.1: *Results of the diagrams in Figure 6.1*

Configuration type	J1	L1	W1
W/S	1767	1767	1767
W/P	0.0525	0.00635	0.0136
W/P_{novf}	0.0610	0.0510	0.0639
T/W	1.225	1.225	1.225

6.2. Class I Mass Estimation

To come up with a first estimate, multiple existing eVTOLs were analyzed to perform a class I weight estimation. The eVTOL data was gathered from multiple reports [1], [9], [10] and online sources [4] [5] [6]. Normal regression was used to determine the maximum take-off mass (MTOM) with the payload as the variable. Initially, all the eVTOLs were taken into account for the regression, as displayed by the red-blue dashed line in Figure 6.2a. This resulted in a R^2 value of 0.73 and RMSE of 850 [kg], which was deemed too unreliable. It was therefore decided to only include eVTOLs that have a flying prototypes, as displayed by the blue dots. This increased the R^2 value to 0.83 and decreased the RMSE to 450 [kg]. The database dimension was reduced from 24 to 10.

[4] Accessed May 10th 2023, https://evtol.news/aircraft
[5] Accessed May 10th 2023, https://www.aerospace-technology.com/projects/archer-aviations-maker-evtol-aircraft/
[6] Accessed May 10th 2023, https://transportup.com/beta-technologies-alia/

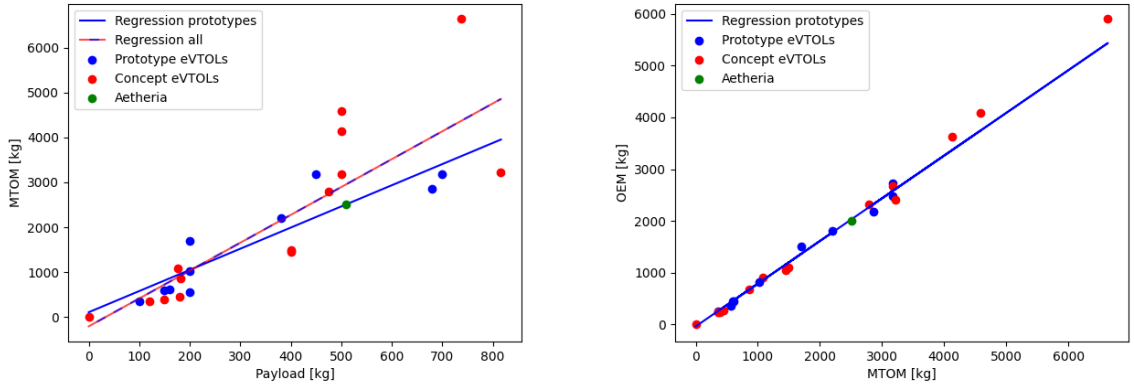

(a) *Payload vs MTOM*

(b) *MTOM vs OEM*

Figure 6.2: *Mass estimation graphs*

For Aetheria, with a payload of 510 [kg], the regression results in a MTOM of 2510 [kg]. Substracting the payload will result in an OEM of 2000 [kg]. These values will later be used as preliminary mass estimations. The OEM calculation can be verified by assessing the relation between MTOM and OEM for other eVTOLs. Figure 6.2b shows that this relation is highly linear (R^2 is 0.99). By applying regression, the OEM is obtained to be 2033 kg, differing by only 33 [kg] from the previous calculation. This is portrayed by the green dot in Figure 6.2b, which is slightly below the regression line. Due to this small discrepancy, the preliminary values for the OEM and MTOM will stay at 2000 and 2510 [kg] respectively.

7

Aerodynamics & Flight Performance

In this chapter, the aerodynamic performance of the J1, W1 and L1 designs are calculated. This is done by forming a wing planform design. Secondly, the flight performance of each design is evaluated by calculating the total required mission energy.

7.1. Aerodynamics

To acquire the required mission energy, the lift-to-drag ratio (L/D) of the three designs during cruise and climb needs to be calculated. The software XFLR5 is used throughout this section to analyze the aerodynamic performance of the airfoil and the wing planform. The drag will first be calculated using a Class I drag estimation (using wetted area), followed by a Class II drag estimation (component drag method).

7.1.1. Initial Aerodynamic Parameter Estimations

The main aerodynamic parameters for the preliminary design of the aircraft have been designed based on literature [11].

Sweep angle and taper ratio Given that the design cruise velocity is well below Mach 0.7, a quarter chord sweep angle ($\Lambda_{c/4}$) of 0 [deg] is most efficient [12]. The leading edge sweep angle (Λ_{LE}) is found using Equation 7.6 [4]. It is a function of the sweep angle at x/c chord length, so by using the quarter chord sweep angle, the sweep at the leading edge can be calculated. A taper ratio of 0.4 is used based on the succesful performance reported in Güzelbey et al. [13].

Aspect Ratio The aspect ratio (AR) for the J1 is calculated using an assumed Oswald efficiency factor (e) of 0.8, using Equation 7.2 [12]. This gives an aspect ratio of 8.4. The aspect ratio of the W1 is assumed to be similar to the Wigeon design, namely 9.5 for the first wing, and 10.0 for the second wing [1]. The L1 aspect ratio is assumed similar to the Lilium Jet. It is found by inspecting a 2D top-view drawing of the Lilium Jet. The resulting aspect ratio is 5.8 for the front wing, and 10.3 for the second wing.

$$e_{tandem} = e_{ref} \cdot \left(0.5 + \frac{1 - 0.66 \cdot \frac{h}{b}}{2.1 + 7.4 \cdot \frac{h}{b}}\right) \tag{7.1}$$

$$e = 1.78 \cdot (1 - 0.045 \cdot AR^{0.68}) - 0.64 \tag{7.2}$$

Oswald efficiency factor The Oswald efficiency factor is required to calculate the C_{D_i}. For the J1, an efficiency factor between 0.75 and 0.85 is assumed [11], therefore 0.8 is used. Next, the Oswald efficiency factor of the W1 can be calculated using Equation 7.1 [4]. The vertical distance between the two wings h is 0.3 m and the span b is 8.4, giving an efficiency factor of 0.73 (assumed the same for both wings). For the L1, an efficiency factor of 0.83 is assumed [14].

Wing surface area and span Dividing the first mass estimation of 2510 kg by the wing loading (W/S) (Section 6.1), the total wing surface area (S) is found to be 14.0 [m^2] for all three designs. This area will change for each design after going through the design convergence script (Section 8.7). This script iterates through all the designs until the performance criteria are met and the designs parameters converge. Using the new wing area and the aspect ratio, the wing span (b) can be calculated through Equation 7.3 [15].

Root chord and tip chord The root chord (c_r) needs to be calculated in order to find the leading edge sweep angle. The root chord is calculated using Equation 7.4 [12]. The tip chord (c_t) is calculated by multiplying the taper ratio by the root chord.

$$b = \sqrt{S \cdot AR} \tag{7.3}$$

$$c_r = \frac{2S}{(1+\lambda) \cdot b} \tag{7.4}$$

$$C_{L_{des}} = \frac{W}{0.5 \cdot \rho \cdot V^2 \cdot S} \tag{7.5}$$

$$\tan \Lambda_{LE} = \tan \Lambda_{x/c} + \frac{x}{c}\frac{c_r}{b}(1-\lambda) \tag{7.6}$$

Design lift coefficient Then, the design lift coefficient ($C_{L_{des}}$) is calculated using Equation 7.5 [12]. The wing loading of the aircraft is 1767 [N/m^2], as found in Section 6.1, while the cruise velocity is 83.3 [m/s] [16]. The final calculated parameters can be found in Table 7.1, which are found after running the convergence script (Section 8.7). Also, the 3D wing planforms from XFLR5 are illustrated in Figure 7.1.

DATCOM method Using the empirical equations from the DATCOM method, values for aerodynamic parameters [11], values for the lift curve gradient (C_{L_α}) and maximum lift coefficient ($C_{L_{max}}$) are easily computed. Using Equation 7.7 [11] yields a value for the C_{L_α} of the finite wings. Next, the $C_{L_{max}}$ is computed with Equation 7.8. For $\left[\frac{C_{L_{max}}}{C_{l_{max}}}\right]$, a value of 0.9 can be assumed. Then, from the value for $C_{l_{max}}$ of 1.67, a value of 1.50 for $C_{L_{max}}$ was found.

$$\frac{dC_L}{d\alpha} = C_{L_\alpha} = \frac{2\pi AR}{2 + \sqrt{4 + \left(\frac{AR\beta}{\eta}\right)^2 \left(1 + \frac{\tan^2(\Lambda_{0.5c})}{\beta^2}\right)}} \tag{7.7}$$

$$C_{L_{max}} = \left[\frac{C_{L_{max}}}{C_{l_{max}}}\right] \cdot C_{l_{max}} \tag{7.8}$$

$$C_L = s_1 \cdot C_{L_1} + s_2 \cdot C_{L_2} \cdot (1 - \frac{d\epsilon}{d\alpha}) \tag{7.9}$$

The ratio (s_i) is the ratio of areas of the front and rear wing. For the L1, this is 0.29 and 0.71 respectively, and for the W1, this is 0.5 for both. The downwash coefficient ($d\epsilon/d\alpha$) is assumed to be 0.1 [4]. From Equation 7.9, the total lift coefficient for the entire aircraft can then be calculated.

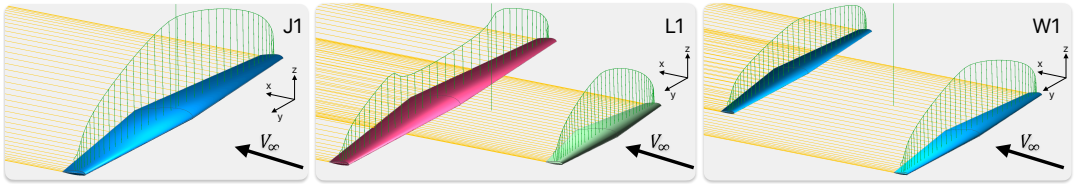

Figure 7.1: *3D wing models built in the XFLR5 software for each design*

Table 7.1: *Initial estimates for wing planform (wing1 + wing2 for tandem wings)*

	J1 (single wing)	L1 (tandem)	W1 (tandem)
AR [-]	8.40	5.80 + 10.3	9.50 + 10.0
e [-]	0.8	0.83	0.73
h/b [-]	-	-	0.0357
S [m^2]	11.2	7.26 + 18.1	9.29 + 9.29
b [m]	9.69	6.49 + 13.67	9.39 + 9.64
c_r [m]	1.65	1.60 + 1.90	1.41 + 1.38
c_t [m]	0.660	0.639 + 0.758	0.565 + 0.551
Λ_{LE} [deg]	0.166	2.12 + 1.19	0.147 + 0.140
C_{L_α} [deg$^-$1]	0.0865	0.0762 + 0.0903	0.0888 + 0.0898
$C_{L_{des}}$ [-]	0.432	0.124 + 0.308	0.216 + 0.216

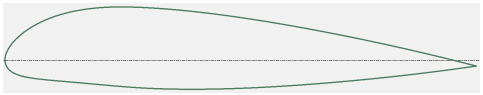

Figure 7.2: *NACA44017: chosen airfoil for all designs*

7.1.2. Airfoil Selection

In accordance to the design characteristics reported in [1], the NACA44017 airfoil has been chosen for all three designs to simplify the study (depicted in Figure 7.2). The aircraft configurations are modelled in XFLR5 and the wing performance parameters follow from simulating the models. XFLR5 uses the Vortex Lattice Method (VLM) using horseshoe vortices [17]. This has a few limitations, namely that is in inaccurate for configurations with a low aspect ratio and a high sweep. Fortunately, all three of the designs have a medium aspect ratio (between 7 and 10) and no sweep. Only the front wing of the L1 design has a slightly lower aspect ratio. The effect this has on the VLM will be neglected for the preliminary aerodynamic sizing. In terms of viscosity, XFLR5 is not sophisticated enough to provide high-fidelity 2D drag estimations under high angles of attack as the interactive boundary layer solver fails when flow detaches from the surface. For the 3D analysis, the viscous module was used in XFLR5 which interpolates the 2D viscous drag over the wing span.

7.1.3. Drag Estimations

To perform the initial drag estimation, a Class I drag estimation was performed calculating the skin friction drag based on an assumed skin friction drag coefficient and ratio of wetted surface area to wing surface area. This yielded a first estimate for the C_L/C_D to be used by other aspects of the design such as power sizing.

Subsequently, a Class II drag estimation is done using the component build-up drag method shown in Equation 7.11 [11]. The total drag coefficient in the drag polar is the sum of the parasite drag and the induced drag, which in turn is a function of the lift coefficient. The parasite and induced drag coefficients are defined by Equation 7.11 and Equation 7.10, respectively.

$$C_{D_i} = \frac{C_L^2}{\pi ARe} \tag{7.10}$$

$$C_{D_0} = \frac{1}{S_{ref}} \sum C_{f_e} \cdot FF_c \cdot IF_c \cdot S_{wet_c} + C_{D_{misc}} \tag{7.11}$$

Here, S_{ref} is the reference wing area, which is the same as the total wing area [1]. C_{f_e} is the flat plate skin friction coefficient, which depends on the flow. For turbulent flow, the C_{f_e} can be calculated using Equation 7.1.3 while for laminar flow Equation 7.1.3 holds. The assumption is done so that 5% of the flow around the fuselage is laminar, and 95% is turbulent [11]. Around the wings 10% is laminar, 90% is turbulent. Using a Reynolds number of $4.5{\cdot}10^6$ for the calculations (cruise conditions), the values of C_{f_e} and $C_{f_{fus}}$ are $6.26{\cdot}10^{-4}$ and $3.40{\cdot}10^{-3}$ respectively.

$$C_{f_{turb}} = \frac{1.328}{\sqrt{Re}} \tag{7.12}$$

$$C_{f_{lam}} = \frac{0.455}{(\log_{10} Re)^{2.58}(1+0.144M^2)^{0.65}} \tag{7.13}$$

The form factor (FF) takes into account the form of the wings and fuselage. t/c is the average thickness to chord ratio, $(x/c)_m$ is the position of maximum thickness, (l/d) is the slenderness ratio, Λ_m is the sweep angle at the position of the maximum thickness ($0.293c$ for NACA 44017) and M is the Mach number. The form factor of the wing and fuselage can be found in Equation 7.14 and Equation 7.15, respectively.

[1] Accessed May 24th, https://aerotoolbox.com/wing-area#:~:text=The%20reference%20wing%20area%20is,area%20of%20an%20aircraft's%20wing.&text=An%20aircraft's%20reference%20wing%20area,the%20wing%20through%20the%20fuselage).&text=Wing%20area%20is%20a%20fundamental,performance%20modelling%20of%20an%20aircraft.

$$FF_w = \left(1 + \frac{0.6}{(x/c)_m}\left(\frac{t}{c}\right) + 100\left(\frac{t}{c}\right)^4\right) \cdot \left(1.34M^{0.18}\cos\Lambda_m{}^{0.28}\right) \quad (7.14) \qquad FF_{fus} = 1 + \frac{60}{(l/d)^3} + \frac{l/d}{400} \quad (7.15)$$

Furthermore, IF is the interference factor, of which values range from 1.0 and 1.5. The S_{wet} is the wetted area of the aircraft, and $C_{D_{misc}}$ is the drag of other components, such as landing gear and fuselage upsweep [4]. The wetted area of the fuselage can be calculated using Equation 7.16. L1 is the length of the parabolic section, L2 is the length of the cylindrical section and L3 is the length of the conical section.

$$S_{wet_f} = \frac{\pi D}{4}\left(\frac{1}{3L_1^2}\left[\left(4L_1^2 + \frac{D^2}{4}\right)^{1.5} - \frac{D^3}{8}\right] - D + 4L_2 + 2\sqrt{L_3^2 + \frac{D^2}{4}}\right) \quad (7.16)$$

For $C_{D_{misc}}$ the upsweep drag was taken as a drag component, as well as the base drag. To calculate the upsweep drag Equation 7.17 is used, while for the base drag Equation 7.18 is used. A_{max} is the maximum fuselage cross-sectional area, while A_{base} is the fuselage base area.

$$C_{D_{upsweep}} = \frac{3.83u^{2.5}A_{max}}{S_{ref}} \quad (7.17) \qquad C_{D_{base}} = \frac{[0.139 + 0.419(M-0.161)^2]A_{base}}{S_{ref}} \quad (7.18)$$

XFLR5 drag estimation The drag can also be estimated using XFLR5. However, the fuselage drag is not included, meaning that XFLR5 only computes the C_{D_0} and C_{D_i} of the wing. These two parameters were compared to the values computed using the Class II drag estimations after which the highest value for each parameter was chosen for safety measures. Then, adding to the C_{D_0} and C_{D_i} the fuselage drag coefficient, leads to a final value for C_D. Table 7.2 shows the final drag estimates, and the C_L/C_D, after it has been run through the convergence script (Section 8.7).

Table 7.2: *Class II drag estimates*

	J1 (single wing)	**L1 (tandem)**	**W1 (tandem)**
Λ_m [deg]	-0.255	-0.209	-0.368
$C_{D_{upsweep}}$ [-]	0.00328	0.00328	0.00328
$C_{D_{base}}$ [-]	0	0	0
C_{D_0} [-]	0.0231	0.0159	0.00828
C_{D_i} [-]	0.00884	0.00844	0.0174
C_D [-]	0.0319	0.0253	0.0265
C_L [-]	0.432	0.432	0.432
$(C_L/C_D)_{max}$[-]	13.5	17.0	16.3

7.2. Mission Profile

The mission profile will be essential in order to make a preliminary energy estimation. The mission profile for the Aetheria is shown in Figure 7.3. Segments **A**, **I**, and **I'** represent the ground taxi phases in the mission, of which the required energy is neglected due to their insignificant order of magnitude relative to the other phases in the mission. The remaining phases and their meaning are listed below.

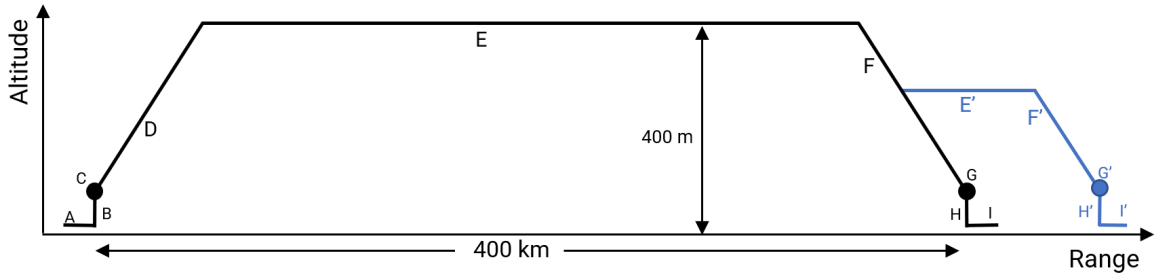

Figure 7.3: *Mission profile of the Aetheria*

- **B** - Take-off to transition altitude (t = 15 [s])
- **C** - Transition to horizontal flight (t = 10 [s])
- **D** - Climb to cruise (t = 74 [s])
- **E** - Cruise (t = 78 [min])
- **F** - Descend from cruise (t = 123 [s])
- **G** - Transition to vertical flight (t = 10 [s])
- **H** - Landing (t = 15 [s])
- **E'** - Loiter cruise (t = 10 [min]
- **F'** - Descend from loiter cruise (neglected)
- **G'** - Transition to vertical flight (t = 10 [s])
- **H'** - Landing (t = 15 [s])

7.3. Mission Energy

The mission energy defines the total energy required by the aircraft to perform the mission. As the mission energy is a trade-off criterion and must be carefully assessed.

Take-off to transition altitude First of all, determining the required energy during take-off requires knowledge of the altitude at which transition takes place and the vertical velocity during take-off. As energy is a function of power and time, both should be kept at a minimum. From regulations set by EASA, a specified altitude 30.5 [m] (100 ft) [6] was set for the minimum transition altitude. Moreover, the rate-of-climb (RoC) is set to be 2.0 [m/s] which might be changed in the optimization stage. Knowing the RoC and transition altitude, the total take-off climb time was estimated to be 15 seconds. Next, the power required to ascend at a RoC of 2 [m/s] follows from Equation 7.19 [4]. The value of κ can be taken as 1.2 [18]. Multiplying the power by the time required for take-off, the energy was found.

$$P = T \cdot ROC + \kappa T \left(-\frac{ROC}{2} + \sqrt{\frac{(ROC)^2}{4} + \frac{T}{2\rho A_{\text{disk}}}} \right) \tag{7.19}$$

Transition to horizontal mode For the transition from take-off configuration to horizontal flight mode configuration, the average power of the take-off and climb phases is taken as a first estimate of the required power during transition. Multiplying this power by the transition time yields the total required energy during transition. In the optimization stage, a model will be made to track every step of the transition phase.

Climb During the climb a constant speed is assumed. This might not be the most fuel-efficient, but the energy calculation serves as a comparison between the designs, hence the assumption. Equation 6.2 is rewritten to P_{br}/W and multiplied by the fuel cell and battery efficiency. Then, this is multiplied by the MTOW to find the thrust needed. The cruise altitude is set at 400 [m], which is comparable to the cruise altitude of the Wigeon design. Finally, the climbing time can be calculated with Equation 7.20 [4].

$$t_{climb} = \frac{h_{cruise} - h_{transition}}{ROC} \tag{7.20}$$

Cruise The energy used in the cruise phase follows from the analysis performed in Chapter 10, and Equation 10.8. The power is found by multiplying the drag by the cruise velocity. Then, the required power during cruise is computed and then multiplied by the time spent in cruise, yielding the total required energy.

Descent To keep the total mission energy at a minimum, an almost gliding descent is suggested, with the power being only 20% of the cruise power [14]. However, a more accurate estimation is to use the climb equation (Equation 6.2) and use a negative ROC. The descent from cruise altitude to transition altitude is assumed to have a rate of descent (RoD) of 3 [m/s]. Then, using the same method as for climb, the required power can be computed. Again, the product of the required power and the descent time yields the total required energy during descent.

Loiter The total loitering time was set at 10 [min] for horizontal mode and 30 [s] [4] for hovering during final approach. The configuration which requires the least amount of power ensures maximum endurance as well as maximum climb rate. Therefore, the power for loiter can be found similarly as for the climb, but setting the RoC to zero. For the hovering, the required power for take-off can be used while keeping the RoC at zero. Finally, the time spent in loiter cruise multiplied by the required power setting and the loiter hovering time multiplied by the required power setting are summed to find the total energy required for loitering.

Transition to vertical mode The transition from horizontal flight back to vertical flight closely resembles the transition from horizontal to vertical flight. However, as less power is needed to decelerate the aircraft with respect to acceleration, the total required energy will be lower. For simplicity reasons, the final transition is assumed to consume the same amount of energy as the transition after take-off. This approach suggests a conservative required energy, allowing some margin for errors.

Landing For the landing velocity, a value of -2 [m/s] is taken to allow for a smooth and comfortable landing. The hover landing starts at the transition altitude of 30.5 [m], resulting in a landing time of 15.3 [s]. The required mission energy is then found by multiplying this landing time by the required power (Equation 7.19.

The total mission energy for all designs is tabulated in Table 7.3. A more detailed distribution of the required energy per mission segment is illustrated in Figure 7.4.

Table 7.3: *Mission energy for each design*

	J1	L1	W1
Total energy [kWh]	199.0	527.3	313.9

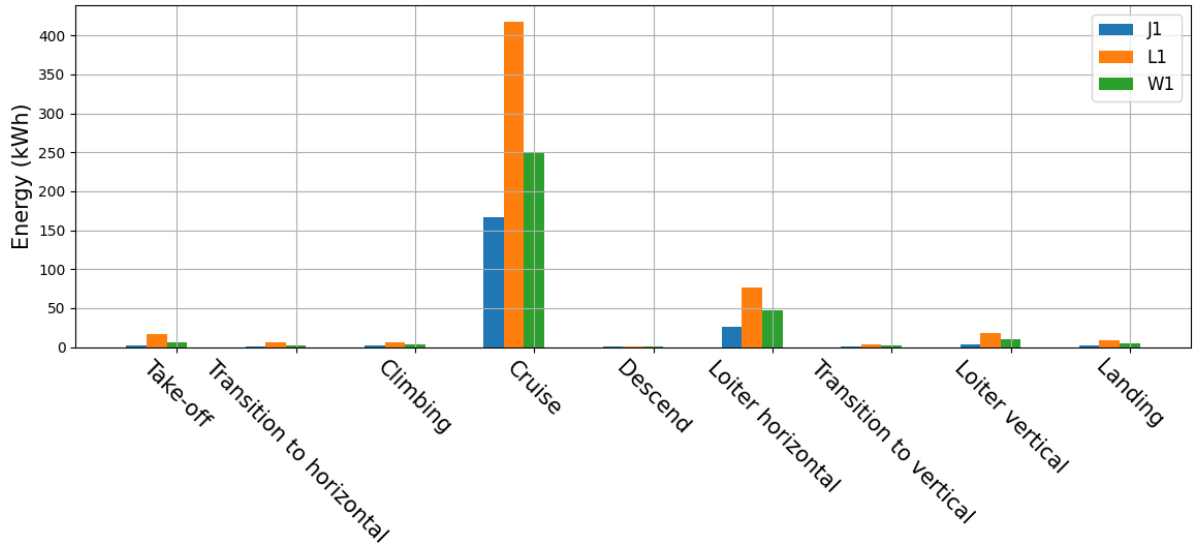

Figure 7.4: *Energy of the different mission segments*

7.4. Mission Energy Criterion Scores For Different Designs

To conclude, the J1 design is the winner in terms of required mission energy. From Figure 7.4 it becomes obvious that the cruise phase is by far the most energy-demanding phase. The J1 performs significantly better compared to L1 and J1 in this phase, giving it a high advantage. The cruise energy is directly proportional to the weight of the aircraft, and as the weight of the J1 design was found to be much lower compared to the other designs, it makes sense the J1 comes out on top for this analysis. The designs are evaluated for mission energy on a score from 0 to 3, where 0 is unacceptable and 3 is excellent. Since all designs are feasible, none was given a score of 0. J1 was given a score of 3 since it has an exceptionally low mission energy. The second best (W1) has been given a score of 2 and lastly, the L1 has been given a 1. The L1 uses by far the most energy per mission, more than twice the energy the J1 uses. This relates mostly to the high weight, which causes the cruise power to be very high.

7.5. Sensitivity Analysis

A sensitivity analysis was conducted to assess the impact of changes in mission segments, lift and drag estimations of the aspect ratio, and disk loading on the final mission energy. The analysis aimed to identify the variables that significantly influence the design outcomes. Wing placement, on the other hand, was evaluated solely for the final design.

7.5.1. Aspect Ratio

The aspect ratio is one of the parameters which is taken from sources and not calculated. It is also used to calculate the lift over drag and thus the mission energy. A sensitivity analysis is done on the aspect ratio to see whether changes significantly affect the MTOM and the mission energy. For the tandem wings, both aspect ratios have been changed but only the most aft wing is shown in Figure 7.5 and Figure 7.6. From these figures, it can be concluded that changing the aspect ratio has a large impact on all configurations. This is because a wing with a higher aspect ratio relates to a larger span, which causes more bending forces on the wing. Therefore it is required to reinforce it, which increases the mass. From Figure 7.6 it can be seen that there is an optimal aspect ratio for each design. A low aspect ratio increases the induced drag, while a high aspect ratio increases the weight.

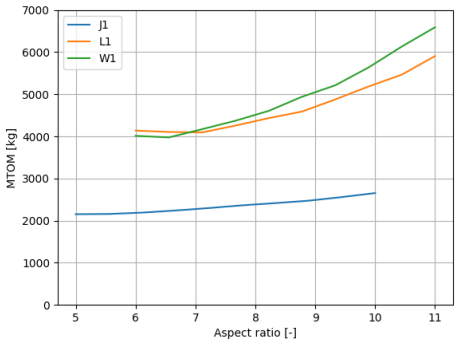

Figure 7.5: *MTOM compared to different aspect ratios*

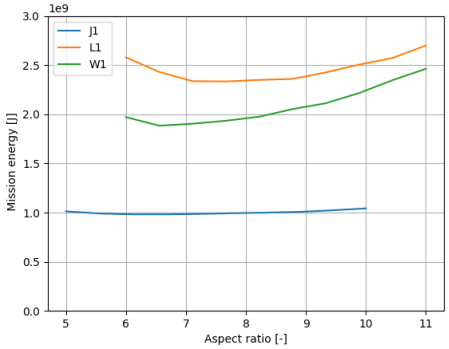

Figure 7.6: *Mission energy compared to different aspect ratios*

7.5.2. Disk Loading

As mentioned before, the disk loading is derived from outside sources beforehand, additionally, it is the variable characterizing each design. Hence, it was decided that a sensitivity analysis should be performed on the disk loading. In order to do so, a suitable disk loading range was selected for each design concept as shown in Table 7.4. This range was selected based on the original value of the disk loading that was chosen for the respective design concept. Then for each data point in the range of disk loading, the design was converged using 10 iterations. The result is as shown in Figure 7.7, please note the use of a logarithmic scale on both axis.

Table 7.4: *The chosen disk loading range for each design concept to perform the sensitivity analysis*

Design Concept	Disk loading [kg/m^2] range
J1	45 to 500
L1	1000 to 2000
W1	200 to 1000

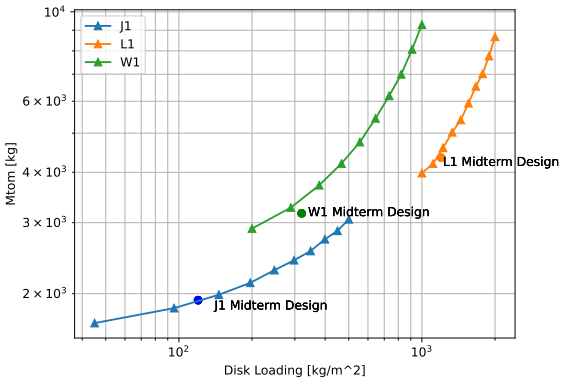

Figure 7.7: *The converged weight of the three design concepts as a variable of the disk loading used.*

A logarithmic scale was chosen due to the wide range of data and the greater importance of relative changes. As can be seen, all design concepts are significantly influenced by a change in disk loading. An interesting occurrence is that J1 has a better performance than W1 for the same disk loading. The same can be said for the L1 compared to W1 for a disk loading of 1000 [kg/m^2], this difference is most likely caused by the ducted fans of the L1 design. Additionally, it is observed that relative changes in disk loading are not as significant as J1 experiences the greatest amount of relative change but is affected the least. The absolute value of the

disk loading has a more significant role, this can be seen in the fact that all designs have the same slope in the overlapping disk loading range, but are shifted vertically due to their different designs. Finally, important to note is that the design points have a slight offset from the sensitivity lines, this is caused by the limited iterations performed per datapoint.

7.6. Verification and Validation

To verify the mission energy code, numerous checks have been performed. First of all, all equations were manually checked by engineering judgment. Furthermore, a pytest was run for each module, making sure that each function gives a correct value. For future verification, extra tests will need to be performed on the code. Furthermore, additional sources will need to be looked into to verify whether the used equations relate to the chosen design configurations.

To validate the aerodynamic sizing, a number of tests can be performed. The objective of the validation is to ensure the results correspond to experimental or established data. To meet this objective, several tests are required. Firstly, during the DSE, the results are compared to data of similar aircraft. This can be seen as a preliminary validation method. However, this is not sufficient for the final prototype. Therefore, other tests lying outside the scope of this DSE will need to be performed in order to properly validate the entire design. A wind tunnel test is required to validate the aerodynamic part of the design. For this test a 3D model will be used, which will be printed by a group member to validate the aircrafts topology. Then, a large scale model must be build with which a flight test will be performed. The data of this flight test will serve as a better validation of the aerodynamics of the aircraft.

8
Structural Design

This chapter presents the structural design for the three configurations. Maximum load factors are firstly obtained in Section 8.1, which are utilized in Section 8.2 to analyse the stresses at the wingroot of each design option. This analysis will exhibit the design's structural ability and lay a basis for the crashworthiness study in Section 8.8. As the hydrogen system poses dangers regarding passenger safety, assessing the crashworthiness of each configuration is of uttermost importance.

8.1. Manoeuvre & Gust Envelope

In order to obtain the maximum load factor that the eVTOL will experience, it is useful to construct a manoeuvring and gust envelope. The maximum load factor for the manoeuvring envelope is firstly determined by the maximum lift coefficient until it reaches the maximum prescribed load factor. This is defined by EASA to be 2.5 for the upper limit and -1.0 for the lower limit [6]. This part can be calculated with Equation 8.1.

For the gust envelope, the load factor is calculated with Equation 8.2, where u is the gust velocity. Three points are plotted based on three gust velocities and aircraft velocities. The gusts at V_b, V_c and V_d are given by EASA to be 20.12, 15.24 and 7.62 [m/s] respectively. V_b is the design velocity for maximum gust velocity and is obtained from requirements from EASA [19] and Introduction to Aerospace Flight Vehicles [20]. V_c is cruise velocity and multiplying that value by 1.25 gives the dive velocity, V_d. The envelope is completed by mirroring the three points around the line $n = 1$ and connecting the points with straight lines.

$$n = \frac{\rho V^2 C_{L_{max}}}{2W/S} \tag{8.1}$$

$$n = 1 + \frac{\rho V C_{L_\alpha} u}{2W/S} \tag{8.2}$$

The density for both envelopes is considered to be the one at cruise, as the aircraft will mostly fly at this altitude. The combined flight envelope of J1 is shown in Figure 8.1. The flight envelopes for L1 and W1 are

not displayed as there shape is similar. The maximum load factor can be obtained from this by taking the highest point in the flight envelope. It is apparent that gust loads exceed manoeuvring loads. Subsequently, the maximum load factor is multiplied by a safety factor of 1.5 to obtain the ultimate load factor. During the structural design, this value should be kept in mind, as it is the highest load that the aircraft should withstand without failing catastrophically. The maximum and ultimate load factors, obtained from the flight envelopes, are summarised in Table 8.1.

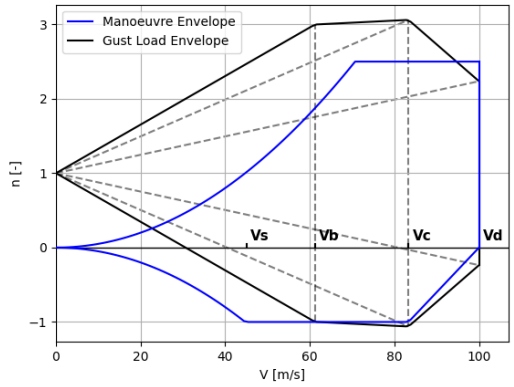

Figure 8.1: *Flight Envelope of J1*

Table 8.1: *Design load factors*

Configuration type	J1	L1	W1
n_{max}	3.06	3.15	3.14
n_{ult}	4.59	4.72	4.7

To conclude, the ultimate load factors are similar for the three configurations and are in an acceptable range compared to other general aviation aircraft. J1 has the lowest ultimate load factor, which will allow for a lighter structural design.

8.2. Structural Analysis Method

The most critical load cases were investigated for each configuration. For the trade-off, a complete structural analysis is not feasible, so only the limiting cases were considered. The loads will be analysed in the wing box at the root of the wing in two different load cases: vertical flight and hover.

The current design phase does not determine the use or quantity of composites. The final trade-off will consider both metallic and composite components. This report focuses on 2024-T3 Aluminium, commonly used in wing-box structures for its high tensile strength [21]. According to Leishman [22], critical defect types for metallic components include fatigue, corrosion, creep, and overload, while composite components face fatigue, disbonds, delamination, and fiber breakage. Creep, corrosion, disbonds, and delamination will not be considered in the trade-off. Overload and fiber breakage depend on applied stress. Stresses at the root of the wing box, where it connects to the fuselage, will be investigated as they are the highest. Shear forces, bending stresses, and critical buckling stresses will be discussed in Section 8.2.1. Fatigue performance analysis will be covered in Section 8.2.2.

8.2.1. Stress Analysis

The normal stresses are generated by the resultant force in the y direction and the resultant bending moments around the x and z axes. For the bending stress and normal stress Equation 8.3 and Equation 8.4 are used. Note that σ_y is not the yield stress here but the normal stress in the y-direction.

$$\sigma_y = \frac{M_x I_{zz} - M_z I_{xz}}{I_{xx} I_{zz} - I_{xz}^2} z + \frac{M_z I_{xx} - M_x I_{xz}}{I_{xx} I_{zz} - I_{xz}^2} x \quad (8.3) \qquad \sigma_y = \frac{F_y}{A} \quad (8.4) \qquad \tau = \frac{q}{t} = \frac{T}{2tA_m} \quad (8.5)$$

The shear stresses depend on the resultant moment around the y axis (torque), which can be calculated with Equation 8.5. The rest of the shear stresses are caused by the resultant forces in the x and z directions. Since this is a closed section, a cut will first have to be made to perform the analysis with Equation 8.6 to determine the basic shear flows (q_b). After this, the sum of the moments around the centre of gravity is taken to determine $q_{s,0}$.

$$q_s = q_b + q_{s,0}$$
$$= -\frac{V_z I_{zz} - V_x I_{xz}}{I_{xx} I_{zz} - I_{xz}^2} \int_0^s t y ds - \frac{V_x I_{xx} - V_z I_{xz}}{I_{xx} I_{zz} - I_{xz}^2} \int_0^s t x ds + q_{s,0} \quad (8.6)$$

$$\sigma_{cr} = C \frac{\pi^2 E}{12(1-\nu^2)} \left(\frac{t}{b}\right)^2 \quad (8.7)$$

These equations are from Dr. Calvin Rans' Structural Analysis lectures [23]. The critical buckling stress is important to consider. The top plate experiences compressive stresses due to bending. The buckling stress for a plate is given by Equation 8.7 [24].

The constant C depends on the clamping mode, while E represents Young's modulus, ν is Poisson's ratio, t is plate thickness, and b is plate width. A buckling coefficient of 4.00 is assumed for both SSSS and CCSS cases [24]. The material properties used are from the widely used aluminium 2024 T3 alloy in the aerospace industry [**?**]. The design of stiffeners, such as stringers, can be customized for the chosen configuration and will not be discussed here. The buckling and crippling of stiffeners and stiffened panels are more complex and will be analyzed in the final design phase.

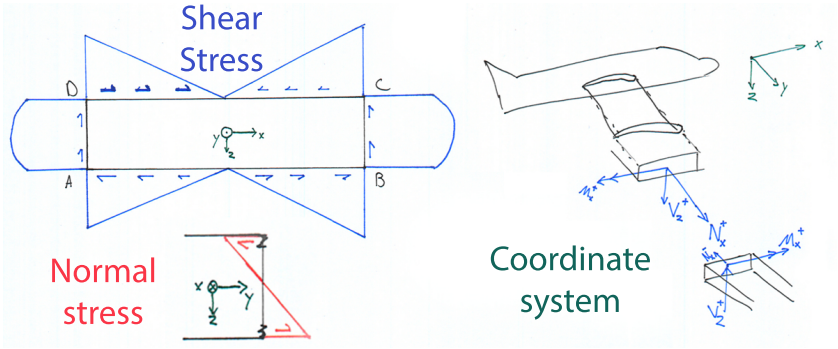

Figure 8.2: *Loads and coordinate system visualised*

8.2.2. Fatigue Analysis

The fatigue analysis shown in Figure 8.3 has been largely inspired by the fatigue analysis of the wigeon group[4] since they design a similar aircraft with the same method. Fatigue depends on two factors, crack initiation and crack growth. Now combining Equation 8.8 and Equation 8.9 results in Equation 8.10. These are determined using a Wöhler's curve (Figure 8.3) and the Paris equation (Equation 8.10) respectively. The Wöhler's curve is determined by Basquin's Law $S_a^m \cdot N = C$ where S_a is the load level, m = 4.10 and C = $3.15 \cdot 10^{14}$ [25].

$$N_{a_0 \to a_f} = \int_{a_0}^{a_f} \frac{1}{f_R(\Delta K)} da \quad (8.8)$$

$$\frac{da}{dN} = C \Delta K^m = C(\beta \Delta \sigma \sqrt{\pi a})^m \quad (8.9)$$

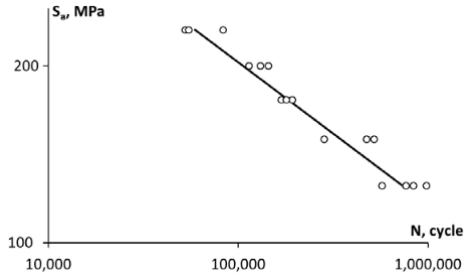

Figure 8.3: *Wöhler's curve for 2024-T3 aluminium alloy [25]*

$$N = \frac{1}{C \Delta \sigma^m} \int_{a_0}^{a_f} \frac{1}{(\beta \sqrt{\pi a})^m} da = \frac{1}{C \Delta \sigma^m} \frac{1}{(\beta \sqrt{\pi})^m} \cdot \left[-\frac{2}{(m-2) \cdot a^{\frac{m-2}{2}}} \right]_{a_0}^{a_f} \quad (8.10)$$

C and m are material properties taken from 2024-T3 aluminium alloy. The number of cycles can easily be determined with this formula and by looking at Figure 8.3. The Paris equation describes the fatigue crack growth where a is the crack length and $f_r(\Delta K)$ is the resistance to crack growth of the material. Since the case where the crack is initiated at the edge is most critical, β is assumed to be 1.225 [4]. a_0 is the initial crack length

and this is chosen to be 0.45 [mm] since this is the smallest length detectable by the mechanoluminscence film [26]. The final crack length a_f is assumed to be half the thickness of the wing box which results in a value of 1.5 [mm]. The results of these equations can be found in Table 8.3.

8.3. Wing-box Geometry

The wing box for now has been assumed to be rectangular with a height of 80% of the root chord height and a width of %60 of the root chord. The body axis coordinate system was used as shown in Figure 8.4[1]. Since the wing box is symmetrical, the product moment of inertia is zero ($I_{xz} = 0$). Also, since the wing thickness is for now assumed to be 3 [mm], the section is thin-walled. The equations for the geometry are described by Equations 8.11, 8.12, 8.13, 8.14 and 8.15 [23]. For the tandem wing configurations (W1 & L1) the rear wings were analyzed since for L1 the rear wing carried more load and for W1 the rear wing is smaller but it assumed the loads will be the same so this will be more crucial.

$$w = c_{root} \cdot 0.6 \tag{8.11}$$

$$A = w \cdot h - (w - 2t) \cdot (h - 2t) \tag{8.12}$$

$$A_m = (w - t) \cdot (h - t) \tag{8.13}$$

$$I_{xx_{thinwalled}} = \frac{w \cdot h^2 \cdot t}{3} \tag{8.14}$$

$$I_{zz_{thinwalled}} = \frac{h \cdot w^2 \cdot t}{3} \tag{8.15}$$

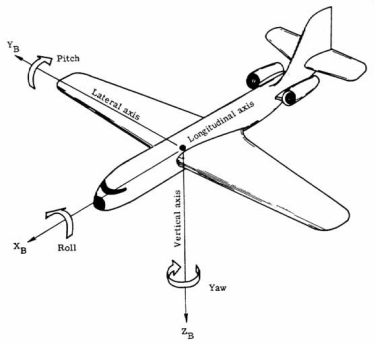

Figure 8.4: *Body-axis coordinate system*

8.4. Load Cases

Two load cases will be considered in the structural design: vertical flight (Table 8.2) and cruise (Table 8.3). For J1, the stresses are generally the lowest which makes this concept the winner. Regarding buckling, W1 performs the best, followed by J1 and L1. Note that the critical buckling stresses here are quite low. This is because the wing box was modelled without stringers since these will be added at a later stage. But, from this result, one can conclude that W1 would need the least amount of stiffeners.

Table 8.2: *Maximum stresses for the vertical flight case*

	J1	L1	W1
$\tau_{max}[MPa]$	8.4	15.67	12.61
$\sigma_{max}[MPa]$	55.41	62.58	82.16

Table 8.3: *Maximum stresses for the cruise case*

	J1	L1	W1
$\tau_{max}[MPa]$	65.29	156.5	311.1
$\sigma_{max}[MPa]$	238.3	423.4	287.3
$\sigma_{cr}[MPa]$	2.48	1.87	3.55
$N_{paris}[10^3]$	56.5	5.352	26.25
$N_{S-N}[10^3]$	308.0	54.87	175.7

[1] Accessed May 23rd 2023, https://www.aerospacemanufacturinganddesign.com/article/aluminum-alloys-for-aerospace/

8.5. Fuselage Design and Hydrogen Storage

The fuselage design will be the same for the three configurations, so its shape will not be considered for the trade-off. It is included here as it is required for the departments' design. The dimensions used in this section are based on the lecture slides from the first-year ADSEE course and Airplane Design Part III by Roskam [27]. If possible, the dimensions for private jets will be chosen as Aetheria will compete with private jets and other luxurious means of transport. The fuselage design is initiated with the design of the cross-section which is seen in Figure 8.5.

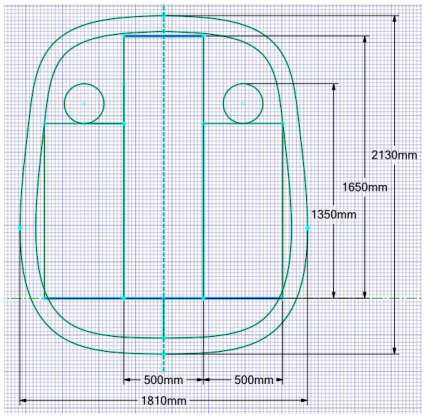

Figure 8.5: *Initial fuselage cross section*

Following the cross-section set-up, the initial fuselage planform can be designed which can be seen in Figure 8.6. The cabin is separated by a firewall from the tail, where the hydrogen power system is stored. The fuel cell system, batteries and hydrogen storage have been sized based on Chapter 9. Some margin has been left around the hydrogen storage to allow for energy absorption, this is something that is analyzed in more detail in later reports. This is because it is not relevant for the trade-off since the fuselage is the same for each design.

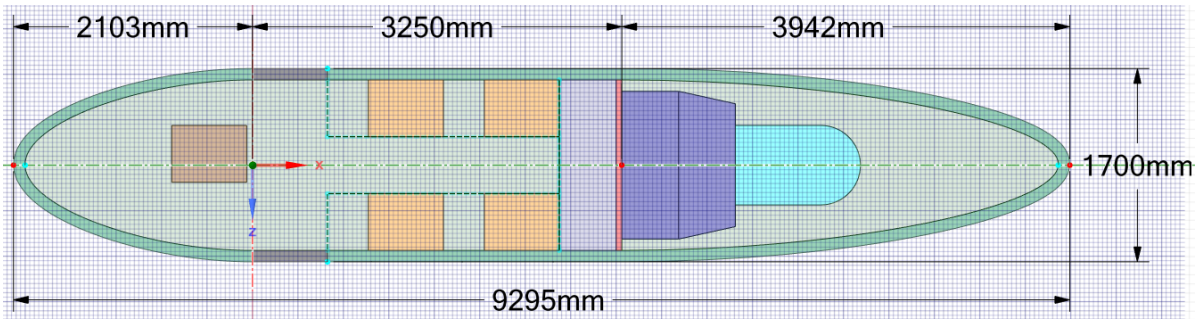

Figure 8.6: *Initial fuselage planform*

8.6. Class II Weight Estimation

To estimate the structural weight of different VTOL concepts, a Class II weight estimation will be performed. Since there are no existing methods specifically for VTOLs and limited data is available, it has been decided to utilize methods for general aviation planes as outlined in [2]. According to Roskam, the structural weight of an aircraft consists of several components, including the wing, fuselage, landing gear, empennage, and nacelles. Additionally, the powerplant- and powertrain weight have to be estimated. Finally, one can consider miscellaneous subsystem such as Flight Control, furnishing et cetera.

However, not all of these components are applicable to the chosen design concepts. For a summary of the selected components for each design, please refer to Table 8.5. It should be noted that the weight of the front canard/wing in design L1 is modelled as a wing component, following Roskam's recommendation to use the wing weight equation for significantly loaded canards [2, pg. 72].

Table 8.4: *All variables utilized in Table 8.6 including a description and their units used in the class II weight estimation*

Variable	Description	Unit
w_{to}	Maximum take-off weight	[lbs]
A	Aspect ratio of the wing	[-]
S	Wing surface area	[ft^2]
l_f	Length of the fuselage	[m]
n_{pax}	Amount of passengers including pilot	[-]
Φ_f	Maximum perimeter of fuselage	[m]
A_h	Aspect ratio of the horizontal tail	[-]
S_h	Surface area of the horizontal tail	[ft^2]
t_{r_h}	Maximum root thickness of horizontal tail	[ft]
P_{max}	Maximum power outputted by engine(s)	[hp]
$P_{density}$	Power density of powertrain (engines, propellers, shaft et cetera)	[lbs/hp]

Table 8.5: *Components utilized in the different concepts for performing the Class II weight estimation.*

Component	J1	L1	W1
Wing	1	2	2
Fuselage	1	1	1
Landing gear	1	1	1
Horizontal tail	1	0	0
Powertrain	1	1	1
Power system	1	1	1
Nacelles	1	1	1
Flight Control system	1	1	1
Electrical system	1	1	1
Instrumentation & avionics	1	1	1
Air conditioning	1	1	1
Furnishing	1	1	1

The method in which each component in Table 8.5 is computed is tabulated in Table 8.6. Source [2] offered four methods for component weight estimation: General Dynamics, United States Air Force, Torenbeek and the Cessna method. The respective method used for each component is also listed. The variables used in Table 8.6 are listed in Table 8.4 including their descriptions and the units they should be substituted with. Note that they are not in SI units and hence the outcomes of the equations in Table 8.6 should first be converted to [kg]. Additionally, the equation for the landing gear has been simplified from the original in [2] as the parameters required were not yet available.

Table 8.6: *Equations and methods used for computing the components in Table 8.5.*

Component	Equations	Method
Wing	$0.04674\, w_{to}^{0.397} S^{0.36} n^{0.397} A^{1.712}$	Cessna
Fuselage High wing	$14.86\ w_{to}^{0.144} \left(\frac{l_f}{\Phi_f}\right)^{0.778} l_f^{0.383} n_{pax}^{0.455}$	Cessna
Fuselage Low wing	$0.04682\ w_{to}^{0.692} \Phi_f^{0.374} l_f^{0.59}$	Cessna
Landing gear	$0.04\, w_{to} + 6.2$	Cessna [2]
Horizontal Tail	$\frac{3.184 w_{to}^{0.887} S_h^{0.101} A_h^{0.138}}{174.04 t_{r_h}^{0.223}}$	Cessna
Powertrain	$\frac{P_{max}}{P_{density}}$	Bespoke
Power system	See Section 9.3	Bespoke
Nacelles	$0.24 P_{max}$	Cessna
Flight Control System	$0.0168\, w_{to}$	Cessna
Electrical system	$0.0268\, w_{to}$	Cessna
Instrumentation & Avionics	$0.008\, w_{to} + 40$	Torenbeek
Air conditioning	$0.018\, w_{to}$	Torenbeek
Furnishing	$0.412 n_{pax}^{1.145} w_{to}^{0.489}$	Cessna

Finally, a note on computing the fuselage weight is required. As can be seen in Table 8.6, two equations for the fuselage weight are available dependent on the wing configuration. The J1 design concept has a high-wing configuration thus the corresponding equation should be utilized. However, the L1 and W1 design concepts have tandem wings positioned in both low and high-wing configurations. In order to accommodate this feature, the value between the high and low wings is averaged. After convergence of the designs, the results are as shown in Table 8.7 and Table 8.8 for L1 and W1, and J1 respectively.

[2] Simplified from the original Cessna method for the landing gear.

Table 8.7: *Final result of the class II weight estimation after convergence of the design concept had been completed.*

Component	L1 [kg]	W1 [kg]
Front Wing	149.3	335.1
Back Wing	555.09	365.9
Fuselage	287.9	254.6
Landing gear	185.9	136.7
Powertrain	314.3	167.9
Power system	1455.03	816.7
Nacelles	321.2	171.6
Miscallenous [3]	434.7	333.9
OEM with 10% contingency	4073.9	2840.6
Payload	510	510
Total	4583.9	3350.6

Table 8.8: *Final result of the class II weight estimation of J1 after convergence of the design concept had been completed.*

Component	J1 [kg]
Wing	234.8
Horizontal Tail	30.7
Fuselage	267.7
Landing gear	83.4
Powertrain	61.8
Power system	404.9
Nacelles	63.2
Miscallenous [3]	220.8
OEM with 10% contingency	1504.08
Payload	510
Total	2014.1

In conclusion, the J1 design option is significantly lighter primarily due to its lower mission energy consumption, which reduces the weight of the hydrogen system. On the other hand, L1 becomes excessively heavy due to high energy consumption, leading to a snowballing effect on all other weight components. This further increases energy consumption and results in a significant weight increase for L1. It should be noted that the snowballing effect may not be as severe in reality, as the miscellaneous weight component would not change significantly across design concepts. However, the Cessna and Torenbeek methods estimate these weight components based on take-off weight, causing a divergence in the miscellaneous weight component. Despite this divergence, no suitable alternative was found, and the decision was made to continue using the Cessna and Torenbeek estimations. Furthermore, an increase in take-off weight may lead to unforeseen weight penalties for the sub-components within the miscellaneous component.

8.7. Convergence

When designing an aircraft, there is no predetermined sequential manner for computing the aircraft parameters. Instead, one aims to compute the various subsystems in a way that minimizes feedback. In the case of Aetheria, the order illustrated in Table 2.1 was chosen. Although this order limits the amount of feedback, it is still present. Therefore, it was necessary to iterate through the various subsystems multiple times to ensure that all designs converged. A divergent design would be infeasible and not meet the expected weight and performance requirements. The convergence history of J1, L1, and W1 is depicted in Figure 8.7.

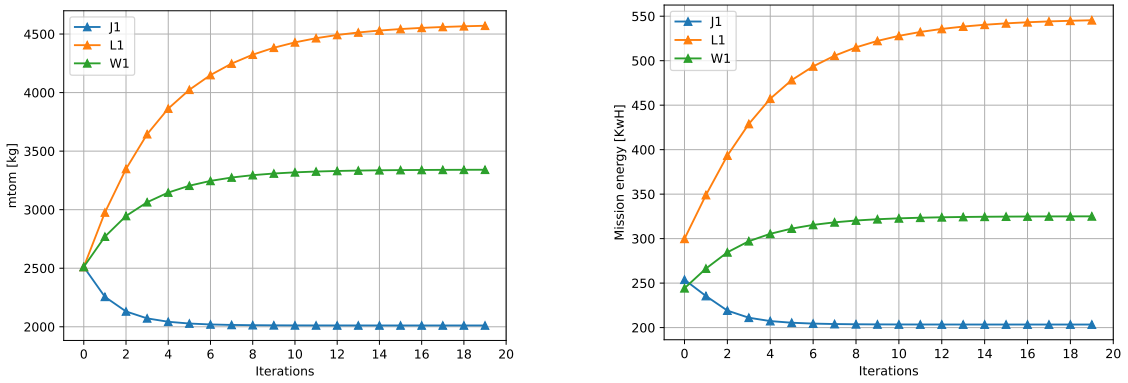

(a) *Convergence history of the MTOM of all design concepts*

(b) *Convergence history of the energy consumption of all design concepts*

Figure 8.7: *Two parameters illustrating the convergence history of the Aetheria Package*

As can be seen from Figure 8.7a, the weight of the various design concepts can safely be assumed to have converged. It can be noted that the L1 and W1 take longer to converge as they have a larger offset from the

[3] Contains Flight Control system, Electrical system, Instrumentation & Avionics, Air Conditioning and Furnishing

initial class I weight estimation, resulting in the snowball effect being stronger for their design. The design concept can hence safely be assumed to meet the performance requirements set.

8.8. Crashworthiness Study

Comparing the different designs on their crashworthiness is an important part of the trade-off. Regulations and certifications have long been present in the aircraft industry to make sure safety is always guaranteed, especially because crashes can have serious consequences. EASA has recently released some safety regulations for eVTOLs [6], including a part on crashworthiness [28]. This is a big step because, in the past, manufacturers would take regulations from small aircraft (CS23) and rotor-craft (CS27). This is due to no regulations being present on eVTOLs yet. The main trade-off criteria are listed below and are taken from the above-mentioned regulations and the requirements determined in the baseline report.

Post-crash fire

This mainly constitutes that the chances of a fire breaking out should be minimized with different measures. Mainly since eVTOLs make use of batteries or fuel cells and these have a risk of catching fire after a crash as the integrity of their storage might get compromised. Batteries also have a special condition that they should be isolated from the cabin, to eliminate the risk of a sudden release of energy which could electrify the cabin. Conditions state that any flammable energy source should be kept away from ignition sources as much as possible. Energy sources should also be placed as far away from the cabin as possible, including separation by a firewall[4]. Hydrogen tanks feature a special release valve, this system notices if the integrity of the tank has been compromised in case of a crash. Detecting whether the integrity has been compromised could be performed utilizing Fibre-Optic Sensors (FOS) embedded into the composite structure of the tank. According to Güemes et al., FOS have reached a technology readiness level of 8-9 as strain sensors [29]. By measuring strains given by the embedded FOS, damage within the tank's structure can be predicted. Article [29] presents two methods for translating strains into a damage detection model. However, discussing these methods is beyond the scope of the midterm report. Once damage has been detected, it results in the valve slowly releasing the hydrogen to lower the pressure and decrease the risk of an explosion. Since a compromised fuel tank might not be able to handle all of the hydrogen content, it is preferable to slowly release the hydrogen in a controlled fashion instead of a catastrophic failure where all of the hydrogen is released at once[5].

Engine & wing configuration

Since the fuselage design and the fuel system is roughly the same for all of the different concepts, the crashworthiness study will for now mainly focus on the different wing and engine configurations. The crashworthiness of the engines mainly depends on the size and speed of the propellers since these introduce a risk. This is the risk of fragments with high energy being released and possibly endangering the aircraft and its passengers in case of failure as shown in Figure 8.8a. In this case, the aircraft suffered a bird strike causing loss of a propeller blade. Due to the high momentum of the blade it completely penetrated into the cabin (no occupants were injured). The L1 concept has small ducted fans (total area of $4[m^2]$), resulting in the lowest risk. While the J1 has the highest risk since this features 6 large propeller rotors ($17[m^2]$). The Wigeon poses a moderate level of risk as its propellers are smaller than the propellers of J1 ($10[m^2]$). However, still significantly heavier than L1.

[4] Accessed May 17th 2023, https://www.easa.europa.eu/sites/default/files/dfu/moc-2_sc-vtol_-_Issue_1_-_23-06-2021.pdf

[5] Accessed May 17th 2023, https://www.hydrogenfuelnews.com/how-safe-are-hydrogen-fuel-cell-vehicles-in-a-crash/8539783/?utm_content=cmp-true

(a) *Propeller detachment resulting from a birdstrike: The damage on a BAE Jetstream 41.* [6]

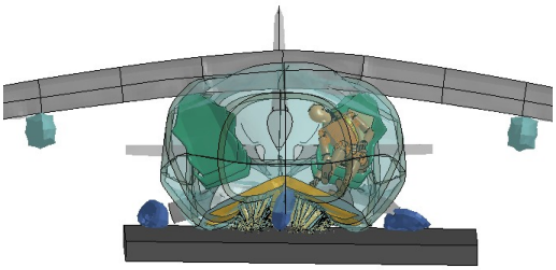

(b) *Structural Deformation of a Lift-Plus-Cruise eVTOL Aircraft under 10.6 [m/s] Vertical Loading [30]*

Figure 8.8: *Figures illustrating complications of the wing and engine configuration.*

The different wing configurations each have a score as well. Low-wing configurations are generally not preferable since the structure goes through the fuselage. Since wing structure are comparably stiff, it is not useful for absorbing crash energy, instead it will be introduced into the cabin. Additionally, no space is available to install deployable energy absorbers (DEA). These DEAs are materials that are put below the cabin to protect the passengers in case of a crash [31], DEAs are further discussed in the section below.

High-wing configurations are also not always feasible. Having a structure above the cabin introduces new calamities. In case of a crash landing, the inertia of the wing will exert a downward force on the fuselage, which would increase the amount the fuselage is crushed, thus reducing the safety of the passengers [30]. However, Ryan Miller suggests a controlled wing failure mechanism can be used to shed the wing and nacelle mass in crash landings [32]. This would allow the fuselage to retain more of its usable cross sectional area.

Mid-wing aircraft are the safest in case of a crash, but this has it's own disadvantages. Mid-wing configurations require additional structural strength since the wing box can't be made out of one piece because it is interrupted by the cabin. The configuration comparison and trade-off score justification of each design can be found in Section 8.9.

Energy Absorption System

The eVTOL requires an energy-absorbing structure beneath the cabin for passenger safety, as depicted in Figure 8.9a. A preliminary estimation of this rectangular box crash structure with a honeycomb structure and isentropic properties is discussed. The structure aims to absorb all kinetic energy by allowing for significant travel distance, thereby reducing in-cabin decelerations. Crash absorption is guided by maximum deceleration in g's (a) and kinetic energy. The maximum deceleration depends on crash velocity and vertical displacement of the crushed structure. The crushed state of the crash structure, which remains the same across all configurations, is illustrated in Figure 8.9b. This aspect will not be considered in the trade-off.

(a) *Deployed Energy Absorbers in Pre-Crushed State [33]*

(b) *Deployed Energy Absorbers in Crushed State [33]*

Figure 8.9: *Deployable Energy Absorber System*

[6] Accessed May 31th 2023, https://aerossurance.com/safety-management/j41-birdstrike-propeller-mine/

Crash absorbing energy shall be equal to the kinetic energy and is given by:

$$E_k = \frac{1}{2}mv^2 \quad (8.16) \qquad E_{cr} = \sigma_{cr} As = \sigma_{cr} A \frac{v^2}{2a} \quad (8.17) \qquad A = \frac{ma}{\sigma_{cr}} \quad (8.18)$$

Where v is the crash velocity, A is the required area, σ_{cr} the compression strength and s the crash structure displacement. Equating and rewriting these formulas gives Equation 8.18 for the crash-absorbing structure's area. The compression strength is based on the material chosen and can be assumed the same for each configuration for comparison purposes. The deceleration is set by EASA requirements and the required area is therefore mostly dependent on the maximum take-off mass. A higher required area is not necessarily worse, but it should fit under the cabin. A preliminary calculation of the required area is therefore conducted. The requirement is that cabin loads should not exceed 30 g at an impact velocity of 9.1 [m/s] [34]. This leads to a deceleration distance of 141 [mm]. Which, according to Figure 8.5, leads to a maximum energy absorption structure width of 590 [mm]. The required area is calculated with Equation 8.18. The compression strength is assumed to be 0.315 [MPa] [35].

The required length for the deployable energy absorbers will in this scenario be 1.59, 3.63 and 2.65 [m] for J1, L1 and W1 respectively This will fit under the cabin for J1 and W1, but L1's required length exceeds the cabin length of 3.25 [m]. L1 would therefore need a fuselage or crash structure redesign. Next to that, a larger crash structure increases the structural weight.

8.9. Crashworthiness Criterion Scores For Different Designs

Just looking at these stresses J1 comes out as the best. Quantifying this into the trade-off categories is done by assuming that the lower loads will lead to a lighter structure. This lighter structure will mainly have an effect on the crashworthiness and the mission energy which are described below. The crashworthiness has been described above in Section 8.8 and it will be concluded below. The mission energy will be elaborated more on in Section 9.3.

In conclusion, there is no clear winner. Regarding the wing configurations, J1 performs the worst. It sports a high-wing configuration which might push down on the cabin in case of a crash, it does however provide room for DEAs beneath the cabin. The high-wing configuration danger can also be mitigated by making use of a new mechanism that allows the wing root to break in case of a crash so the energy is not released into the cabin[32]. L1 and W1 have both high and low wings but they are placed away from the cabin so the high wing does not push down on the cabin and there is still space for DEAs. With the propellers, J1 also performs the worst, it has large propellers which will introduce high energy fragments flying around. W1 is in the middle and L1 is the safest as it has small ducted fans. However, the weight of J1 is much lower so this will greatly reduce the amount of kinetic energy which will have to be absorbed by the DEAs. As shown in Section 8.8, L1 has correctable deficiencies regarding the crash energy absorbing structure and gets a score of 1 for crashworthiness. J1 and L1 are both not optimal for crashworthiness, but meet all requirements without correction. They, therefore, receive a 2 as their score.

8.10. Sensitivity Analysis

For the stresses, the root chord is a very important variable. This is because for now the geometry is based on fractions of the chord. Doubling or halving the chord results in a maximum shear stress change of -55% and 144% respectively. The same procedure results in a maximum axial stress change of -75% and 300% respectively. Especially for the latter stress the values change dramatically so the chord length very important for the stresses. Skin thickness is a factor that influences the stresses as well, especially the critical buckling load. The thing however is that for the final design, stringers will be included. These stringers will carry the axial loads so it is not necessary to increase the skin thickness, that is why it is not in the sensitivity analysis

8.11. Verification and Validation

This is crucial to make sure the code and the simulations that have been used are trustworthy. If this is not present, one can not assume the aircraft has any structural integrity.

8.11.1. Verification
Up until now, the verification has mostly consisted of writing unit tests and applying engineering judgment to the values that have been computed. The internal stresses have been verified with simple FBDs to check whether the signs obey the right-hand rule. In reality, more verification is needed than this to verify the values. It can also be done by using more sources for the equations and values for the materials used.

8.11.2. Validation
This plan is easier as it mainly consists of testing the load cases. The wing box can be simplified to a simple cantilever beam with a point load or a distributed load. Other tests can also be described and performed to validate the results. They will never be exactly right but this is due to the assumptions that are made and the simplification of the model. This can of course be mitigated by making the model more elaborate and detailed. Another way to validate the results is by using validated Finite Element Analysis (FEA) software.
It has to be taken into account that these values are determined by preliminary guesses of the wing box geometry. Since these are dependent on the chord length and the thickness-to-chord ratio and the assumed ratios for the height and width of the wing box. These do provide a proper comparison between the loads for the configurations so a trade-off can be performed for these.

9
Power Source

In this chapter, trade-offs will be done on the power source subsystems. For power, first, a trade-off will be performed to choose the suitable power concept for the design which will be followed by doing a trade-off between the different fuel cells, batteries, and hydrogen storage.

9.1. Power Options
The two most promising options that made it to this point are the use of hydrogen fuel cells (with battery for hovering) and the hybrid option (with battery for cruise and hovering) as a power source. The battery-only option for the whole mission will also be analysed as means of mass comparison between the two main options. Both options will first be looked at in detail and then a decision will be made following a trade-off on which option is better for the design. An adapted version of the Wigeon design software will be used for comparison of the power design options [4].

Hydrogen Cruise - Battery Hover
This option relies solely on the usage of hydrogen and fuel cells as a power source for the cruise and climb/descend phases, which are the most energy-demanding. However, batteries will also always be required for fuel cell start-up, to power onboard electronics during fuel cell start-up, for hovering which is power demanding, for throttle response since batteries have a swift response and to match the demand from the electric motors [16]. In other words, the power system sizing for trade-off will be done by sizing the batteries for hovering; whereas, the sizing for hydrogen (hydrogen, tanks, fuel cells) will be made for the rest of the mission excluding hovering.

Hybrid Cruise
In the hybrid option, batteries will be used for the reasons stated in the previous subsection as well as for part of the cruise. The optimum division between batteries and fuel cells will be computed and used to compare this design option with the hydrogen fuel cell option in Section 9.3.

9.2. Power Source Trade-off

In this section, trade-offs will be made regarding the type of battery, fuel cell and hydrogen storage. First, the criteria for comparison will be determined, assigning weights based on their design importance. Then, a trade-off table will be created to compare these criteria across different configurations. The table will use the colour coding and scores as shown in Table 9.1.

Table 9.1: *Scores for the colour coding*

Green	Blue	Yellow	Red
Excellent - 3	Very Good - 2	Acceptable - 1	Undesired - 0

It is important to note that the weight of each criterion is graded relative to the other options. Hereafter, a score will be calculated for each configuration to establish a quantitative comparison. The score will be calculated by multiplying the score of the option by the weight of the parameter. These values obtained for all parameters will be summed up to obtain a total value for each configuration. After completion, a decision will be made on the type of configuration for the battery, fuel cell and hydrogen storage system based on the results from the trade-off.

9.2.1. Battery Trade-off

Following the Design Option Tree, three different battery types were considered for further analysis and trade-off. These were, Lithium-ion and solid-state batteries and supercapacitors. In addition, Lithium-sulfur batteries will also be analysed and included in this trade-off since it has promising potential [4]. This trade-off will consist of quantitative and qualitative analysis. Following a literature study, Table 9.2 contains values found for the parameters for the different battery types.

Table 9.2: *Characteristics of different battery types*

Parameter	Li-ion [1] [2] [36]	Li-sulfur [3], [37], [38]	Solid State [4], [39], [40]	Supercapacitor [5] [36] [41]
P. Density [kW/kg]	3	10	10	10
E. Density [kWh/kg]	0.3	0.422	0.4	0.015
V. Density [kWh/L]	0.45	0.4	1	0.113
Cost [$/kg]	30.3	61.1	82.2	150
Life [cycles]	1000	1000	10000	10000

From the parameters mentioned in Table 9.2, the power density (P. Density) is crucial as it is the main parameter used for sizing the batteries for the hover phase. Furthermore, to size the batteries for cruise, energy density (E. Density) will be looked at. Following the sizing of the batteries for a particular phase, the volume of batteries can be calculated using the volumetric energy density (V. Density). Finally, cost and lifetime can also be seen.

For a perfect design, the highest power and energy densities are desired since high values in these parameters will result in less battery mass needed to satisfy the mission power and energy requirements. Furthermore, high volumetric density is also desired since this would result in the smallest battery volume meaning smaller space would be necessary to fit the batteries. A high lifetime is desired since it would mean that the battery will need to be renewed after longer periods resulting in lower maintenance costs. Furthermore, having the lowest cost per kg is preferred since it would result in the cheapest design resulting in lower production costs and thus cheaper tickets.

For the qualitative part, the two important considerations to take into account are safety and technological readiness level (TRL). TRL will be applied as a strong pass-or-fail criterion following the trade-off scores,

[1] Accessed May 12th 2023, https://eepower.com/capacitor-guide/types/supercapacitor
[2] Accessed May 12th 2023, https://www.ionblox.com/air
[3] Accessed May 12th 2023, https://news.umich.edu/1000-cycle-lithium-sulfur-battery-could-quintuple-electric-vehicle-ranges/
[4] Accessed May 12th 2023, https://www.etechnophiles.com/solid-state-battery/
[5] Accessed May 12th 2023, https://eepower.com/capacitor-guide/types/supercapacitor

whereas, safety will be given a weight and included in the trade-off.

To perform a balanced trade-off between all aspects, criteria must be assigned appropriate weights. The power density is crucial because battery sizing is based on power requirements. Energy density and safety are the next important criteria to ensure sufficient energy during hover and to prevent explosions. The cost and life were given the same weights since the cost of batteries is a very small portion of the unit variable cost (less than 1% from Chapter 13). Life is given the same weight as cost because they both influence the unit variable cost and go hand in hand. The volumetric density was given the same weight as cost and life since it does not outweigh the rest. The weights, on a scale of 1 can be seen in Table 9.3:

Table 9.3: *Weights of the Battery trade-off Criteria*

Power Density	Energy Density	Safety	Volumetric Density	Life	Cost
0.4	0.15	0.15	0.1	0.1	0.1

Following the weight assignment, a trade-off table can be seen in Figure 9.1.

	P. Density	E. Density	Safety	V. Density	Life	Cost
Lithium-Ion	Blue	Blue	Yellow	Blue	Yellow	Green
Lithium-Sulfur	Green	Green	Blue	Blue	Yellow	Blue
Solid State	Green	Green	Green	Green	Green	Blue
SuperCapacitor	Green	Red	Green	Yellow	Green	Yellow

Figure 9.1: *Battery Trade-Off Table*

The colour coding in Figure 9.1 follows from Table 9.1. As can be seen from Figure 9.1, Solid-state batteries seem to have the best overall performance, however, them being not very technologically ready (TRL) is an important consideration. To make the comparison more quantitative, an overall score can be calculated for each battery type. This will be done using the method discussed in Section 9.2. By doing this, the overall scores are the following:

Table 9.4: *Scores of different battery configurations*

Lithium-ion	Lithium-Sulfur	Solid-State	Supercapacitor
1.85	2.45	2.9	2.15

As can be seen from the total scores, solid-state batteries seem to be the best followed by lithium-sulfur, supercapacitors and finally lithium-ion. As mentioned before, TRL is a pass/fail criterion and thus lithium-sulfur batteries will be automatically discarded. Furthermore, solid-state batteries are also not developed enough. However, as they have the highest potential and overall score, they will also be analysed later on in the power sizing system for possible future designs. Super-capacitors, on the other hand, are more developed than lithium-sulfur and solid-state batteries but have extremely low energy densities. This is infeasible since, even though, they have high power densities to supply the high power requirement for hovering, the low energy densities would result in an unfeasible heavy design. Therefore, by discarding this option, the only remaining feasible design option is lithium-ion batteries, although obtaining the lowest score. This is a consequence mainly due to the hard pass/fail criteria imposed by the TRL. As aforementioned, for the sake of completeness and possible futuristic designs, solid-state batteries will also be analysed in Section 9.3 as they have the highest score.

9.2.2. Fuel Cell Trade-off

Currently, there are many types of fuel cells, however, the ones presented in Design Option Tree were; Polymer Electrolyte Membrane (PEM), Alkaline (AFC), Phosphoric acid (PAFC) and Solid Oxide (SOFC) fuel cells. In order to decide which out of these 4 is the best and most suitable for the design, a trade-off will be performed similar to the battery trade-off. Following a literature study, information obtained regarding the characteristics of the different fuel cells can be seen in Table 9.5.

Table 9.5: *Characteristics of different Fuel Cells*

Parameter	PEM, [6], [42], [43]	AFC, [6], [44], [45], [43]	PAFC, [6], [7], [46], [43]	SOFC, [6], [47], [43]
Operating Temp [°C]	60-110	70-130	175-210	500-1000
Power Density [mW/cm^2]	300-1000	150-400	150-300	250-350
Electrical Efficiency [%]	55	70	45	72
Cost [$/kW]	75	175	4000-4500	2400
Safety	Safe	Safe	Safe	Safe
TRL	Most Mature	Mature	Mature	Mature

In terms of safety, all the fuel cells are considered safe due to not involving combustion. However, it is important to note that the potassium hydroxide electrolyte in the AFC and the phosphoric acid electrolyte in the PAFC are corrosive. This does not make them unsafe but rather considered to be handled with higher caution.

In terms of technological readiness level, all of the fuel cells considered are at a mature level allowing for use in designs. One assessment tool that considers all previous TRL assessment tools is the fuel cell technology readiness level (FCTRL). According to the FCTRL, the fuel cells considered are above level 5 and into level 6, bringing the risk down to 20% [48]. However, out of all these options, the PEM fuel cells are the most developed [48] and widely used technology currently, especially in transportation-related activities [8]. Thus, PEM fuel cells have a slight advantage in this aspect with respect to the rest in the trade-off.

The fuel cell operating temperature, power density and efficiency are equally important as they all have equal influence on the number of fuel cells that will be needed to comply with the energy requirement for cruise. A low operating temperature is desired [49] in order to supply as little power as possible to the fuel cell for it to start operating, even though a higher operating temperature is better for cooling applications. Furthermore, high efficiency is desired so that the amount of power loss is minimum. High power density is also desired as it reduces the fuel cell's weight. Once again cost is of low importance as fuel cell cost is less than 1% of the unit variable cost from Chapter 13. Safety is weighed low since all of the fuel cells are considered safe with very minor differences. TRL on the other hand will not be given weight since all of them pass the hard pass/fail condition; with PEM cells having a slightly higher TRL, which will be used as a qualitative analysis. The criteria considered in the trade-off and their respective weights are therefore seen in Table 9.6, followed by the trade-off seen in Figure 9.2.

Table 9.6: *Weights for Fuel Cell trade-off*

Operating Temperature	Power Density	Efficiency	Cost	Safety
0.25	0.25	0.25	0.15	0.1

Table 9.7: *Fuel Cell scores*

PEM	AFC	PAFC	SOFC
2.75	2.6	1.3	1.3

	O. Temperature	Power Density	Efficiency	Cost	Safety
PEM	Green	Green	Blue	Green	Green
AFC	Green	Blue	Green	Blue	Green
PAFC	Blue	Yellow	Yellow	Red	Green
SOFC	Red	Yellow	Green	Red	Green

Figure 9.2: *Fuel Cell trade-off Table*

From the table, the PEM fuel cells seem to be the best option, however, for a better comparison, a more quantitative result can be used by calculating a score for each fuel cell. The method previously described will be used. By doing this, the overall scores can be seen in Table 9.7:
Based on these overall scores, PEM fuel cells indeed seem to show the most promising score with alkaline fuel cells closely behind. Since PEM has better power density, is cheaper than AFC, has slightly higher TRL,

[6] Accessed May 15th 2023, https://www.energy.gov/eere/fuelcells/comparison-fuel-cell-technologies
[7] Accessed May 15th 2023, https://phosphoricacidfuelcells.com/
[8] Accessed May 15th 2023, https://www.energy.gov/eere/fuelcells/comparison-fuel-cell-technologies

as well as higher overall score, it is preferred, even though it has lower efficiency. Therefore, to conclude this trade-off, PEM fuel cells are the best type for this design and thus will be used.

9.2.3. Hydrogen Storage Trade-off

There are two different methods to store hydrogen, either by liquefying it or by compressing it using really high pressure. The former will require cooling the hydrogen to cryogenic temperatures of below 33K and storing it at approximately 20K; whereas, the latter can be achieved by compressing the hydrogen using pressures between 350 to 700 bars. Furthermore, there is also a new type of storage method that combines the previously mentioned 2 methods; namely, the cryo-compressed hydrogen method.

This trade-off will be performed by gathering data from a literature study about compressed and liquid hydrogen tanks and implementing the results into the python script for power system sizing used in Section 9.3. Later, the results obtained from the python script for the two storage methods are compared. To make this comparison using the python script, the data obtained from the literature study that was implemented into the script can be seen in Table 9.8.

Table 9.8: *Hydrogen Tank Characteristics*

Type	Tank E.density [kWh/kg]	V.Density [kg/L]
Liquid [9]	6.666	0.271
Cryo-compressed [10]	1.550	0.627
Compressed -700 bar [10]	1.91	0.695
Compressed-350 bar [10]	1.784	0.435

Based on these values obtained, all the storage options seem similar, with the exception of the liquid storage option, which seems to show higher energy density and lower volumetric density compared to the rest. Therefore, this seems like the best option since it would result in the lowest tank mass and volume. However, for a more specific analysis, a trade-off table can also constructed that can be seen in Figure 9.3 based on a performed literature study [50] [51] [52] [53].
To construct the trade-off table, the criteria for comparison have to be given weights. The volumetric density refers to how much mass of hydrogen can be stored in a given amount of volume in [kg/L]. Safety is crucial too as hydrogen is highly explosive. Energy loss [%] refers to the loss of energy content due to the processes of cooling and compressing. The energy required refers to the amount of energy necessary for the liquefaction and compression processes. Efficiency [%] is the loss of energy in terms of heat due to the type of insulation of the tank. Boil-off losses are the inevitable loss of hydrogen in the form of evaporation "due to heat flow from the environment into the tank" [50]. The cost once again is not a very important factor since the storage cost is a very small portion of the unit variable cost Chapter 13. TRL was not considered as a criterion, since both storage options are technologically ready except the cryo-compressed storage. However, this option is also being considered despite not being at a sufficient TRL [50], for possible applications in the future when it is technologically feasible. For the construction of the table, the given weights for each parameter can be seen in Table 9.9:

Table 9.9: *Weights for storage trade-off*

Volumetric Density	Safety	Energy loss	Efficiency	Energy required	Boil-off loss	Cost
0.2	0.2	0.15	0.15	0.1	0.1	0.1

	V. Density	Safety	Energy Loss	Efficiency	E. Req.	B.Off Loss	Cost
Liquid	Blue	Green	Yellow	Green	Blue	Yellow	Blue
Compressed	Yellow	Blue	Green	Blue	Green	Blue	Green
C-L	Green	Green	Green	Blue	Yellow	Green	Yellow

Figure 9.3: *Storage Trade-Off Table*

[9] Accessed May 15th 2023, http://hylium-industries.com/tank
[10] Accessed May 15th 2023, https://hyfindr.com/

To get a more overall result, a score can be calculated for each type using the method discussed in Section 9.2. The results can be seen in Table 9.10:

Table 9.10: *Storage scores*

Liquid	Compressed	Compressed-Liquid
2.1	2.15	2.45

As can be seen from the overall scores, the combination of compressed and liquid seems to be the best option, however, the cost of this storage method as well as the infrastructure is currently a major problem since it is not fully developed, thus, limiting the viability of this option [50]. Therefore, for current designs, this option will be neglected and looked at in the future with the advancement of technology and infrastructure. From the remaining two options, both seem to be similarly good with compressed being slightly better. Furthermore, it is important to note that current vehicles mainly use compressed hydrogen tanks as a storage method [54], thus, this option seems a bit better as it is a method already tested on vehicles. Furthermore, a liquid storage system is a far more complex system than a compressed hydrogen storage system since it is much more difficult to cool the hydrogen and keep it at cryogenic temperatures rather than compressing it. This aspect was not included in the trade-off as it can not be quantified. Therefore, to avoid this complexity a compressed storage would be preferred and chosen. This conclusion was further justified by an engineer responsible for fuel cells and storage methods at Zeroavia following a meeting.

9.3. Power Sizing

In this section, the initial mass and volume of Aetheria's power system will be estimated. This will be done for the three concept designs mentioned in Section 9.1. Furthermore, there are three load cases that the power system should be sized for. These are the average power during cruise, peak power, and total mission energy.

Hydrogen has a very high energy density (33.3 kWh per kg) compared to the battery (0.3 kWh per kg). However, this does not take into account the weight of the tank in which the hydrogen is stored. Therefore, it is better to use the energy density of the hydrogen tank to do the sizing. The energy density of a hydrogen tank can be calculated with Equation 9.1. m_{h2} is the mass of the hydrogen that can be stored in the tank, $m_{empty,tank}$ is the mass of the empty hydrogen tank and $(E_{sp})_{h2}$ is the energy density of hydrogen.

$$(E_{sp})_{tank} = \frac{(E_{sp})_{h_2} \cdot m_{h_2}}{m_{h_2} + m_{empty,tank}} \tag{9.1}$$

At this point, the fraction ν is introduced which relates the amount of power coming from the fuel cell to the average power during cruise flight. If $\nu = 0$, then all the power comes from the batteries during cruise and if $\nu = 1$ all the power during cruise comes from the fuel cell. Since the cruise power has a much longer duration than the peak power it is assumed that most of the total is consumed during cruise at this stage. Using this, the mass of the hydrogen tank and the battery due to the mission energy can be calculated with Equation 9.2 and Equation 9.3.

$$m_{Tank} = \frac{E \cdot \nu}{(E_{sp})_{tank}} \frac{1}{\eta_{FC}} \tag{9.2}$$

$$m_{bat} = \frac{E \cdot (1-\nu)}{(E_{sp})_{bat}} \frac{1}{\eta_{bat}} \tag{9.3}$$

The fuel cell mass can be derived using the power required during the cruise segment and the power density of the fuel cell. This can be seen in Equation 9.4. Initially, the power density of the fuel cell is estimated using statistical data from hydrogen fuel cells that are available on the current market.

$$m_{FC} = \frac{P_{cruise} \cdot \nu}{(P_{sp})_{FC}} \tag{9.4}$$

$$m_{bat,cruise} = \frac{P_{cruise} \cdot (1-\nu)}{(P_{sp})_{bat}} \tag{9.5}$$

The fuel cell requires additional systems to work. These subsystems supply the hydrogen and air to the fuel cell and also do thermal management for the fuel cell. The weight of these subsystems is not trivial. It was found after a discussion with a fuel cell engineer at ZeroAvia that the weight of the fuel cell subsystems is approximately the same as the weight of the fuel cell itself. The estimated mass of these subsystems will be re-evaluated in the detailed design phase. The battery size required for power requirement during cruise is estimated in the same way. This results in Equation 9.5

The battery sizing for the peak power consumption for the concepts are done with Equation 9.6. It is important to note that by using these equations, it is possible that most of the peak power will come from the fuel cell. In that case, the numerator of Equation 9.4 should be rewritten to use the power that is desired from it during the hover phase.

$$m_{bat} = \frac{P_{peak} - P_{FC,max}}{(P_{sp})_{bat}} \quad (9.6) \qquad m_{power} = m_{FC} + m_{Tank} + m_{FC,subsystems} + max(m_{bat}) \quad (9.7)$$

The mass of the power system can be calculated by adding the mass of the battery, fuel cell, hydrogen tank and the fuel cell subsystems. The mass of the battery is the maximum of the battery mass calculation from Equation 9.6, Equation 9.5 and Equation 9.3. This can be seen in Equation 9.7. The relation between the fuel cell cruise power fraction and the mass of the power system can be calculated. It is clear from Figure 9.4 and Figure 9.5 that there is a value of ν for which the power system mass is minimum. The location of this minimum is dependent on the maximum requirements for Aetheria and the relation with the battery size for it. The battery power requirements results in the battery carrying quite a significant amount of energy. However, hydrogen is way more efficient in carrying energy and thus carrying energy in the battery is not beneficial. This can be seen best in Figure 9.4 as there the low power density of the lithium-ion battery greatly shows this effect between the three different designs.

The J1 has the lowest maximum power requirements which results in the ν being closest to the 1. The W1 and L1 follow logically on the basis of the maximum power required. This is confirmed when comparing Figure 9.4 with Figure 9.5 for each design separately. This clearly indicates that for a higher battery power density (solid-state battery has an advantage of around 300%) the location of the minimum power system mass is closer to $\nu = 1$. Therefore, increasing the power density of the battery shifts the value of ν closer to 1 which is beneficial for the weights as relatively more energy is stored in the form of hydrogen.

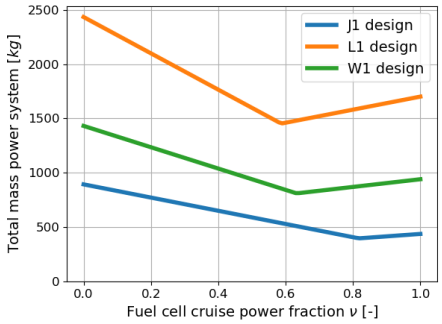

Figure 9.4: *Power system mass depending on the cruise power fuel cell fraction with lithium-ion battery*

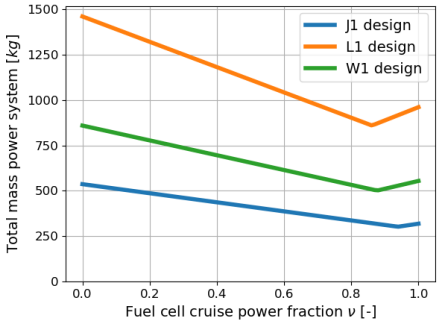

Figure 9.5: *Power system mass depending on the cruise power fuel cell fraction with solid-state battery*

However, the simple fact that the mission energy requirements significantly affect the value of ν for the minimum power system mass as well. This can be seen in Figure 9.4 where the location of the minimum power system mass for the W1 and L1 design is relatively close to each other while there is a significant difference in maximum power required. This happens because the larger amount of mission energy reduces the fraction of energy stored in the batteries which is due to the maximum power requirement. Therefore, the fraction of energy stored in hydrogen is increased which raises the fuel cell cruise power fraction.

Finally, the volume required to store hydrogen can be a limiting factor due to its low density. It has to be shown that the volume of the power system is reasonable to fit within the aircraft considering that the hydrogen has to be stored in the fuselage. The general equation to calculate the volume of the specific subsystem is given in Equation 9.8 where E_V and m are the volumetric energy density and mass for the specific power subsystem.

$$V = \frac{E_{sp}}{E_V} m \quad (9.8)$$

It was found that with compressed hydrogen the volume for the J1 design is in the range of 400 to 500 liters depending on storage pressure. This is not limiting and therefore Aetheria will be using a storage pressure of 350 bar.

9.4. Final Power Source Trade-Off

From the trade-offs performed earlier and the python script used for the sizing of the whole power system, a final trade-off can be performed in which the final choices for the battery, fuel cell, and hydrogen storage type can be made.

From Section 9.3, for battery type, it can be seen that usage of lithium-ion batteries suffices for now as it does not result in a heavy design. Although, clearly, solid-state batteries result in a lighter design with a 25% deduction in power system mass for J1, showing its high potential for the future. However, for now, from battery trade-off results and the power system sizing conclusions, a lithium-ion battery is the final choice to be used in the design of Aetheria. From the fuel cell trade-off, the clear winner was the polymer electrolyte membrane (PEM) fuel cell. Therefore, other options were not even considered during the power system sizing. As a result, PEM fuel cells will be the final choice for this design. Finally, following the trade-off for the storage method, the compressed hydrogen storage system was preferred over liquid. The use of compressed hydrogen storage was also feasible in terms of power system mass and volume. Therefore, Aetheria will use a high-pressure storage system to store the hydrogen in a compressed form at 350 bar. A summary can be seen in Table 9.11

Table 9.11: *Final Choices for the Power System*

Battery	Fuel Cell	Storage
Lithium-ion	PEM	350 bar compressed Hydrogen

9.5. Verification and Validation

The different verification and validation methods performed for this chapter will be discussed in this section. The power sizing code will be verified by using system tests and unit tests. Furthermore, a verification and validation plan will be discussed to be implemented for the final report.

For the power sizing system test, it is checked whether the energy in the battery and in the hydrogen is equal to or larger than the required mission energy. Obviously, it would be best if the required energy is the total energy that is stored in the system. Second, it is checked whether the fuel cell and the battery are capable of at least providing the required cruise power and hover power.

The functions that are responsible for power system sizing for a specific segment of the mission profile are verified that they conserve energy and power. Furthermore, it is checked that they produce logical results. For example, if all the power during the cruise is coming from the fuel cell, then the mass of the battery should be zero for the cruise segment and vice versa.

In addition to verification, validation should also be performed in order to make sure that the results obtained have credibility. Given the significant divergence of Aetheria's power source from existing eVTOLs, a direct comparison of results would be inefficient due to the usage of hydrogen as a primary source of power. Therefore, viable validation would be to use the models to size the power systems of both hydrogen-powered cars and battery-powered existing eVTOLs. This compares our model predictions to existing designs for both the battery and hydrogen aspects of the power system. This method of validation is known as comparison.

10
Propulsion & Power

In this chapter, the propulsive subsystems in terms of disk theory, power and noise will be compared and scored for each conceptual design.

10.1. Propulsive Configuration for Each Design

The J1 is a tilt-rotor design with two large rotors on each wing and with smaller rotors on each horizontal stabilizer. All rotors can tilt, meaning they can be used for all mission phases. The L1 features distributed podded engines on its tandem wings that can tilt. The number of engines is an optimization parameter. For the W1 a tandem wing is also used, each wing with its own distributed rotors. The number of rotors on each wing will be optimized, thus there is no constraint.

10.1.1. Propulsion Factor Effects on Designs

In Table 10.1 the propulsive factors are listed, and how each design measures relative to these factors. Once the advantages and disadvantages are listed, quantitative measures will be used to contrast the different designs with respect to the propulsive factors. The factors used, and some of the (dis)advantages have been taken from the Wigeon group [4].

Table 10.1: *(Dis)advantages of Each Configuration*

	J1 - Large Rotor System	L1 - Ducted Pod System	W1 - Distributed Rotor System
Noise	- The large rotors emit a lot of noise, with minimal opportunities to reduce noise	+ The ducted pods can mask the noise using acoustic liners	- The distributed rotors emit a lot of noise, with minimal opportunities to reduce noise
Engine Placement	± The front rotors have good placement but the aft rotor is likely to be affected by the slipstream of the fronts	+ The different heights in wings increase the efficiency of the rear pods	+ The different heights in wings increases the efficiency of the rear rotors
Distributed Propulsion	+ The rotors can locally increase the flow over the wing, increasing the lift and decreasing the required wing surface area	+ The pods can locally increase the flow over the wing, increasing the lift and decreasing the required surface area	+ The rotors can locally increase the flow over the wing, increasing the lift and decreasing the required surface area
Redundancy	+ A large number of rotors ensure that if one engine is inoperative, it is still stable	+ If one engine is inoperative, the effect is almost negligible due to the distributed pods	+ If one engine is inoperative, the effect is almost negligible due to the distributed rotors
Disk Loading	+ Low disk loading due to high rotor area	- High disk loading due to smaller duct area	± Medium disk loading, since there are quite a lot of rotors each with a decent area

10.2. Actuator Disk Theory

Actuator disk theory is a method to estimate the preliminary power, thrust, rotor area and efficiency by assuming the rotor can be replaced by infinitely many blades that form a disk. The flow is accelerated through this disk, which induces a pressure change, that produces thrust due to the momentum equation. The disk is assumed to be ideal, meaning there is no friction and no rotational wake component [1]. Some assumptions are made regarding steady, inviscid, and incompressible flow, which will have an inflating effect on the efficiencies of the rotors[2]. Figure 10.1 shows how actuator disk theory is modeled.

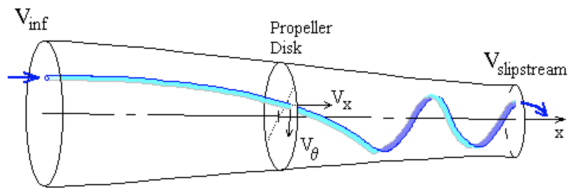

Figure 10.1: *Actuator Disk Theory Depiction* [3]

[1] Accessed May 10th 2023, https://www.mechnflow.com/post/wind-turbine-momentum-theory#viewer-aec5s
[2] Accessed May 10th 2023, https://web.mit.edu/16.unified/www/FALL/thermodynamics/notes/node86.html
[3] Accessed on June 1st 2023, http://www-mdp.eng.cam.ac.uk/web/library/enginfo/aerothermal_dvd_only/aero/propeller/prop1.html

As mentioned, all the configurations have an unspecified number of engines, which is an optimization parameter. Due to this, an engine number will be given from the existing design (Joby, Lilium, or Wigeon) that the configurations are mimicking. From the actuator disk theory, the parameters that can be estimated are the total propeller area, the propulsive efficiency, required power, and noise.
For the required propeller area, the relationship is as follows:

$$A_{total} = \frac{MTOM}{DL} \tag{10.1}$$

$$A_{rotor} = \frac{A_{total}}{N} \tag{10.2}$$

where DL stands for disk loading, the ratio of the total aircraft weight to the total area the rotors sweep, and N stands for the number of engines. Disk loading should usually be minimized for efficiency reasons [4]. The disk loading of each configuration has been estimated based on a literature study, as shown in Table 10.2. The disk loading of Joby was calculated based on their MTOM [5], and their rotor diameter [6]. The exhaust velocities for both cruise and hover can be found using the slides from the AE4135 master's course [7] and are displayed in Equation 10.3 and Equation 10.4. Equation 10.4 will be important to determine the propulsive efficiency, and Equation 10.3 for the power during hover. Finally, propulsive efficiency in cruise can be determined using Equation 10.5 [8].

$$V_h = \sqrt{\frac{2MTOW}{\rho A_{total}}} \tag{10.3}$$

$$V_{cr} = \sqrt{\frac{2MTOW}{\rho A_{total}} + V_\infty^2} \tag{10.4}$$

$$\eta_{cr} = \frac{2}{1 + \frac{V_{cr}}{V_\infty}} \tag{10.5}$$

Using the MTOW for each configuration, 300 [km/h] for the cruise speed, and an air density at an altitude of 400 [m], Table 10.2 is given.

Table 10.2: *Propulsive Parameters*

	J1	**L1**	**W1**
Disk Loading $[kg/m^2]$	120	1200 [55]	320 [56]
Number of Engines [-]	6	36	12
Total Rotor Area $[m^2]$	16.78	3.82	10.46
Area per Rotor $[m^2]$	2.80	0.11	0.87
Propulsive Efficiency in Cruise [-]	0.93	0.77	0.89

This shows that there is a difference in the propulsive efficiencies of each configuration, where the J1 clearly wins. The L1 suffers from its high disk loading. For the disk loading values themselves, since each design imitates an already existing eVTOL, the respective eVTOL's disk loading is given to the configurations.

10.3. Power

Next, the power of the phases can be found using other literature. For the required power during hover, Equation 10.7 has been used for the L1 (ducted), and Equation 10.6 for the J1 and W1 (open). In these equations, T is thrust, which is equal to the MTOW.

$$P_{h-open} = \frac{T^{3/2}}{\sqrt{2\rho A_{total}}} \tag{10.6}$$

$$P_{h-duct} = \frac{T^{3/2}}{2\sqrt{\rho A_{total}}} \tag{10.7}$$

For the maximum required power, these equations can also be used, but with a higher value for T, since hovering is the most power-intensive phase. T would be the MTOW multiplied by the highest thrust-to-weight ratio achieved during hover, which has been found in Chapter 6 as 1.225 for the W1, and 1.233 for J1 and L1. For cruise power, Equation 10.8 is used. Then, the relation in Equation 10.9 can be used, so that Equation 10.10 can be obtained. Finally, Table 10.3 can be constructed.

[4] Accessed May 10th 2023, https://www.krossblade.com/disc-loading-and-hover-efficiency
[5] Accessed May 22nd 2023, https://evtol.news/joby-s4
[6] Accessed May 22nd 2023, https://newatlas.com/aircraft/joby-aviation-toyota-evtol-air-taxi/
[7] Accessed May 10th 2023, https://brightspace.tudelft.nl/content/enforced/498753-AE4135+2022+3/2.1.1_From%20momentum%20to%20vorticity-Actuator%20disc%20theory(1).pdf?_&d2lSessionVal=DSSP3YfSuJ7cTrBD4vhWz2nDT&ou=498753
[8] Accessed May 11th 2023, https://web.mit.edu/16.unified/www/FALL/thermodynamics/notes/node81.html

$$P_{cr} = \frac{D_{cr} V_\infty}{\eta_{cr}} \quad (10.8) \qquad \frac{W}{D} = \frac{C_L}{C_D} \quad (10.9) \qquad P_{cr} = \frac{W V_\infty}{\eta_{cr}} \frac{C_D}{C_L} \quad (10.10)$$

Table 10.3: *Power Requirements of Each Design*

	J1	L1	W1
Hover Power [kW]	433	2,204	1,176
Maximum Power [kW]	593	3,018	1,595
Cruise Power [kW]	132	285	188

It seems that due to the high disk loading, L1 seems to have a very power-demanding system. The J1 has shown that it requires the least amount of power while maintaining a very high propulsive efficiency, which would easily make it the winner of the three configurations.

10.4. Noise

The eVTOL's noise also has a significant effect on the stakeholders, specifically the passengers and the people surrounding the vertiports, and the regulatory bodies, since noise is an EASA requirement. Therefore the configurations must also be ranked in terms of the noise that they produce in hover, and in cruise. For this, an empirical formula has been taken from the reader of the course AE4431 [57]. The SPL in the equation calculates the noise at a distance of 1 [m] in the direction where it is maximal.

$$SPL = 83.4 + 15.3 \log(P_{br}) - 20 \log D + 38.5 M_t - 3(B-2) + 10 \log N_p \quad (10.11)$$

In Equation 10.11, the sound pressure level (SPL) of each propeller is given as a function of P_{br}, the power required per engine, D, the propeller diameter, B, the blades per propeller, and N_p, number of propellers per engine. There is one more term, M_t, which is the rotational tip Mach number. This in itself is calculated with Equation 10.12, where c is the speed of sound at a given altitude, and n_p is the propeller rotational speed in rpm.

$$M_t = \frac{\pi D}{c} \frac{n_p}{60} \quad (10.12)$$

In Equation 10.11, P_{br} can be found by dividing the total required power divided by the number of engines, D can be found from the rotor area, B will be found from literature, and N_p is 1. In Chapter 11, configuration J2 is introduced. For M_t, the speed of sound will be assumed at sea level as during hover, the eVTOL is close to the ground, and cruise is at above 400 meters which has a negligible effect on the speed of sound. The equation, being empirical, takes into account all factors that contribute to the propeller noise, such as exhaust velocity noise, blade tip noise, mechanical noise, etc.

For each configuration, the value for B and n_p will be different. It should be noted that B will also be an optimization parameter, like N. That is why a value will be assumed for B but this will be optimized. These depend on the type of propulsion that is integrated into the configurations and typical values for existing designs. For example, the more blades there are, the lower the noise will be, due to the smaller vibrations [9]. This means that the design choice of how many blades there are will drastically impact the noise emissions of each configuration. For the L1, B is assumed to be 25. This number is based on the number of blades per engine that Lilium has on its jet, which is 27 (found by observation). Since the L1 is based on the Lilium, it seems quite feasible. For the J1 and W1, a value of 5 will be used to mimic the Joby S4 and Wigeon respectively.

For the revolutions per minute, the W1 has been given a design rpm of 1350, copying the Wigeon group, as they have a lot of support behind this value which could be a good preliminary estimate for this team's eVTOL. The Joby S4 has a rotor diameter of 2.9 meters and rotor tip speed of 113 meters per second [58]. From this, an rpm of 750 can be calculated, which will be used for the J1. For the L1, values will be assumed for M_t itself, as this is available from Lilium. For hover, M_t is 0.45, and 0.26 for cruise [55]. Using a different value for the L1

[9] Accessed May 12th 2023, https://hartzellprop.com/are-more-propeller-blades-better/

is actually beneficial since for the J1 and W1, variable pitch propellers can be used to improve their efficiency [10], but this is not feasible for L1 due to the small and high number of engines.
The propeller noise can now be found since all parameters are known, but the total eVTOL noise must also be estimated. This can be found by using Equation 10.13.

As mentioned, the equation calculates the SPL at 1 [m]. For hovering, the SPL will be calculated for a distance of 30 [m] which is an arbitrary value chosen that represents the distance to the people that are nearest to the vertiports. As stated in the baseline report [16], the noise requirements for an eVTOL weighing more than 1417 [kg], measured 150 [m] below a specific flight path, should be stated as Equation 10.14.

$$SPL_{total} = 10\log[\Sigma 10^{SPL_i/10}] \quad (10.13) \qquad \text{Noise} = 80.49 + 9.97log(M) \quad (10.14)$$

where M is the mass in kilograms. Using this calculation and inputting the MTOW of each design shows that all configurations are well below this limit. These are not shown in Table 10.4 as they are not part of the trade-off, only to verify that they all fit the regulations. Therefore Table 10.4 will show the noise level at 400 [m] for cruise, and the hover noise level at 30 [m]. Finally, Table 10.4 can be produced.

Table 10.4: *Noise Emissions*

	J1	**L1**	**W1**
Max Noise per Propeller, Hover [dB] (30 [m])	78.32	40.69	83.65
Total Noise, Hover [dB] (30 [m])	86.10	56.26	94.44
Max Noise per Propeller, Cruise [dB] (400 [m])	47.90	-2.71	48.98
Total Noise, Cruise [dB] (400 [m])	55.69	12.85	59.77

These parameters seem very insignificant and would not be a key parameter in the propulsive trade-off, except that the L1 has an extremely low noise level at hover, which is an advantage. The L1 even has a negative value for cruise, indicating that it falls below the threshold of human hearing. The validity of Equation 10.11 must be called into play as well since this formula is used more for conventional fuel-burning engines. Electric engines are known to be quieter than fuel-burning engines, meaning that the produced noise could be even less than what Table 10.4 shows. Once the selected configuration is evaluated in the final report, a detailed noise estimation should be made further.

Although SPL is a good measure of the amount of sound that is produced, looking at psychoacoustic annoyance is also beneficial to determine how irritating a sound can be. There are a few metrics to indicate the psychoacoustic annoyance (PA) of a sound, such as loudness, sharpness, tonality, roughness, and fluctuation strength [57]. The computation of each of these factors will take some time and estimations based on other literature. Therefore, this will be done for the final report as only one design will be evaluated.

10.5. Noise Criterion Scores for Different Designs

Based on the noise estimation, these scores have been given. The scores are given out of 3. It should be noted that in Chapter 11, the design J2 is also considered with a double engine for the rear rotors. This is also considered in Table 10.5. The J2 will have the exact same propulsive characteristics and thus has the same noise emissions.

Table 10.5: *Noise scores*

	J1	**J2**	**L1**	**W1**
Scores	2	2	3	2

Most designs have been given a 2, as they are relatively good, and meet all regulations. However, the L1 has been given a 3 since it is an extremely quiet configuration that exceeds the requirements.

[10] Accessed May 12th 2023, https://hartzellprop.com/3-key-benefits-constant-speed-propellers/

10.6. Sensitivity Analysis

To determine which of the parameters affects the final results the most, a sensitivity analysis can be performed. This gives the advantage that if, for example, the hover power needs to be reduced the parameter that reduces it the most for a given decrease in percentage should be considered.

Doubling and halving the thrust in Equation 10.7 and Equation 10.6 results in a power increase of 180% and a decrease of 65%, respectively. The same result is achieved if the thrust-to-weight ratio is doubled and halved. This shows that the power is quite sensitive to these two parameters, which is something to consider if they need to be increased to increase stability and control. Doubling and halving the thrust also decreases and increases the propulsive efficiency by 2% and 1.2%. It seems that at this thrust level, the propulsive efficiency is biased toward decreases which is something to consider too.

The disk loading does not have a very large effect on the parameters, yet it affects almost every parameter. It has an effect on the hover and maximum power, and also on the hover noise. Therefore it is very important that the disk loading is an accurate value. Since this value was taken from literature, the values it affects must be recalculated in the future.

Two final parameters to consider, are the blade numbers and number of engines, since these will be optimized, and is therefore important to see which values they affect. They have no effect on the power but affect the noise. The blade number has a large effect on the SPL, as it is found by using $-3(B-2)$. This means increasing the blades from 5 to 10, decreases the SPL by 15. The number of engines affects the power per engine, which is logarithmically scaled, thus the impact of the number of engines on the power is minor. This concludes that all these parameters are very important to the final results, and any change to these parameters could change the trade-offs.

10.7. Verification and Validation

Verification can be done for both a product and a model. In this report, several models and equations have been used to determine parameters that will be used for the trade-off. These models must be verified to increase confidence in them, by cross-checking using other literature. To verify the power levels, the values will be compared to the values that the other engineering teams in this team have found. In general, using only a few sources is good for a preliminary estimate in the midterm report, but more sources and models will need to be used for the final design which can verify each other.

10.7.1. Verification & Validation Plan

For the final report, a code will also be used to calculate certain parameters. Within the code, the compiler will automatically check for any errors, like a divide by zero error, or a syntax error. In addition to this, unit tests will also be performed in the form of sanity checks.

The models that will be used for the eVTOL can also be used to calculate parameters of existing eVTOLs that are already known, to give an idea of how close the prediction is. Once the final design has been made, it will be validated using analysis and testing. For parameters that are not possible to measure using testing, either due to complexity or lack of a physical product, such as propulsive efficiency, the analysis will be used. The noise levels and used power will also be validated using testing. Once the final parameters are found, these can also be compared with parameters from existing eVTOLs for more validation.

11

Stability & Control Design

In this chapter, the stability and control of each conceptual design is analysed and assessed, in order to provide a trade-off value to each design regarding its stability and control performance. In Section 11.1, the methodology used to find the cg (center of gravity) range envelopes for each design is discussed. Next, in Section 11.2, the conceptual designs are presented, focusing on the parameters that most affect the stability and control. For each conceptual design, the cg envelope is displayed. Lastly, in Section 11.3, the cg envelopes are analysed and compared and a trade-off value is assigned to each conceptual design with respect to its performance in stability and control.

11.1. Methodology

Each of the designs can be assessed in terms of stability and controllability performance based on the allowable cg travel a design offers. If this cg travel is too limited, the aircraft might become unstable or uncontrollable under certain loading conditions. The cg boundaries can be defined in terms of three criteria and hence four boundaries:

- Most forward and aft cg boundary imposed by controllability during vertical flight under one engine failure.
- Most aft cg position imposed by open loop longitudinal stability requirement during horizontal flight ($Cm_\alpha < 0$).
- Most forward cg position imposed by longitudinal controllability requirement during horizontal flight ($Cm = 0$).

11.1.1. Controllability During Vertical Flight

The VTOL needs to be able to achieve a ROC of 2 [m/s] in vertical flight. The aircraft also needs to be operational under one engine failure. Hence, the strictest requirement in vertical flight becomes: "The aircraft must be controllable in vertical flight at a rate of climb of 2 [m/s] when one engine is inoperative".

The controllability can be obtained by ensuring that the sum of moments and forces equals 0. This assumes that the control response of the rotors is quick enough such that the aircraft can be evaluated in static conditions. Assuming that the rotors are pointed vertically, the relevant equations of forces and moments become:

$$\Sigma T - D = W \qquad \Sigma M_x = 0 \qquad \Sigma M_y = 0 \qquad \Sigma M_z = 0 \tag{11.1}$$

It has been determined that the drag is much smaller ($\approx 82[N]$ for design W1) at a rate of climb of 2 [m/s] and hence can be neglected making the force equilibrium simply thrust equals weight.

A simple 2D decoupled analysis was proven to not be possible due to the strong coupling between the thrust and torque produced by the rotors which makes yawing often the limiting condition. Hence, the system must be treated in 3D as a matrix of equations with the individual forces produced by each of the rotors as unknowns. However, since there are more unknown forces than equations, the system is underdetermined and multiple solutions exist. This leads to the problem that feasible designs may be falsely penalized due to only solutions that require extreme thrusts on some rotors being needed when there actually exists a solution that does not impose extreme requirements on the thrust & power required by each engine.

The problem of matrices can be avoided using the (Available Control Authority Index) ACAI method. It was determined that when the ACAI is greater than 0, a multicopter is controllable [59]. The basic ACAI method takes as input the locations and rotational directions of the propellers, their efficiency (0 or 100% depending on whether the engine has failed or not), aircraft weight, the cg location, a limit on maximum thrust per propeller, and a limit on the minimum thrust per propeller (which equals 0). The output is the ACAI parameter indicating whether the multicopter is controllable or not. It has been verified that the physical meaning of ACAI = 0 is that forces and moments equilibrium can be barely satisfied for a given limit on the maximum thrust produced by each rotor. ACAI > 0 indicates that there is more thrust available per engine than required to satisfy the static equilibrium requirements.

The ACAI method can be further extended to construct an 'envelope of controllability'. By looping over various possible thrust limits, possible cg locations, and all possible one engine failures, the cg locations where

the eVTOL is controllable can be plotted as a function of maximum available thrust per engine. In this envelope, two lines can be drawn (one for aft cg and one for the forward cg limit) corresponding to ACAI = 0 at different available thrust per engine limits marking the limits of vertical flight controllability.

A limit on thrust does not impose physical limitations on aircraft design. However, the maximum thrust per engine required to obtain controllability at a certain cg position can be related to the maximum power required by the most power demanding engine. Since the most power intensive phase of flight is the vertical ascent, the maximum power required by a certain engine for controllability during vertical ascent can be used to size the engines in the later stages of the design. The engine thrust (T) for a rotor with disk area A_{disk} can be related to the engine power required at a certain rate of climb (ROC), taken to be 2m/s through Equation 7.19.

11.1.2. Longitudinal Stability and Control During Horizontal Flight

The longitudinal stability requirement during cruise sets a limit for the most aft cg of the aircraft. To achieve longitudinal stability, $Cm_\alpha < 0$ condition must be satisfied. Denoting the front wing with subscript 1 and the horizontal tail or the rear tandem wing with subscript 2, the limit on cg imposed by stability requirements can be expressed as:

$$x_{cg} < \frac{-C_{m1_\alpha} + C_{L1_\alpha} \cdot \frac{x_1}{c_1} - C_{m2_\alpha} \cdot (1 - \frac{d\epsilon}{d\alpha}) \cdot \frac{S_2 c_2}{S_1 c_1} \cdot (\frac{V_2}{V_1})^2 + C_{L2_\alpha} \cdot (1 - \frac{d\epsilon}{d\alpha}) \cdot \frac{x_2 S_2}{c_1 S_1} \cdot (\frac{V_2}{V_1})^2}{\frac{C_{L1_\alpha}}{c_1} + \frac{C_{L2_\alpha}}{c_1} \cdot (1 - \frac{d\epsilon}{d\alpha}) \cdot \frac{S_2}{S_1} \cdot (\frac{V_2}{V_1})^2} \tag{11.2}$$

x_1 and x_2 refer to the position of the forward and rear wing with respect to the fuselage nose. It is important to note that Cm_α of a wing equals 0 if the aerodynamic forces of the wing are placed at the aerodynamic center of the mean aerodynamic chord. However, XFLR5 yields a distribution of Cm as a function of span. This distribution is integrated to get a final Cm. Since the integrated Cm is not necessarily at the aerodynamic center of the MAC, Cm_α gets a small, yet non-zero value.

The most forward cg limit is set by the controllability requirements, which become most stringent near stall landing conditions. At this conditions it must be possible to obtain $Cm = 0$ leading to constraint for the cg location:

$$x_{cg} > \frac{-C_{m1} + C_{L1} \cdot \frac{x_1}{c_1} - C_{m2} \cdot \frac{S_2 c_2}{S_1 c_1} \cdot (\frac{V_2}{V_1})^2 + C_{L2} \cdot \frac{x_2 S_2}{c_1 S_1} \cdot (\frac{V_2}{V_1})^2}{\frac{C_{L1}}{c_1} + \frac{C_{L2}}{c_1} \cdot \frac{S_2}{S_1} \cdot (\frac{V_2}{V_1})^2} \tag{11.3}$$

Since controllability is required until stall conditions: $C_L = C_{L_{max}}$. The Cm of the wings are evaluated at $C_{L_{max}}$.

In Section 11.2, it is possible to see that the longitudinal stability and controllability impose much more stringent limits on the cg travel compared to the vertical ascent controllability limits. This makes it necessary to perform a sensitivity analysis on the wing placement to see to what extent the longitudinal cg range is affected. Two independent sensitivity analysis are performed. Firstly, the location of the front wing is shifted while keeping the rear wing at its nominal position, determined based on existing similar designs in the market. Secondly, the location of the rear wing is varied while keeping the front wing at its nominal position and the minimum cg and the maximum cg allowed for a longitudinally stable and controllable aircraft is plotted, as shown in Section 11.2.

11.1.3. CG Range Envelope

By superposing the cg limits based on vertical flight in Subsection 11.1.1 and the horizontal flight in Subsection 11.1.2, the overall cg limits for controllability can be plotted. This leads to two envelopes per design:

1. Hover cg limits as a function of the maximum power available for the most power demanding engine, together with the cg range for different positions of the front wing, for a fixed rear wing position.

2. Hover cg limits as a function of the maximum power available for the most power demanding engine, together with the cg range for different positions of the rear wing, for a fixed front wing position.

Based on the cg range determined from these envelopes for each design, a conclusion on whether the design can be controlled and stabilized can be made. If stability and controllability can be obtained in a very limited cg range, the design might not be stable and controllable at a later design stage depending on the placement of the passengers, fuselage tanks, and loading conditions.

11.1.4. Existing Verification & Validation & Planning

The base ACAI method has been verified against the static balance of forces and moments by the control and stability department. Additionally, it has been peer-reviewed and published [59]. This demonstrated that both methods lead to consistent cg limits in vertical flight. The additional code developed for iterating over various values for maximum thrust limit per engine, different engine failures, and cg positions have been verified separately. This involves choosing a thrust limit, then manually plugging the base ACAI function into each of the different engine failures and determining the cg limits for those. The cg limits determined from this procedure are compared against the cg limits determined via the looping code. Unit testing can be used to verify the lines of code that convert thrust to power (based on Equation 7.19) and the lines of code that calculate the cg limits based on horizontal flight stability and controllability limitations (based on Equation 11.2 and Equation 11.3). Validation of the cg limits during the hover under one engine inoperative conditions and the cg limits during horizontal flight can be validated via flight testing once the design is finalized.

11.2. Design Options & CG Envelopes

In this section, the parameters of each conceptual design that affect stability and control of the aircraft are introduced and defined. The cg range envelope is shown, calculated as described in Subsection 11.1.3.

Table 11.1: *Longitudinal stability and control parameters*

Parameter	Description	J1	J2	W1	L1
$MTOM$ [kg]	Maximum Take-off Mass	2014	2014	3351	4584
S_{proj} [m^2]	Vertically projected surface area	13.4	13.4	22.3	30.5
$n_{engines}$ [-]	Number of engines	6	6	12	36
A_{disk} [m^2]	Rotor disk area	2.8	2.8	0.87	0.106
$C_{m_{\alpha_1}}$ [-]	C_{m_α} of foremost wing	-1.596	-1.596	-1.644	-1.466
$C_{m_{\alpha_2}}$ [-]	C_{m_α} of aftmost wing	0	0	-1.664	-1.675
C_{m_1} [-]	C_m of foremost wing	-0.0391	-0.0391	-0.0319	-0.0317
C_{m_2} [-]	C_m of aftmost wing	0	0	-0.032	-0.032
C_{L_1} [-]	C_L of foremost wing, assuming $C_{L_{max}}$ during landing	1.638	1.638	1.638	1.638
C_{L_2} [-]	C_L of foremost wing, assuming $C_{L_{max}}$ during landing	-0.636	-0.636	1.638	1.638
$C_{L_{\alpha_1}}$ [-]	C_{L_α} of foremost wing	4.8665	4.8665	4.996	4.403
$C_{L_{\alpha_2}}$ [-]	C_{L_α} of aftmost wing	4.3	4.3	5.05	5.075
$\frac{V2}{V1}$ [-]	Ratio of flow velocities over both wings	1	1	1	1
$\frac{d\epsilon}{d\alpha}$ [-]	Downwash ratio	0.1	0.1	0.1	0.1
x_1 [m]	x-location of foremost wing	3	3	0.5	0.5
x_2 [m]	x-location of aftmost wing	8.5	8.5	9	8
c_1 [m]	Chord length of foremost wing	1.224	1.224	1.05	1.19
c_2 [m]	Chord length of aftmost wing	0.736	0.736	1.023	1.41
S_1 [m^2]	Surface area of foremost wing	11.17	11.17	9.29	7.26
S_2 [m^2]	Surface area of aftmost wing	3.25	3.25	9.29	18.14
l_{fus} [m]	Fuselage length	9.295	9.295	9.295	9.295

The parameters that affect longitudinal stability and control can be found in Table 11.1 for all aircraft. The parameters that affect the vertical flight control and the final cg envelope will be presented individually for each concept design.

11.2.1. Concept J1

This design is very similar to Joby. Hence, the relative positions of the rotors can be kept the same with respect to the Joby when the longitudinal positions are normalized with respect to fuselage length and the spanwise positions are normalized with respect to wing span. This yields the following locations for the 6

rotors, depicted in Table 11.2.

Table 11.2: *J1 Rotor Locations*

Rotor numbers	Longitudinal position (m)	Spanwise position (m)
1 and 2	0.57	2.3
3 and 4	3.4	5.4
5 and 6	6.8	2.3

For the inputs from Table 11.1, together with those from Table 11.2, the following plot is created.

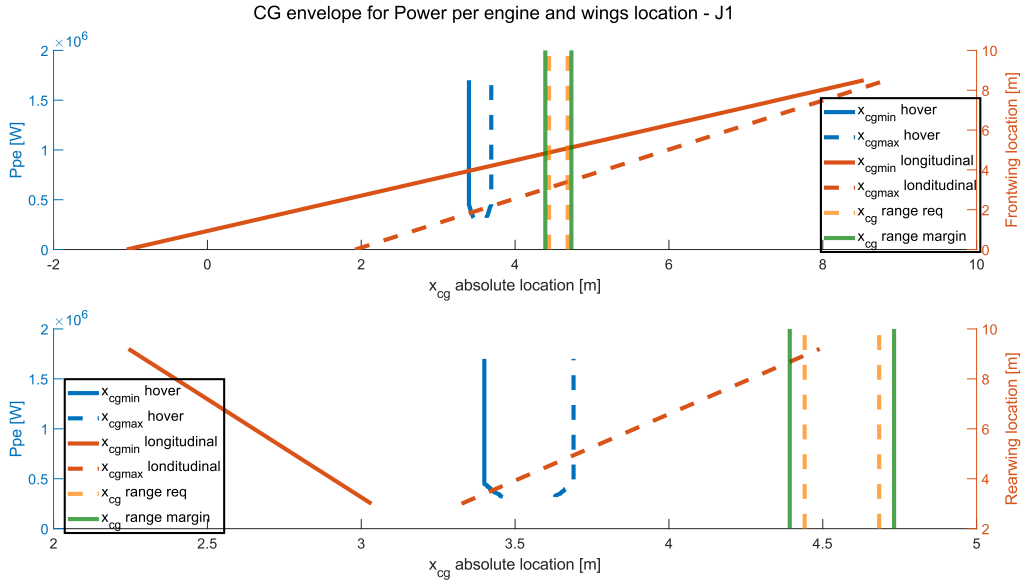

Figure 11.1: *J1 cg envelope*

It can be seen from Figure 11.1, that this aircraft design concept must be discarded. The orange dotted lines correspond to the expected cg excursion, and the green solid lines correspond to a 20% margin on the cg excursion on each side. The design concept's allowable cg range space is that to the right of the solid red and blue lines, and to the left of the dotted red and blue lines. It is with the comparison of the allowable cg range space to the expected cg excursion that a value is given for each design in the trade-off matrix, as explained below in Section 11.3. For this design, the trade-off value is 0 and it is automatically discarded.

11.2.2. Concept J2

In order to counter the limited cg range of J1 it is decided to include two engines, that provide half of the required maximum thrust power each, per rotor. This is a proven concept that is used in high-payload helicopters and that is easily adaptable for electric engines. For this reason, the rotor locations are similar to those of J1, shown in Table 11.2.

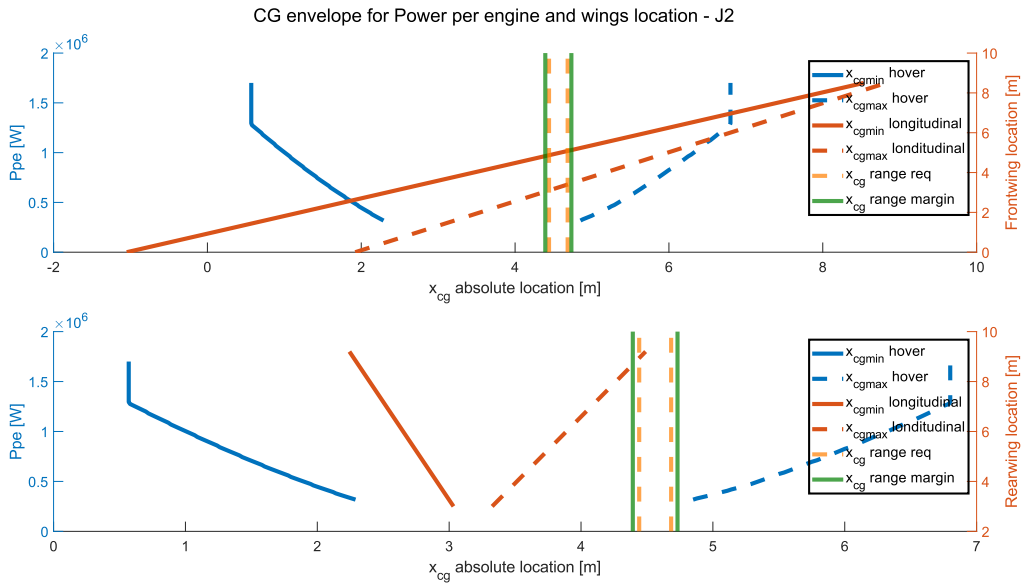

Figure 11.2: *J2 cg envelope*

As observed, the cg envelope is very favourable for this concept. The cg locations limits allow for a large range of possible frontwing positions. The power per engine can be kept to a minimum while satisfying the the cg excursion requirements, making of this concept a very flexible and low compromise design.
Something to take into account when reading the graph above is that although the free-rearwing plot seems to not allow for an acceptable cg range, it is plotted for a fixed frontwing location which has been pre-established by a first-level estimation, and that falls outside of the correct frontwing locations found from the top plot. However, this can be used in later stages of design to optimise for wing positioning.

11.2.3. Concept W1

In design W1 that is similar to Wigeon, 6 propellers will be placed on the front wing and 6 on the rear wing, leading to a total number of 12 propellers. A clearance of 0.3 [m] between different propellers and the fuselage is used. Propeller radius can be estimated from the total rotor area extracted from Wigeon group of 2.089$[m^2]$ leading to R_p= 0.46 [m]. This value will change with design iterations for the design concept performed by the Aetheria team, but the locations of the rotors will remain equal through the iterations in a preliminary stability and control analysis of the W1 concept. Since from a directional controllability point of view, having the engines near the outer section of the wing is more advantageous, the wings are placed starting from the wing tip (4.2 [m] from fuselage center) with each additional engine placed with 0.3 [m] clearance from one another. In addition, in Wigeon, the lifting surfaces were placed as far apart as possible. Assuming that the propellers are one chord (1.19 [m]) away from the leading and rear edge of the 10.74, fuselage, the locations of the propellers were determined, displayed in Table 11.3.

Table 11.3: *W1 Rotor Locations*

Rotor numbers	Longitudinal position [m]	Spanwise position [m]
1 and 6	1.19	4.2
2 and 5	1.19	2.99
3 and 4	1.19	1.78
7 and 12	9.55	4.2
8 and 11	9.55	2.99
9 and 10	9.55	1.78

With the above-specified inputs, the cg envelope is created, as displayed below, in Figure 11.3.

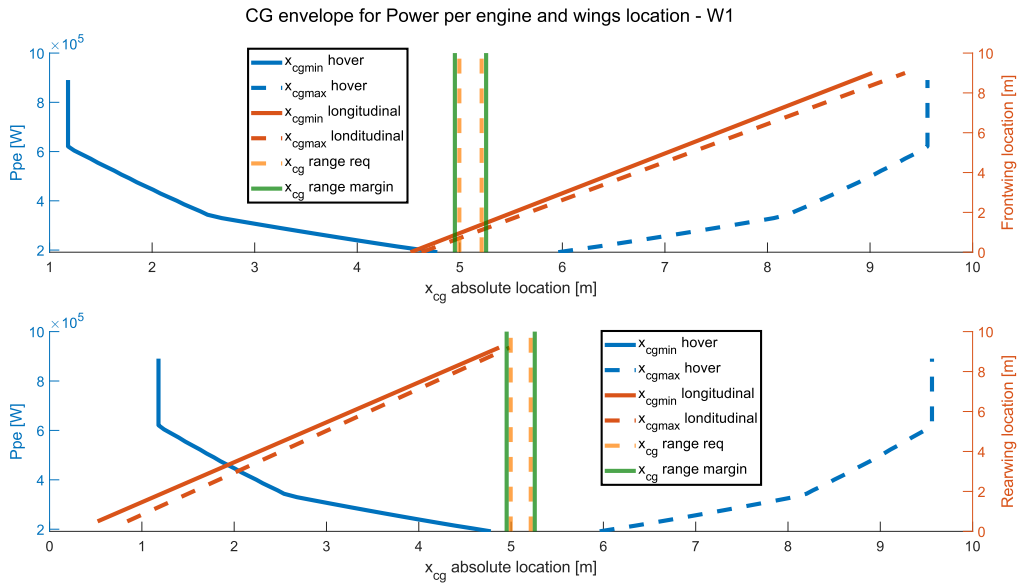

Figure 11.3: *W1 cg envelope*

It is seen in Figure 11.3 that the cg excursion required can barely be satisfied with this design concept. It is for that reason that an alternative plot is created in which the lift coefficient of the rear wing during approach is reduced to 80% of its original value, which is achievable with a reasonable trim surface.

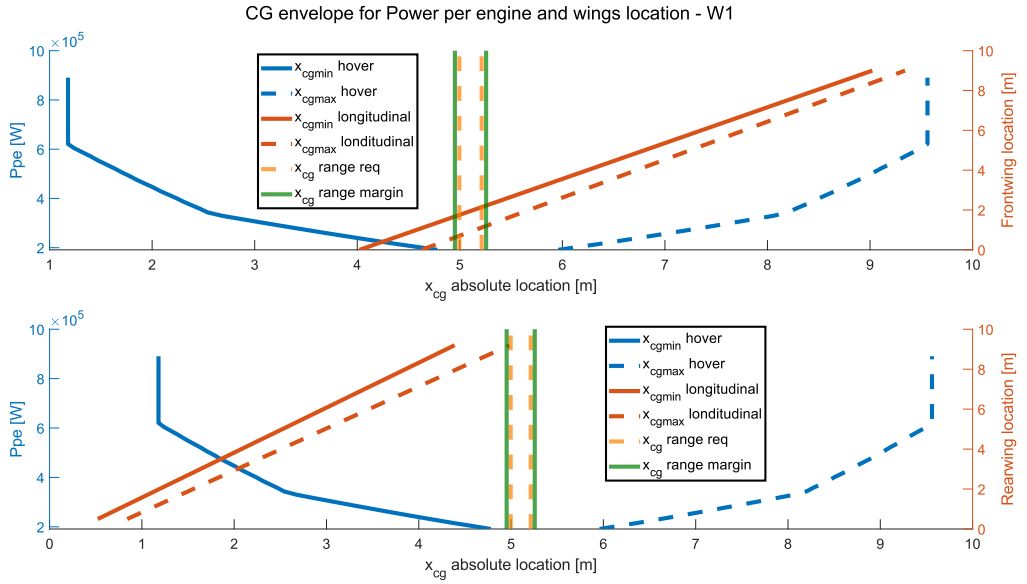

Figure 11.4: *W1 cg envelope with CL2 reduced to 80%*

It can be observed in Figure 11.4 that the cg envelope is slightly improved. The concept design can now satisfy the cg excursion requirements. However, the cg range space is still very limited and this concept allows for little design freedom, making the aircraft's stability and control a very constraining factor in the future development of the design.

11.2.4. Concept L1

Concept L1 is based on the existing Lilium Jet. The concept contains 36 rotors, distributed 12 on the front wing and 24 on the rear wing. The locations of the rotors have been obtained from scaled drawings of the

Lilium Jet. The rotors 1 to 12 are placed on the front wing, 0.9 metres behind the nose. The spanwise locations are 1.91, 1.64, 1.37, 1.1, 0.82, and 0.55 metres from the centre of the fuselage. The rotors 13 to 36 are located on the rear wing, 6.9 metres behind the nose. The spanwise locations are roughly 0.27 metres apart, with the closest rotor to the fuselage positioned at 1.17 metres from the fuselage centre.
In order to create the cg envelope for this concept design, the condition of one engine inoperative condition has been neglected for vertical flight controllability criteria. This can be done because of the high number of rotors and close positioning respect to each other. Doing so enormously reduces the computation cost of this cg envelope, without great consequences. Contingency factors can be used to counteract the effect of the assumption in later stages of design, when more precision is needed.

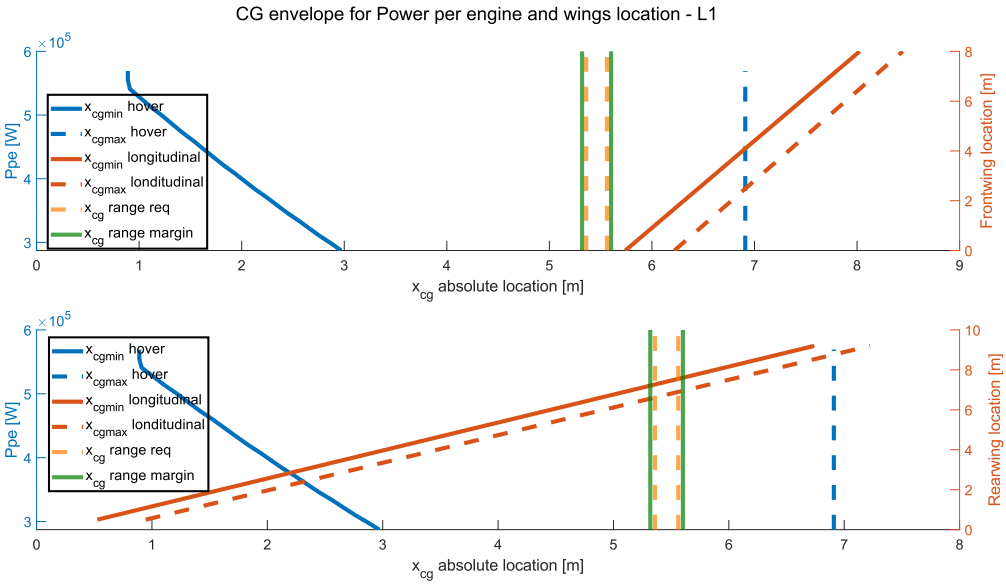

Figure 11.5: *L1 cg envelope*

Similarly to W1, this concept design barely satisfies the cg excursion requirements. It is for this reason that the CL of the rear wing has been reduced to 80% of its value during approach and the cg envelope is reevaluated.

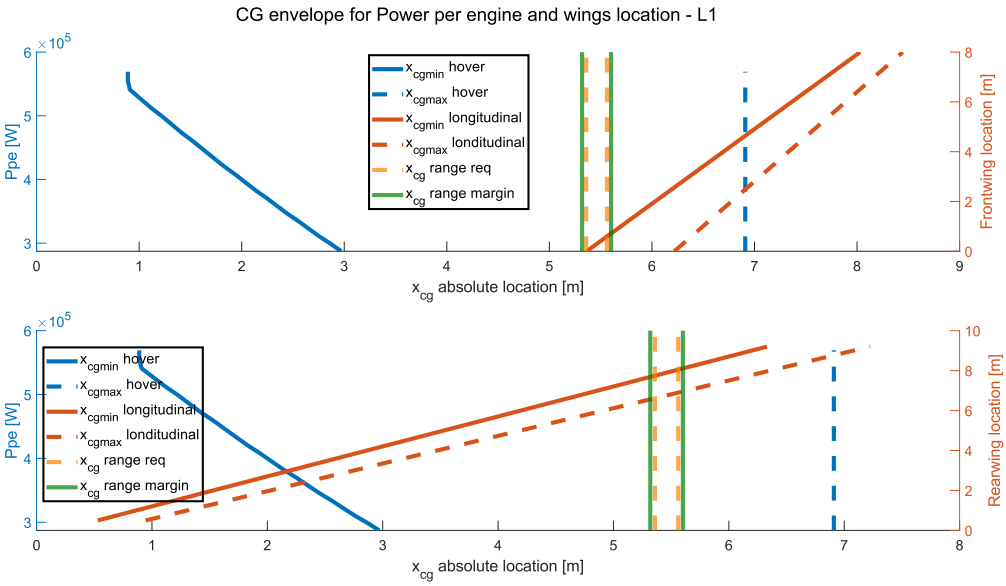

Figure 11.6: *L1 cg envelope with CL2 reduced to 80%*

In Figure 11.6, one can observe a large improvement on the cg envelope by reducing the lift coefficient of the rear wing during approach. This increases drastically the design flexibility and, when compared to W1, proves to be a better concept for stability and control criteria.

11.3. Stability & Control Criterion Scores For Different Designs

The designs can be evaluated on the basis of whether the allowable cg travel (where stability and controllability can be provided) is enough to cover the operational cg travel shown in the loading diagrams for each of the designs (Figure 11.7a, Figure 11.7b and Figure 11.7c). A design is awarded a '3' if the cg range required (determined by its loading diagrams) can be achieved for a variety of wing locations, indicating a flexible design. A '2' is awarded if for a specific wing location, the cg range found in the loading diagrams can be covered with reasonable trim. A '1' is awarded if a design does not immediately meet the required cg travel but can be forced to cover the required cg range at a cost of excessive drag induced by large trim or by using low C_L/C_D reflex airfoils. If under no circumstances, a cg range where the aircraft can be stabilized or controlled is found, the aircraft is given a score of 0 out of 3, eliminated, and thus discarded in the trade-off.

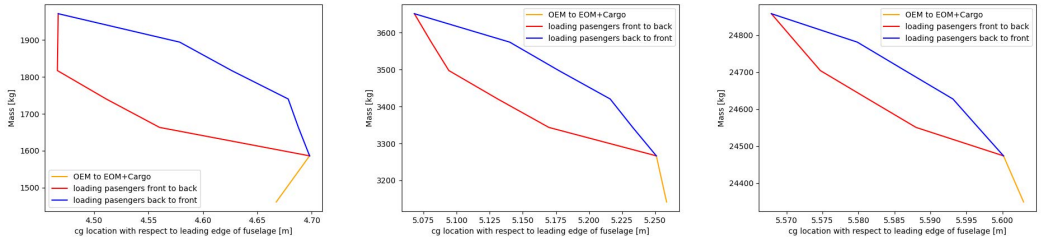

(a) *J1 and J2* **(b)** *W1* **(c)** *L1*

Figure 11.7: *Loading Diagram for Different Designs*

The values assigned for the trade-off for each concept design are summarized in Table 11.4.

Table 11.4: *Trade-off values for stability and control*

J1	J2	W1	L1
0	3	2	3

12 Operations, Logistics & Sustainable development

In this chapter, the operations and logistics of the three designs will be evaluated. Furthermore, the RAMS characteristics of the designs will also be discussed. Lastly, the sustainability aspects will be looked at.

12.1. In Operation

When the aircraft is in operation, its operational profile consists of multiple steps, as seen in Figure 12.1.

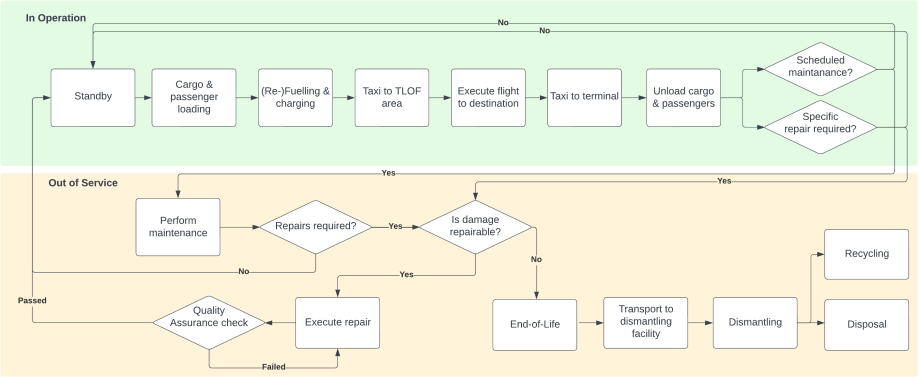

Figure 12.1: *Operations & Logistics Flow Diagram*

Standby The standby/parking phase of the operational logistics relates to the time when the aircraft is not in use, but waiting for its next mission. The aircraft can be outside on a VTOL parking spot or inside a hangar. This will limit the maximum wing span as this is mainly what dictates the parking size. The main stakeholders regarding standby operations are the customer and the vertiport operator. The wing span of the L1 is the highest (13.67 [m]) while the J1 and W1 have similar wing spans. This makes the J1 and W1 more suitable for standby operations.

Cargo & passenger loading The cargo and passenger loading trade-off delves into passenger comfort and cargo space. The main stakeholders are therefore the passengers and the customers. The customers would prefer easily accessible cargo space to ensure a short turn-around time. Furthermore, the passengers prefer embarkment to be as smooth as possible. A high-wing configuration provides easy embarkment, favouring the J1 design. However, tandem wings aircraft are also easy to enter as the entry door can be positioned in between the wings. So, there is no clear winner in terms of cargo and passenger loading.

(Re-)Fuelling & charging The (re-)fuelling and charging part of ground operations are similar to standard airports. The fuelling of compressed hydrogen will happen similarly to that of fuelling hydrogen cars. The charging of the batteries will happen on-site thus a refuelling station will need to be present. The effect of refuelling on the designs is discussed in Section 12.3.

12.2. Out of Service

Following each flight performed by Aetheria, it is assessed whether or not there is scheduled maintenance or whether a specific repair is required. If maintenance is scheduled, Aetheria will be out of service until the required checks and repairs have been done.

Perform maintenance For scheduled maintenance, the complexity and duration may vary significantly for each design configuration. Maintenance services for complex tilting wing or rotor mechanisms are obviously more time-consuming and costly compared to conventional fixed-wing aircraft. Brown and Harris present interesting results on OPEX costs for different eVTOL configurations such as lift + cruise, tilt-wing, and tilt-rotor [60]. Purely looking at the maintenance costs for the tilt-wing and tilt-rotor configuration, there is no clear winner. Due to the lack of available literature on tilt wings, it is hard to quantitatively favour one design over the other.

Repairs Next, following the performed maintenance, the question arises whether or not repairs are required. If not, the aircraft can return to service and will be made ready for the next flight. If it turns out repairs are required, the damage has to be assessed to see if the damage is repairable without leading to significant costs. If the damage is repairable and within reasonable cost, the damage will be fixed. After the repair, the quality assurance will inspect the aircraft one final time before clearing it for return to service. Should the damage be beyond repair, the aircraft proceeds to the end-of-life phase. This is similar to each of the designs.

End-of-life When arriving at the end-of-life phase, the aircraft will be transported to a dismantling facility where the aircraft will be dismantled. For sustainability purposes, as many components as possible should be recycled or repurposed. Any components not suitable for recycling will be disposed of as sustainably as possible. Since the parts of the designs are similar, no design is favoured for end-of-life operations.

12.3. RAMS

The Reliability, Availability, Maintainability and Safety characteristics of the three designs are to be maximized to ensure the aircraft will fulfill the mission for which it is designed [1]. Hence, these criteria will be evaluated.

Reliability The reliability is the probability that the system will perform its task[2]. The chances of failure are the highest in the beginning and end-of-life[3], which can be related to the 'bath-tub' curve. Production errors will always cause some failures. Since the hydrogen fuel cells are still in an early development stage their chance of failure is relatively high. Moreover, if opted for a solid-state battery system, the reliability of such a system is not guaranteed and should be carefully looked into, as it is not at an acceptable TRL (Technology Readiness Level) at the moment.

Availability The availability of a product is determined by its likeliness to perform its tasks in the product lifetime[4]. The availability of Aetheria largely depends on the time spent between missions (the turnover time) as well as the time spent in repairs when the aircraft is inoperable. Minimizing the turnover time increases availability. The use of hydrogen is beneficial in this aspect as filling a hydrogen tank with compressed hydrogen for a fuel cell vehicle can be done in under 3 minutes, showcasing the little time it would take Aetheria to refill the hydrogen tank [61]. On the other hand, the most powerful Tesla supercharger can currently deliver up to 250 [kW] of power[5], resulting in a charging time of more than one hour for a 250 [kWh] battery pack. Since the J1 only has a battery pack consisting of about 50 [kWh], the charging time is around 10 minutes, while L1 has the biggest battery pack (300 [kWh]) which would take more than an hour to charge. This is not beneficial for the turnaround time.

Maintainability As discussed in Section 12.2, the difference in maintainability for tilt-wing and tilt-rotor configurations is not substantial. However, from comparing the maintenance of such tilting mechanisms to conventional fixed-wing aircraft, it becomes clear that the increased complexity is unfavorable for maintainability. For this reason, the aircraft should provide easy access for mechanics to inspect and maintain the aircraft and all its complex components.

Safety The safety of the aircraft is a critical aspect of the design, as the incorporation of hydrogen as a power system in an aircraft is rather novel and might be dangerous given the great amounts of pressure the system is under. The crashworthiness of the aircraft determines the ability to avoid catastrophic events in the case of a crash. There is no guarantee that for a crash from 300 [m] the aircraft will stay intact, but a proper placement and protection of the hydrogen tanks may be the difference between life and death for a small crash. This is described in more detail in Section 8.8.

12.4. Environmental Analysis

Currently, the main factor influencing environmental sustainability is mission energy. The reason is that the majority of energy is still not green (produced from non-renewable sources [62]). Hydrogen is currently largely produced as grey/blue hydrogen (produced from fossil fuels). It is expected that the production of green hydrogen will grow by 9.2% each year up to 2030 [63]. Thus, the feasibility of utilizing green hydrogen will increase and therefore the mission energy will become less constraining. The only negative aspect of fuel cells is that the fuel cells use a rare earth metal, platinum. However, researchers at the Imperial College have developed a fuel cell that substitutes platinum with iron, but this technology is not ready to be implemented

[1] Accessed May 8th 2023, https://www.byhon.it/rams-engineering-analysis/#:~:text=The%20RAMS%20(Reliability%2C%20Availabilitby%2C,availability%20and%20well%2Ddefined%20safety.
[2] Accessed May 8th 2023, https://asq.org/quality-resources/reliability
[3] Accessed May 8th 2023, https://www.code7700.com/aircraft_reliability.htm
[4] Accessed May 22nd 2023, https://www.byhon.it/rams-engineering-analysis/
[5] Accessed May 22nd 2023, https://www.tesla.com/support/supercharger

within aviation yet [64].

Another environmental aspect that requires analysis is the type of battery utilized. Lithium batteries show the most promising life-cycle analysis [65]. An aspect to consider is the distance traveled during life cycle operations, a decrease in distance traveled will lower the CO_2 emissions per kilometer. The batteries are also limited by the materials used. Lithium, Cobalt, and Nickel are not sustainable unless recycled [66]. Assuming this will happen in the future, hydrogen, and batteries are both environmentally stable. A lighter aircraft will increase sustainability as the mass of batteries will decrease, thus this should be kept in high regard in the designs. If recycling the rare earth metals will not be performed in the future, the best choice is to invest in an iron based fuel cell.

Furthermore, the material used is an essential factor of the environmental sustainability. Currently, most aircraft use aluminium and composites. Using CFRP might decrease the weight [16], however CFRP is not recycled but buried in landfill sites. Airbus does state that it aims to recycle 95% of its CFRP [67], thus this might not be a negative factor in the future. [16].

12.5. Sustainable Economic Analysis

In order for the design to be economically sustainable it should be presented in a market with great potential, such as the energy market, in the future, so that the design can attract as many customers as possible for revenue generation. In this way, the eVTOL will be generating profit over the long run after reaching the break-even units. This design is emission-free, which is important since there is a worldwide aim to reduce emissions as a result of global warming. Furthermore, there is leniency towards new concepts that take advantage of resources that have not been used, due to the depletion of highly used current resources. Therefore, the use of hydrogen for transport is a high-potential market that promises a good breakthrough for Aetheria as it is the first design in this area. Furthermore, due to the design configuration of Aetheria, a very low number of break-even units are projected to be necessary for the design to generate profit at a very early stage, presenting a high degree of economic sustainability.

12.6. Social Analysis

In order to be socially accepted and adapted, eVTOLs must comply with all different kinds of constraints. Some of the constraints originate from regulations set by EASA on perceived noise at a specified distance from an aircraft. An analysis of the produced noise for each design is done in Section 10.4. From these results, it becomes clear that all designs comply with the requirements from EASA for helicopters weighing less than 3175 [kg] (the most relevant comparable aircraft type). The L1 design stands out due to its excellent noise characteristics. It produces merely 15.2 [dB] of noise perceived on the ground for a flying altitude of 305 [m] (less than the noise level of a quiet natural area with no wind[6]). However, the produced noise during hover may be more constraining from a social perspective as takeoff may take place in between office buildings or residential areas. But even in the hovering phase, the L1 produces only about 56.3 [dB] of noise (which is less than the average business office noise level[6]). The maximum produced noise is about 94.4 [dB] for the W1 design during hover (equivalent to a subway train at 200 [ft][6]).

13
Financial Analysis

This chapter provides the financial analysis for Aetheria.

[6]Accessed May 23rd 2023, https://ehs.yale.edu/sites/default/files/files/decibel-level-chart.pdf

13.1. Cost Estimation Equations

Estimating all the parameters that affect the cost, and the cost itself involves using many empirical methods. For this eVTOL, a paper for empirical methods to determine the cost of a GA aircraft is used [3]. This method is called the Eastlake method, which is a modified version of the DAPCA-IV method. The author has added his own inputs to the equations, therefore making them more reliable and inclusive of more factors.

13.2. Cost Breakdown

In this section, the calculations performed to obtain the costs for Aetheria will be presented. The method used was adapted from the Eastlake method [3]. A complete breakdown can be seen below.

13.2.1. Unit Variable Cost

A few equations are used to determine the number of man-hours required for the production of the eVTOL.

$$H_{ENG} = 0.0396 \cdot W_{\text{airframe}}^{0.791} \cdot V_H^{1.526} \cdot N^{0.183} \cdot F_{\text{CERT}} \cdot F_{\text{CF}} \cdot F_{\text{COMP}} \cdot F_{\text{PRESS}} \tag{13.1}$$

$$H_{TOOL} = 1.0032 \cdot W_{\text{airframe}}^{0.764} \cdot V_H^{0.899} \cdot N^{0.178} \cdot Q_m^{0.066} \cdot F_{\text{TAPER}} \cdot F_{\text{CF}} \cdot F_{\text{COMP}} \cdot F_{\text{PRESS}} \tag{13.2}$$

$$H_{MFG} = 9.6613 \cdot W_{\text{airframe}}^{0.74} \cdot V_H^{0.543} \cdot N^{0.524} \cdot F_{\text{CERT}} \cdot F_{\text{CF}} \cdot F_{\text{COMP}} \tag{13.3}$$

Equation 13.1, Equation 13.2, and Equation 13.3 describe the engineering, tooling, and manufacturing man-hours required. Here $W_{airframe}$ is the OEW (found from previous chapters), V_H is the true airspeed in knots (assumed to be cruise speed), N is the number of units to be produced in the next five years (arbitrarily assumed to be 1000), and Q_m is the estimated number of eVTOLs produced per month. F_{CERT}, F_{CF}, F_{TAPER}, F_{COMP}, F_{PRESS} are, respectively, values to determine how the eVTOL was certified, and indicate the complexity of the flaps, show whether it has a tapered wing, indicate the ratio of composite materials to other materials, and state if it's pressurized or not.

Finally, the man hours can be multiplied by the cost per hour of the workers. For the cost of engineering, tooling, and manufacturing, the paper states that 92 dollars, 61 dollars, and 53 dollars should be used, respectively. In Equation 13.4, the cost has been given. This is simply the man hours multiplied by the cost per hour. The value 2.0969 is the CPI (the price of an average "basket" of goods and services, which tracks inflation [1]) of the years 1986 to 2012, and CPI_{2012} is the CPI from now till 2012. It is given this way since this paper was published in 2013 and thus a correction factor from now till then is needed. H is the number of man-hours as shown above, and R is the cost per hour.

$$C = 2.0969 \cdot H \cdot R \cdot CPI_{2012} \tag{13.4}$$

On top of these costs, the cost of purchasing the materials necessary for production is calculated as:

$$C_{MAT} = 24.896 \cdot W_{\text{airframe}}^{0.689} \cdot V_H^{0.624} \cdot N^{0.792} \cdot CPI_{2012} \cdot F_{\text{CERT}} \cdot F_{\text{CF}} \cdot F_{\text{PRESS}} \tag{13.5}$$

Costs are also taken into account for quality control, where technicians and equipment are used to ensure the quality of the eVTOL. This equation makes use of the manufacturing hours, as calculated in Equation 13.3.

$$C_{QC} = 0.13 \cdot C_{MFG} \cdot F_{\text{CERT}} \cdot F_{\text{COMP}} \tag{13.6}$$

Furthermore, the cost of landing gear is considered, but this depends on if it is fixed or retractable, which will be known in the final report. The retractable landing gear is already implemented in the calculations, therefore the paper instructs to subtract 7,500 dollars per aircraft if a fixed landing gear is used.

Cost of avionics depends on what type of certification the aircraft has obtained. This paper differentiates between LSA certification, and 14 CFR part 23 certification. While neither of these is what the team's eVTOL has used, the eVTOL would fit more into the 14 CFR part 23 due to its weight. Therefore, since this design is certified to 14 CFR part 23, 15000 dollars must be added (in 2012), or more specifically this cost multiplied by

[1] Accessed on May 24th 2023, https://www.bls.gov/cpi/

the CPI resulting in a total cost of 19500 dollars.

Finally, the cost of the engine and propellers are needed. The type of engine used depends on the configuration. For the J1 and W1, turboprops will be used as an approximation with constant-speed propellers. For the L1, an electric turbojet is used, therefore its cost is different. These are:

$$C_{PP} = 377.4 \cdot N_{PP} \cdot P_{SHP} \cdot CPI_{2012} \quad (13.7) \qquad C_{PP} = 868.1 \cdot N_{PP} \cdot T^{0.8356} \cdot CPI_{2012} \quad (13.8)$$

Where Equation 13.7 is the cost for a turboprop engine, and Equation 13.8 is for a turbojet. Here, N_{PP} is the number of engines, P_{SHP} is the rated shaft-horsepower (assumed to be the power required for each engine found in Table 10.3), and T is the rated thrust (the MTOW times the thrust-to-weight ratio divided by engine number). For the constant-speed propellers, an extra cost is needed.

$$C_{CSTPROP} = 209.69 \cdot N_{PP} \cdot CPI_{2012} \cdot D_P^2 \cdot \frac{P_{SHP}}{D_P}^{0.12} \quad (13.9)$$

Where D_P is the propeller diameter in feet found using the disk area. Now that all costs are defined, the total unit variable cost can be found.

13.2.2. Fixed Costs

The fixed costs, in this context, are the costs related to the certification of the eVTOL. This can be calculated as,

$$C_{CERT} = C_{ENG} + C_{DEV} + C_{FT} + C_{TOOL} \quad (13.10)$$

where C_{ENG} and C_{TOOL} have already been defined and calculated in Equation 13.4. The other two are calculated as follows:

$$C_{DEV} = 0.06458 \cdot W_{\text{airframe}}^{0.873} \cdot V_H^{1.89} \cdot N_P^{0.346} \cdot CPI_{2012} \cdot F_{\text{CERT}} \cdot F_{\text{CF}} \cdot F_{\text{COMP}} \cdot F_{\text{PRESS}} \quad (13.11)$$

$$C_{FT} = 0.009646 \cdot W_{\text{airframe}}^{1.16} \cdot V_H^{1.3718} \cdot N_P^{1.281} \cdot CPI_{2012} \cdot F_{\text{CERT}} \quad (13.12)$$

Here, C_{DEV} is the cost of development support, such as HR, facility maintenance, administration, or logistics. C_{FT} is the cost of flight test operations. In these equations, all parameters have been previously defined except for N_P, which is the number of prototypes. Here, 3 has been assumed for simplicity's sake.

13.2.3. Additional Costs for Hydrogen eVTOL

The following equations were determined in order to calculate the costs for the components of our design not covered by [3]. The cost of the fuel cell and the hydrogen storage system that will be used can be calculated using Equation 13.13 and Equation 13.14.

$$C_{FCELL} = C_{kW} \cdot P_{mission} \quad (13.13) \qquad C_{H2tank} = C_{H2system} \cdot E_{mission} \quad (13.14)$$

C_{kW} refers to the cost of fuel cells [$/kW] and $P_{mission}$ refers to the total mission power needed for which the fuel cells will be used [kW]. $C_{H2system}$ is the storage cost system [$/kWh] according to [68]. $E_{mission}$ refers to the total energy mission [kWh]. In addition, batteries and their replacement cost [4] will also be necessary and can be calculated with the equations below.

$$C_{BAT} = M_{BAT} \cdot C_{BATKG} \quad (13.15) \qquad C_{BATREP} = \frac{M_{BAT} C_{BATKG} Q_{\text{FLGT}}}{F_{\text{cycle}} N_{cycles}} \quad (13.16)$$

M_{BAT} refers to the mass of the battery used in the design [kg] and C_{BATKG} refers to the cost of the battery [$/kg]. Fuel cells and storage tanks have a very long lifetime (more than 15 years), thus their replacement will not be necessary during the operational lifetime of the eVTOL. Finally, to calculate the cost of energy necessary for the batteries, the following equation can be used [4]:

$$C_{ELEC} = \frac{M_{BAT} C_{kWh} E_{kg} Q_{\text{FLGT}}}{F_{\text{cycle}}} \quad (13.17)$$

The parameters used in this equation are the following: C_{kWh} refers to the cost of electricity [$/kWh], E_{kg} refers to the specific energy density of battery [kWh/kg], Q_{FLGT} is the number of flight hours per year (arbitrarily assumed to be 1800), N_{cycles} refers to the number of battery discharge cycles and F_{cycle} is the number of flight hours per cycle [4].

13.2.4. Break Even Point

To calculate the break-even unit number, the total fixed cost and the unit variable cost are determined. This is done using the following equations:

$$\text{Unit Variable Cost} = \frac{C_{MFG} + C_{QC} + C_{MAT}}{N} + C_{AV} + C_{CSTPROP} + C_{PP} + C_{LG} + C_{INS} + C_{FCELL} + C_{TANK} + C_{BAT} \tag{13.18}$$

$$\text{Total Fixed Cost} = C_{CERT} \tag{13.19}$$

$$N_{BE} = \frac{\text{Total Fixed Cost}}{\text{Unit Price} - \text{Unit Variable Cost}} \tag{13.20}$$

13.2.5. Operational Costs

The annual costs for fuel, insurance, maintenance (C_{AP}), and inspection can be calculated. Furthermore, the engine overhaul fund can be calculated.

$$C_{AP} = F_{MF} \cdot R_{AP} \cdot Q_{FLGT} \tag{13.21}$$

$$C_{FUEL} = FF_{CRUISE} \cdot Q_{FLGT} \cdot R_{FUEL} \tag{13.22}$$

Here, R_{AP} refers to the hourly rate for the certified airframe, FF_{CRUISE} refers to the total fuel flow in gallons per hour and R_{FUEL} refers to the price of fuel in dollars per gallon. It is important to note in the equation above, the fuel being referred to is hydrogen and not kerosene.

$$C_{INS} = 500 + 0.015 \cdot C_{AC} \tag{13.23}$$

$$C_{INSP} = 500 \tag{13.24}$$

$$C_{OVER} = 5 \cdot N_{PP} \cdot Q_{FLGT} \tag{13.25}$$

Where C_{AC} is the insured value of the eVTOL, assumed to be 2.5 million dollars, as stated in the textbook [3]. Finally, the yearly operation cost of the eVTOL C_{YEAR} can be calculated by summing all the previous costs. From this cost, the cost per flight hour C_{HR} can also be obtained by dividing the yearly costs by the total flight hours per year.

$$C_{YEAR} = C_{AP} + C_{FUEL} + C_{INS} + C_{INSP} + C_{OVER} \tag{13.26}$$

$$C_{HR} = \frac{C_{YEAR}}{Q_{FLGT}} \tag{13.27}$$

13.3. Final Results

To sum up all the individual costs obtained from the formulae, a table was constructed which can be seen in Table 13.1. The yearly operational costs, fixed cost, unit variable cost, and finally the break-even units required can be seen. The unit price was fixed at a value twice the unit variable cost according to the configuration. The table is in dollars.

Table 13.1: *Final Costs*

	J1	**L1**	**W1**
Total Fixed Cost (Millions $)	91	201	151
Unit Variable Cost (Millions $)	1.0	3.1	1.7
Unit Price (Millions $)	2.0	6.3	3.3
Break-Even Units	92	64	93

13.4. Return on Investment

Once the cost breakdown has been finished, a projection of the project's costs and revenue per year can be determined to calculate the net present value of each cash flow and required total investment, which can produce a return on investment. Based on the required steps to fully make the eVTOL operational, the timeline has been set to begin in 2030, which is when the market analysis was also done. At this stage, only 5 eVTOLs will be produced that year, increasing it every year, so that 1000 eVTOLs are being produced each year by 2035 till 2040 (the end date of the projection).

The unit variable cost per eVTOL has been written in Table 13.1, but this will decrease as time goes on. This learning curve is affected by experience gained by the workers, better infrastructure, advanced technology, reduction in prices due to the technology becoming more mainstream, less outsourcing, etc. For this, a learning curve of 90% has been set. This value is quite high but hydrogen-powered eVTOLs are a very new concept,

meaning it will take longer for the costs to decrease. The yearly operational costs are not expected to decrease, other than a potential decrease in the fuel cost due to hydrogen being produced more. Taxes also need to be considered, being 25.8% in the Netherlands for businesses [2].

In Table 13.2 the annual cash flows are stated. The total return on investment is the discounted cash flow (using 4% based on numerous projections) over the total discounted investment required.

Table 13.2: *Return on Investments*

	J1	L1	W1
ROI (%)	128	87	98

J1 clearly has the highest return on investment, even though it has the cheapest asking price. This is clearly the best configuration in terms of costs.

13.5. Production and Operational Costs with Scores for Different Designs

The costs for J1 and J2 are identical, therefore J2 will not be implemented into the table and only J1 will be show. In Table 13.3, the values for the yearly operational costs (both with and without fuel), cost per flight hour and production costs (unit variable costs) can be seen. Finally, the trade-off scores for the different designs can be seen in Table 13.4

Table 13.3: *Production and Operational Costs*

	J1	L1	W1
Yearly Operational Cost	200.5k	735.5k	359.7k
Cost per flight hour	111.4	408.6	199.8
Fuel-less Operational Cost	159.3k	614k	293.7k
Production (unit variable) cost	1,005.5k	3,123.9k	1,677.2k

Table 13.4: *Scores for the different designs*

	J1	J2	L1	W1
Fuel-less operational cost score	3	3	1	2
Production cost score	3	3	1	2

14
Design Configuration Trade-off

In this chapter, the trade-off between the design concepts has been performed. The selection criteria and weights have been determined in Chapter 4. The level of compliance (scores) with respect to each trade-off criteria are awarded between 0 to 3 as explained in Chapter 4 and any design that receives a score of 0 in any criteria is discarded. Based on each design's scores for each criteria and the weight of each criteria, a score was awarded to each design out of 3. A higher score indicates a better design. The scores received by different designs for each criteria as well as the final score for the design is shown in Table 15.2. The colors indicate the score of a design per criteria as shown in Table 14.1.

Table 14.1: *Colors Assigned to Different Scores*

0	1	2	3
Red	Orange	Yellow	Green

To assist people with color vision deficiency, the numerical scores out of three for each criteria has also been provided at the lower right corner of the each criteria in Table 14.2. As seen in Table 14.2, J2 wins with a score

[2] Accessed May 22nd 2023, https://business.gov.nl/amendment/corporate-income-tax-increases/

of 2.4/3 with a big lead on the second best contender (W1 with a score of 1.8/3). Hence J2 is the chosen design.

Table 14.2: *Final Trade-off Table*

Criteria / Design	Mission Energy (30%)	Stability & Controllability (20%)	Crashworthiness (20%)	Production cost (10%)	Operational cost except Fuel (10%)	Noise (10%)	Weighted Total
J1	204kWh (3)	cannot be made stable and controllable (0)	1.59m crash floor required for 3.25m cabin, high wing (2)	1.01 M $ / VTOL (3)	159k $ / year (3)	86dB at 30m (2)	DISCARDED
J2	204kWh (3)	large flexibility in terms of wing positioning and trim (3)	1.59m crash floor required for 3.25m cabin, high wing (2)	1.01 M $ / VTOL (3)	159k $ /year (3)	86dB at 30m (2)	2.4
W1	326kWh (2)	allowable cg range just meets required cg travel (2)	2.65m crash floor required for 3.25m cabin, not high wing (2)	1.68 M $ / VTOL (2)	294k $ / year (2)	94dB at 30m (2)	1.8
L1	547kWh (1)	large flexibility in terms of wing positioning and trim (3)	3.63m crash floor required for 3.25m cabin (can be fixed), not high wing (1)	3.12 M $ / VTOL (1)	614k $/ year (1)	56dB at 30m (3)	1.5

Trade off Sensitivity

A trade-off sensitivity is normally required to see whether adjusting the weights of the different trade-off criteria will lead to a different design choice. In this case, even if the weights of the trade-off criteria were completely different, J2 would still the chosen design. This is because the J2 has received a score of 3/3 on different criteria more than any other design and it has not received a score of 1/3 in any criteria. In comparison, the next best design W1 has received a 2 in all criteria which means that J2 is better than W1 regardless of the weights of the criteria. Based on the scores for different criteria, it can be said that the J2 is at least as good W1, the next best design, in each criteria or better. This means that the design choice would not change even if the weights of the different criteria were altered.

15 Manufacturing, Assembly and Integration Plan

This chapter will give a brief overview of the manufacturing, assembly, and integration plan to produce Aetheria. In the final report, a more detailed plan will be given, as a final design will have been generated by then. Like most aircraft, Aetheria will be produced in a line production. The flow diagram for the Manufacturing, Assembly and Integration can be found in Figure 15.1. It shows a timeline of the production and testing of Aetheria.

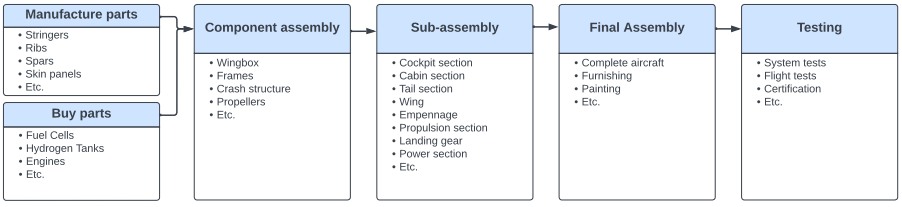

Figure 15.1: *Manufacturing, Assembly and Integration Flow Diagram*

The production process starts with manufacturing simple and specific parts and buying complicated and standardised parts and components. Parts will be manufactured and ordered in batches and stored in a warehouse. Like most aircraft, the assembly will be done in line production. The components, such as the wingbox and frames, are produced in the component assembly lines, which flow into the sub-assembly lines. These lines produce sub-assemblies, such as the cabin and landing gear, and flow into the final assembly lines. This line can be seen as the backbone of the production lines and culminates with a complete aircraft. At the end of the final assembly line, final finishes such as furnishing and painting are performed.
The last important phase before the aircraft can be delivered is testing. Testing will be performed on the (sub)system level, which can be done in parallel with production. After the complete aircraft is produced and all systems have passed the tests, a flight test will be conducted to ensure that the aircraft meets all the performance and safety requirements. When all tests are passed, the aircraft can be delivered to customers.

16
Conclusion & Recommendation

The objective of this report is to outline the process from the three initial designs presented in the baseline report to a single design that will undergo a detailed analysis. Using a multidisciplinary approach as described in Chapter 4, this report evaluates the mentioned designs. The evaluation took into account technical factors such as mission energy and controllability and non-technical factors such as the operating cost.

During the evaluation as can be seen in Chapter 14, it was determined that the J2 design shows the most favourable factors among the three concepts mentioned. The J2 design is similar to the J1 design however, with the incorporation of two engines per propeller such that the controllability requirements are met. The J2 design features a single high wing with 4 propellers and a tail with 2 propellers. In terms of the power system as described in Chapter 9 will consist of a proton exchange membrane fuel cell and a lithium-ion battery.

It is important to note that more work is required for a final design. Several recommendations have been found however not all of them have been included in this report. They consist of determining the wing location, sizing the cooling system, and quantitative analysis for the crashworthiness such passenger safety can be guaranteed.

Bibliography

[1] 06, D. G., "Final Report MultiDisciplinary Design and Optimisation of LongRange eVTOL Aircraft," Tech. rep., 2021.

[2] Roskam, J., *Airplane Design Part V: component weight estimation*, Roskam Aviation and Engineering Corporation, Ottowa, Kansas, 1985.

[3] Gudmundsson, S., "General Aviation Aircraft Design - Chapter 2," *Science Direct*, 2014.

[4] 06, D. G., "Midterm Report MultiDisciplinary Design and Optimisation of LongRange eVTOL Aircraft," Tech. rep., 2021.

[5] Jenkinson, L. R., and Marchman, J. F., "2 - Preliminary design," *Aircraft Design Projects*, edited by L. R. Jenkinson and J. F. Marchman, Butterworth-Heinemann, Oxford, 2003, pp. 6–42. doi:https://doi.org/10.

1016/B978-075065772-3/50004-1, URL https://www.sciencedirect.com/science/article/pii/B9780750657723500041.

[6] EASA, "Second Publication of Proposed Means of Compliance with the Special Condition VTOL," 2021.

[7] Nathen, P., "Architectural performance assessment of an electric vertical take-off and landing (e-VTOL) aircraft based on a ducted vectored thrust concept," Tech. rep., 2021.

[8] Maxim Tyan, S. K. J.-W. L., Nhu van Nguyen, "Comprehensive preliminary sizing/resizing method for a fixed wing – VTOL electric UAV," Tech. rep., 2017.

[9] Polaczyk, N., Trombino, E., Wei, P., and Mitici, M., "A review of current technology and research in urban on-demand air mobility applications," , 2019.

[10] Stoll, A., "Analysis and Full Scale Testing of the Joby S4 Propulsion System," , 2015.

[11] Dr. F. Oliviero, *AE2111-II aircraft part*, September 2021. Academic year 2021/2022.

[12] R. Vos, B. Z., J.A. Melkert, "AE1222-I 2-Class I weight estimation," AE1222-I Aerospace Engineering TU Delft, May 2023. Accessed 11-05-2023.

[13] Güzelbey, I. H., Eraslan, Y., and Doğru, M., "Effects of Taper Ratio on Aircraft Wing Aerodynamic Parameters: A Comperative Study," *European Mechanical Science*, 2019.

[14] Nathen, D. P., "Architectural performance assessment of an electric vertical take-off and landing (e-VTOL) aircraft based on a ducted vectored thrust concept," , May 2023. Accessed 11-05-2023.

[15] Schiktanz, D., "Conceptual design of a medium range box wing aircraft," *Department Fahrzeug technik und Flugzeugbau, Master Thesis, Hamburg, HAW Hamburg*, 2011.

[16] Group 11, *Hydrogen-powered long-range eVTOL designed for crashwor- thiness Baseline Report*, May 2023. Academic year 2022/2023.

[17] "XFLR5: Analysis of foils and wings operating at low Reynolds numbers," Tech. rep., XFLR5, 2023.

[18] Beyne, E. E., and Castro, S. G., "Preliminary performance assessment of a long-range Evtol Aircraft," *AIAA SCITECH 2022 Forum*, 2022. doi:10.2514/6.2022-1030.

[19] Lewis, E., "VTOL Design Loads and Interaction of Systems and Structures," , 2020.

[20] Faisal, N., Ömer Necati Cora, Bekci, M. L., Śliwa, R. E., Sternberg, Y., Pant, S., Degenhardt, R., and Prathuru, A., *Introduction to Aerospace Flight Vehicles*, 2021.

[21] Smye, B., "Aluminum alloys for aerospace," Tech. rep., 2018.

[22] Leishman, J. G., *Structural Health Monitoring Damage Detection Systems for Aerospace*, 2023.

[23] Rans, C., "Structural Analysis Formulas," Tech. rep., 2020.

[24] Curtis, H. D., *Fundamentals of Aircraft Structural Analysis*, McGraw-Hill Higher Education, 1996.

[25] Lipski, A., "Rapid determination of the Wöhler's curve for aluminum alloy 2024-T3 by means of the thermographic method," *AIP Conference Proceedings*, Vol. 1780, No. 1, 2016. doi:10.1063/1.4965936.

[26] Fujio, Y., Xu, C.-N., Sakata, Y., Ueno, N., and Terasaki, N., "Invisible crack visualization and depth analysis by mechanoluminescence film," Tech. rep., 2020.

[27] Roskam, J., *Airplane Design Part III: Layout Design of Cockpit, Fuselage, Wing and Empennage: Cutaways and Inboard Profiles*, Roskam Aviation and Engineering Corporation, Ottowa, Kansas, 1985.

[28] EASA, "Means of Compliance with the Special Condition VTOL," 2021.

[29] Güemes, A., Fernández-López, A., Díaz-Maroto, P. F., Lozano, A., and Sierra-Perez, J., "Structural Health Monitoring in Composite Structures by Fiber-Optic Sensors," *Sensors*, Vol. 18, No. 4, 2018. doi:10.3390/s18041094.

[30] Jacob Putnam, J. L., "Crashworthiness of a Lift plus Cruise eVTOL Vehicle Design within Dynamic Loading Environments," 2020.

[31] Jackson, K., Kellas, S., Horta, L., and Annett, M., "Experimental and Analytical Evaluation of a Composite Honeycomb Deployable Energy Absorber," 2011.

[32] Ryan Miller, J. W. F. T. M. A., Andrea Di Renzo, "Test and Analysis Methodology for Validating Crashworthiness of AW609 Tiltrotor," 2022.

[33] Jackson, K. E., Fuchs, Y. T., and Kellas, S., "Overview of the NASA Subsonic Rotary Wing Aeronautics Research Program in Rotorcraft Crashworthiness," *ASCE 11th Earth and Space Conference*, NASA Langley Research Center, General Dynamics Advanced Information Systems, Long Beach, CA, 2008.

[34] Dühne, A., "VTOL Crashworthiness based on EASA Special Condition," , 2019.

[35] Thomas, T., "Crushing Behaviour of Honeycomb structure: A Review," *International Journal of Crashworthiness*, 2018.

[36] "Supercapacitors: A new source of power for electric cars?" *Economic Analysis and Policy*, Vol. 61, 2019, pp. 93–103. doi:https://doi.org/10.1016/j.eap.2018.08.003, special issue on: Future of transport.

[37] "A Cost- and Energy Density-Competitive Lithium-Sulfur Battery," *Energy Storage Materials*, Vol. 41, 2021, pp. 588–598. doi:https://doi.org/10.1016/j.ensm.2021.06.037.

[38] "Lithium-sulfur batteries: lightweight technology for multiple sectors," *The Faraday Institution*, Vol. 8, 2020, pp. 2–5.

[39] "A dynamic stability design strategy for lithium metal solid state batteries," *Nature*, 2021, p. 218–222. doi:https://doi.org/10.1038/s41586-021-03486-3.

[40] "Battery cost forecasting: a review of methods and results with an outlook to 2050," *Energy Environmental Science*, 2021. doi:10.1039/D1EE01530C.

[41] "Highly enhanced energy density of supercapacitors at extremely low temperatures," *Journal of Power Sources*, Vol. 423, 2019, pp. 271–279. doi:https://doi.org/10.1016/j.jpowsour.2019.03.096.

[42] Wang, Y., Pang, Y., Xu, H., Martinez, A., and Chen, K. S., "PEM Fuel cell and electrolysis cell technologies and hydrogen infrastructure development – a review," *Energy Environ. Sci.*, Vol. 15, 2022, pp. 2288–2328. doi:10.1039/D2EE00790H.

[43] Zhang, X., "Current status of stationary fuel cells for coal power generation," *Clean Energy*, Vol. 2, No. 2, 2018, pp. 126–139. doi:10.1093/ce/zky012.

[44] "Development of low cost alkaline fuel cells," *Journal of Power Sources*, Vol. 18, No. 4, 1986, pp. 317–335. doi:https://doi.org/10.1016/0378-7753(86)80089-1.

[45] "Alkaline fuel cell technology - A review," *International Journal of Hydrogen Energy*, Vol. 46, No. 35, 2021, pp. 18489–18510. doi:https://doi.org/10.1016/j.ijhydene.2021.02.203.

[46] "Chapter 2 - Performance Trends and Status of Microbial Fuel Cells," *Progress and Recent Trends in Microbial Fuel Cells*, edited by P. P. Kundu and K. Dutta, Elsevier, 2018, pp. 7–24. doi:https://doi.org/10.1016/B978-0-444-64017-8.00002-6.

[47] "Paths to market for stationary solid oxide fuel cells: Expert elicitation and a cost of electricity model," *Applied Energy*, Vol. 304, 2021, p. 117641. doi:https://doi.org/10.1016/j.apenergy.2021.117641.

[48] Petrovic, S., and Hossain, E., "Development of a Novel Technological Readiness Assessment Tool for Fuel Cell Technology," *IEEE Access*, Vol. 8, 2020, pp. 132237–132252. doi:10.1109/ACCESS.2020.3009193.

[49] "6 - Operation and durability of low temperature fuel cells," *Polymer Electrolyte Membrane and Direct Methanol Fuel Cell Technology*, Woodhead Publishing Series in Energy, Vol. 1, edited by C. Hartnig and C. Roth, Woodhead Publishing, 2012, pp. 137–177. doi:https://doi.org/10.1533/9780857095473.2.137.

[50] "Chapter 13 - Hydrogen storage," *Electrochemical Power Sources: Fundamentals, Systems, and Applications*, edited by T. Smolinka and J. Garche, Elsevier, 2022, pp. 455–486. doi:https://doi.org/10.1016/B978-0-12-819424-9.00006-9.

[51] "Chapter 6 - Stranded Renewable Energies, Beyond Local Security, Toward Export: A Concept Note on the Design of Future Energy and Chemical Supply Chains," *Polygeneration with Polystorage for Chemical and Energy Hubs*, edited by K. R. Khalilpour, Academic Press, 2019, pp. 157–173. doi:https://doi.org/10.1016/B978-0-12-813306-4.00006-9.

[52] "Chapter 4 - Hydrogen storage systems," *Fuel Cell Modeling and Simulation*, edited by G. R. Molaeimanesh and F. Torabi, Elsevier, 2023, pp. 269–282. doi:https://doi.org/10.1016/B978-0-32-385762-8.00008-7.

[53] "9 - Solid-state hydrogen storage nanomaterials for fuel cell applications," *Mechanical Alloying (Third Edition)*, edited by M. S. El-Eskandarany, William Andrew Publishing, 2020, third edition ed., pp. 229–261. doi:https://doi.org/10.1016/B978-0-12-818180-5.00009-1.

[54] "5 - Cryo-compressed hydrogen storage," *Compendium of Hydrogen Energy*, edited by R. B. Gupta, A. Basile, and T. N. Veziroğlu, Woodhead Publishing Series in Energy, Woodhead Publishing, 2016, pp. 119–145. doi:https://doi.org/10.1016/B978-1-78242-362-1.00005-5.

[55] Nathen, P., "Architectural performance assessment of an electric vertical take-off and landing (e-VTOL) aircraft based on a ducted vectored thrust concept," , April 2021. Accessed 11-05-2023.

[56] Alba Maestre, J., Prud'homme van Reine, T., K.; Sinnige, and Castro, S. G., "Preliminary Propulsion and Power System Design of a Tandem-Wing Long-Range eVTOL Aircraft," Tech. rep., 2021.

[57] D.G. Simons, M. S., "Reader Aircraft Noise September 2022 (part A)," AE4431 Aerospace Engineering TU Delft, August 2022. Accessed 12-05-2023.

[58] Stoll, A., "Analysis and Full Scale Testing of the Joby S4 Propulsion System," Joby Aviation, August 2015. Accessed 11-05-2023.

[59] Du, G.-X., Quan, Q., Yang, B., and Cai, K.-Y., "Controllability analysis for multirotor helicopter rotor degradation and failure," *Journal of Guidance, Control, and Dynamics*, Vol. 38, No. 5, 2015, p. 978–985. doi:10.2514/1.g000731.

[60] Brown, A., and Harris, W. L., "Vehicle design and optimization model for urban air mobility," *Journal of Aircraft*, Vol. 57, No. 6, 2020, pp. 1003–1013.

[61] Zhou, X., Yang, T., Xiao, J., Bénard, P., and Chahine, R., "Estimation of filling time for compressed hydrogen refueling," *Energy procedia*, Vol. 158, 2019, pp. 1897–1903.

[62] Enerdata, "Share of renewables in electricity production," Enerdata, May 2023. Accessed 23-05-2023.

[63] Kanestephanie Gil, M. K., "Green Hydrogen: A key investment for the energy transition," *Energy Transition Journal*, 2023.

[64] Mehmood, G. M. J. F. e. a., A., "High loading of single atomic iron sites in Fe–NC oxygen reduction catalysts for proton exchange membrane fuel cells," *Nat Catal 5*, 2022. doi:https://doi.org/10.1038/s41929-022-00772-9.

[65] Melo, S. P., Cerdas, F., Barke, A., Thies, C., Spengler, T. S., and Herrmann, C., "Life Cycle Engineering of future aircraft systems: the case of eVTOL vehicles," *Procedia CIRP*, Vol. 90, 2020, pp. 297–302.

[66] Mossali, E., Picone, N., Gentilini, L., Rodrìguez, O., Pérez, J. M., and Colledani, M., "Lithium-ion batteries towards circular economy: A literature review of opportunities and issues of recycling treatments," *Journal of environmental management*, Vol. 264, 2020, p. 110500.

[67] Meng, F., Cui, Y., Pickering, S., and McKechnie, J., "From aviation to aviation: Environmental and financial viability of closed-loop recycling of carbon fibre composite," *Composites Part B: Engineering*, Vol. 200, 2020, p. 108362. doi:https://doi.org/10.1016/j.compositesb.2020.108362.

[68] Houchins, C., James, B. D., Huya-Kouadio, J., and DeSantis, D., "Hydrogen Storage Cost Analysis," *Department of Energy*, 2021.